CALIBRATION OF THE OSU PSYCHROMETRIC CHAMBER AND FIRST EXPERIMENTS

By

KASEY WORTHINGTON

Bachelor of Science in Mechanical Engineering

Oklahoma State University

Stillwater, OK

2009

Submitted to the Faculty of the
Graduate College of the
Oklahoma State University
in partial fulfillment of
the requirements for
the Degree of
MASTER OF SCIENCE
July, 2011

CALIBRATION OF THE OSU PSYCHROMETRIC

CHAMBER AND FIRST EXPERIMENTS

Thesis Approved:

Dr. Lorenzo Cremaschi

Thesis Adviser

Dr. Daniel E. Fisher

Dr. Afshin J. Ghajar

Dr. Mark E. Payton

Dean of the Graduate College

ACKNOWLEDGMENTS

During the time, I worked on the Psychrometric Chamber, 11 ton Roof Top Unit Testing, and Pipe Insulation Testing Apparatus (PIT) projects at Oklahoma State University, multiple students, faculty, and employees of Oklahoma State University have been a pronounced influence. I would like to thank a few specifically. First, I would like to thank Shanshan Cai for all her hard work and countless hours spent perfecting the PIT. It was a privilege to work with such an intelligent hard working and meticulous individual. Without her, the PIT would have not been a successful project. Secondly, I would like to thank Gary T hacker for all his help, advice, and hard work. His knowledge and time spent helping with the electrical of every project in the ATRC is a huge reason the work present in this thesis was possible. Gary current position as building manager has allowed our group to communicate and work with the OSU Physical Plant. His patience and consistent help with these logistical issues is another huge reason this work was possible. I greatly appreciate all the hard work and extra hours as well as his dedication and enthusiasm. I would also like to thank Chad (Buck) Rich for all his countless hours of work on the construction, fabrication, and welding of countless components involve with the chamber. I would also like to thank Buck for his advice on practicality of fabrication and his willingness to bringing me back to the real world when my far- fetched ideas were too much for the time and cost available. Without his help there is no possible way the chamber would have been constructed and operating the way it is today. Lastly, I would like to thank all faculty and students involved in the Chamber construction as well as the PIT Project. As their advice, discussions, and support are a definite influence on the quality of my work present in this thesis. Without this collaboration, these would not have reached the success that it is today

TABLE OF CONTENTS

Chapter Page

LIST OF TABLES

Table
Page

LIST OF FIGURES

Figure Page

Figure Page

CHAPTER I

INTRODUCTION

OSU Pychrometric Chamber

The OSU Psychrometric Chamber consists of two adjacent air conditioned rooms that are controlled over a wide range of conditions with and without a live load in it. The main focus of the chamber is to test unitary HVAC equipment, where one room artificially reproduces the outdoor climate conditions while the other room is employed to simulate the indoor environments and replicate indoor comfort conditions with thermal loads up to 20 tons of refrigeration (70 kW). The chamber at OSU is not limited to testing of HAVC unitary systems and independent operation of each room is possible to perform countless experiments that need a controlled uniform ambient conditions. An example is described in this thesis in which the chamber was used to control the environmental conditions surrounding a pipe insulation system. The design temperature ranges for the chamber are from -40°F(-40°C) to 135°F (57°C) and from 50°F (10°C) to 135°F (57°C) for the outdoor and indoor rooms respectively; with both rooms capable of relative humidity from 10% up to 95% R.H. Air is first conditioned to the desired psychrometric states and then circulated in the rooms. Uniform conditions are achieve in each room by first conditioning the air to the desired psychrometric states and then circulating it into the rooms, which are of dimensions approximately 19ft (5.8m) x 21ft (6.4m) floor area and 16ft (4.9m) ceiling elevation. More details about the facility design, construction, and specifications can be found in (Cremaschi and Lee 2008). This thesis describes the calibration work conducted on the OSU psychrometric chamber and presents the first two experiments. The two experiments are (1) testing of performance rating of an 11-ton rooftop unit and (2) measuring the thermal conductivity of pipe insulation system for chiller applications. These two experiments are quite different in nature and scope but they both require an accurate control of the environment with a

live thermal load in it, (i.e. experiment 1) and without a live thermal load in the room (i.e. experiment 2). These experiments demonstrate the capabilities and limitation of the chamber and thus are presented as case studies in this thesis. A brief introduction for each experiment is given next.

Unitary Equipment Testing

Unitary equipment and systems are factory-made assemblies that often provide heating and cooling to buildings all year round. They consist of an evaporator or cooling coil, a combination of compressor and condenser, constant or variable speed fans and motors, and a set of accessories and controls that are configured to cost-effectively run the system either for a single zone or multiple zones at full or at part loads conditions. During recent years, given the critical importance of energy savings during actual field operation, an integrated coefficient of performance (ICOP) is used as a single number figure of merit expressing cooling part-load COP efficiency for unitary air-conditioning and heat pump equipment on the basis of weighted operation at various load capacities for the equipment. Yet, a system with a high ICOP does not necessarily lead to reduced energy costs and unitary equipment systems should also be properly sized, have optimized charge balance, and their energy performance should be carefully evaluated. In addition, advanced unitary equipment systems include a series of accessories and controls that often improve the non-steady-state efficiency and their potential energy savings are not properly quantified by conventional steady state energy performance rating parameters. The chamber was design and constructed to help address these needs.

Moisture Propagation in Chilled Water Pipe Insulation

While the chamber's focus is to test unitary equipment, the chamber can also provide a controlled uniform environment. This controlled environment is needed to conduct experiments that determine the thermal conductivity of pipe insulation and investigate the behavior of the insulation as moisture propagates into the material. One of the largest applications commonly exposed to this scenario is chilled water piping systems and the operation of these systems is largely impacted by the thermal performance of the pipe insulation. Pipes carrying cold fluids such as chilled water as well as in refrigeration and liquid nitrogen systems have to be adequately insulated to prevent moisture

propagation from occurring which will lower the performance and/or shorten the life of the insulation. There are other undesirable effects; such as, the promotion of mold growth, dripping or damp surfaces inside a building, which also need to be avoided. To adequately insulate a piping system the thermal performance and behavior of the pipe insulation should be known allowing for the proper material and thickness to be selected. The selection should to be based on the range of actual conditions that the pipe system operates in; hence employing the chamber for these types of experiments is justified by the need to set extreme environmental conditions for conducting accelerated type laboratory test of pipe insulation thermal conductivity below-ambient temperatures.

CHAPTER II

REVIEW OF LITERATURE

Standards for Performance Rating of Unitary Systems

Two highly recognized organizations set forth standards and testing methods that describe step by step the needed procedure to test and certify Unitary Equipment. These two organizations are the Air-Conditioning, Heating, and Refrigeration Institute (AHRI) and the American Society of Heating, Refrigerating, and Air-Conditioning Engineers (ASHRAE); these two organizations have a strong working relationship and collaborate on numerous topics. The standards and testing methods developed by these two organizations are the bases of the design, construction, and operations for the OSU Psychrometric Chamber.

ASHARE Standard 37(2009) exemplifies ways to test unitary equipment to determine its cooling and/or heating capacities. ASHARE Standard 37(2009) categorizes unitary equipment into groups such as Single Package Units, Split Systems, etc. and demonstrates the needed setup to test all these variations. The setups include the unitary equipment sub-component locations and the type of connection linking them, such as refrigerant lines or air ducts. It also describes the environment each component is supposed to experience during testing, with respect to Indoor or Outdoor conditions. Due to the different setup needed to test each category of unitary equipment, the measurement locations are respectably different as well. This standard illustrates the approximate location of the measuring devices relative to the category of equipment. One of the measuring devices used in the testing setup is the Air Flow Measuring Apparatus. This apparatus utilized the pressure drop across flow nozzles in order to calculate the equipment airflow rate. In this standard, the apparatus exemplified a basic example to guide and suggest the adoption of the apparatus to the available and desired configuration needed. This apparatus is the core to the OSU Psychrometric Chamber's Code

Tester. Some of the other measuring devices on the testing setup are pressure and temperature measurements. For these measurements, ASHARE Standard 37(2009)suggested the locations on the testing setup, but refers to ASHRAE Standard 41 as its means of insuring accurate and precise pressure and temperature measurements. ASHRAE 41 is a widely accepted mean of measuring pressures and temperatures and illustrates in detail the needed steps to achieve these measurements. With these acquired measurements, ASHARE Standard 37(2009) goes on to explain the calculations needed for seven different methods which determine the capacity of the unitary equipment being tested.

These methods include:

- Air-Enthalpy Method, Indoor Side
- Air-Enthalpy Method, Outdoor Side
- Compressor Calibration Method
- Refrigerant Enthalpy
- Outdoor Water Coil Method
- Air Flow Measurement
- Cooling Condensate Measurement

Any of these methods are acceptable methods of determining the unit's capacity, but the Psychrometric Chamber is currently setup to use the Indoor or Outdoor Side Air Enthalpy Method. ASHRAE also has standards to determine the efficiency of unitary equipment, which utilize ASHARE Standard 37(2009). This allows the unit to be quantified to an operational cost and to be comparable to other equipment. One of these is ASHRAE Standard116 (1995) which demonstrates the test methods and calculations needed to determine unitary equipment Seasonal Energy-Efficiency Ratio (SEER). The testing methods and calculations to determine the capacity of the equipment follows ASHRAE 37, but ASHRAE Standard116 (1995)takes this further and specifies a set of standardized testing conditions. Standardized testing conditions allow different equipment to be compared and analyzed fairly. Also, ASHRAE Standard116 (1995)defines the Energy Efficiency Ratio (EER) which justifies the amount of energy used by the equipment compared to the cooling or heating capacity produced by the equipment. This EER allows the operating cost to be estimated. It goes on incorporated numerous EER at different conditions in to one SEER. This SEER tries to

capture the equipment EERs for an entire year, where the unit has experienced countless different operating conditions.

As mentioned earlier both ASHRAE and AHRI have a strong relationship and an extensive reference of AHRI Standard 210/240 is used in ASHRAE Standard116 (1995). This Standard is part of a certification program which defines the tests, data, and tolerance needed to publish ratings such as in manufacture's literature, nameplates, operational requirements, and etc., on Unitary Air Conditioning Equipment up to 65,000 Btu/h (19,000W) capacities. AHRI 210/240 goes step by step though the needed equipment setup, full load testing, part load testing, cycling testing, design conditions testing, off design conditions testing, as well as the calculation need to determine the equipment capacity, EER, and SEER. There is constant referencing back to ASHRAE standards 37, 41, 51, 116 and etc. where the content is presented in more or less detail.

Not one of these standards appears to stand-alone as they are all associated, but AHRI 210/240 and AHRI 340/360 are the focal points within this thesis. AHRI 340/360 is much the same as AHRI 210/240 which is a standard stating the needed requirements to publish rating, but AHRI 340/360 covers larger capacity equipment from 65,000 Btu/hr (19,000 W) to 250,000 Btu/hr (73,200 W). There are minor differences between the two standards to account for the feasibility and limitations with testing the larger equipment. One main difference is the overall number of needed tests to meet AHRI 340/360 is less than AHRI 210/240. The unitary equipment tested and presented in this thesis fall into the range covered by Standard AHRI 340/360, but some of the AHRI 210/240 tests were also explored in thesis with the larger equipment.

Review of Chamber Control Strategies

Wong and Li (2010) developed a model or approach that allows engineers to select and evaluate available controls or control strategies to build a HVAC control system. This approach is designed and geared towards intelligent commercial building operating systems that are becoming more and more sophisticated. The Psychometric Chamber does not quite fit inside this category, but a very closely related sophisticated control scheme is needed to control the chamber's set points within the

desired accuracy. There has been a lot of work done with controls of HVAC systems, mainly because of the "Green Energy Push", and narrowing down these works to a smaller list that is relevant and useful for the Psychometric Controls is an overwhelming task. It is believed that this approach can be slightly modified to fit the needs of the chamber and be utilized to speed up and optimize the controls' development. Wong and Li (2010) was able to develop this approach by conducting a study that took a wide range of opinions into account. These opinions are from a community that deals with HVAC systems from day to day, this included occupants, contractors, service personnel, building owners, engineers, and control experts. To obtain such a wide range of opinions a number of surveys were performed. The results of the surveys allowed for the development of a systematic and structured approach to select the optimal control scheme for the application. Within this structured approach are weighted selection criteria and from the surveys 'total energy use' is perceived as the top priority, followed by the 'system reliability and stability', 'operating and maintenance costs', and 'control of indoor humidity and temperature'. To utilize this approach for the chamber a very obvious modification would have to be made. The first and last priority would need to be switched, because the top priority for the chamber is to precisely and accurately control the humidity and temperature in the chamber rooms.

Rentel-Gomez and Velez-Reyes (2001) understood that in some cases, like with the Psychometric Chamber, it is important to be able to control temperature and relative humidity independently and accurately. In most HVAC applications this independence is not important and the tolerance for relative humidity is a large range. In normal applications the conditioned space is controlled to a temperature set point and as long as the relative humidity is within the comfort zone range the space is considered controlled. In more recent days this relative humidity comfort zone has been explored to decrease the energy consumption of the building by adjusting the relative humidity in the space. Even still those works have not completely decoupled the temperature and relative humidity relationship. The Psychometric Chamber main goal is to maintain the chamber at very accurate and precise set temperatures and relative humidity with conserving energy being one of lowest priority. The temperature and relative humidity will be a user specified set point that should not be limited by one

another. Rentel-Gomez and Velez-Reyes (2001) developed a nonlinear non-interacting controller for temperature and relative humidity in a thermal-space, the controller takes into account the coupling dynamics between these variables. Without the controller accounting for this relationship it becomes difficult to set one without affecting the other, therefore the importance of understanding Rentel-Gomez and Velez-Reyes (2001) decoupling techniques to achieve accurate controller is time well spent before starting the development of the automatic controls for the Chamber. Rentel-Gomez and Velez-Reyes (2001) goes on to demonstrate, through simulations in MatLab, how a decoupled controller is possible using a multivariable cascade control with two loops. The inner-loop is the non-interacting control law used for decoupling, and the outer-loop is a PD controller used for stabilization and control. One of the major drawbacks of Rentel-Gomez and Velez-Reyes (2001) work is that it has only been validated through computer simulations and has not been implemented or proven on a real working system. Even within some of the simulations, there were cases where the controller was not stable and was out of control. On a real system this could possibly cause damage to one of the components and if utilized will have to be protected against.

Bai, Wang et al.(2008) investigated how a Smith predictor-based self-tuning PI controller would work for controlling an air-conditioning system test room. This test room is very similar to the Psychrometric Chamber at OSU where there are two rooms appropriately called Indoor and Outdoor In these rooms the temperature and humidity is controlled, so HVAC equipment can be tested. A simple PID control was found not to be adequate enough for the test room. This was because of the large range of operating conditions and drastically different internal loads experienced in the testing room. Therefore, (Bai, Wang et al. 2008) proposed a more sophisticated control scheme. These schemes use the concept of a PID controller, where proportional, integral, and derivative gains manipulate the error of the set point to determine a new output signal. The difference is in a simple PID controller these gains remained constant, but in a Bai, Wang et al.(2008) controller these gains change as the system and conditions change. Empirical data were taken from the actual test room where a parameter estimation study was used to find an equation that describes how the proportional gain and time constant relate to the controller output. Also, with this empirical data, a time delay

range for the system was determined. A good controller adjusts the system to reach its desired set point quickly, but changing control inputs to the system too fast can cause the system to become unstable and possibly out of control. To optimize this time delay range a Smith Predictor was utilized in the control scheme. The Smith Predictor is a model of the system that predicts the system outcome due to the current inputs. The model output is compared with the actual system output/feedback allowing the controls to adjust the system inputs to insure accurate control. Not only does the Smith Predictor help optimize the time delay, allows error comparison of model output with the actual system output/feedback, along with the parameters found with the empirical data, but it also utilized the Integral of Time and Absolute Error (ITAE) tuning rules to adjust the proportional, integral, and divertive gains for the PID controller. This control scheme shows very promising results and usability for the OSU Psychometric Chamber, but there are some concerns with Bai, Wang et al.(2008) work. Bai, Wang et al.(2008) control scheme was simplified and was only developed for one output. In most air-conditioning systems, as well as the OSU Chamber, multiple outputs are needed to completely achieve the desired control. Also, the validation of the control scheme was only done through simulation using Simulink. It is hard to determine if the scheme is useful, when it has not been implemented or tested on actual systems. One positive finding is the simulation results demonstrated that the proposed scheme achieves better performance with respect to the common PID controller when taking into consideration the effects of set-point changes, parameter variations, or load disturbances in HVAC systems.

Qu and Zaheeruddin (2004) investigated two common adaptive control schemes. An adaptive control is where the controller's parameters change as the system changes. The two controls considered are, a first-order-plus-dead-time (FOPDT) with the H1 loop-shaping tuning rules and LQR optimal adaptive models, these models update the PID parameters/gains depending on the system operating conditions. Qu and Zaheeruddin (2004) explored and proved, through simulations, both models where able to track the desired set point changes very well. Many others have also proven this, but one difference in Qu and Zaheeruddin (2004) work is how disturbance in the system effected the control of the system. This is not only interesting to the psychrometric controls, but any HVAC control system. These

disturbances could be caused by chilled water temperature change, electric surges, fouling of heat exchanger, etc. One disturbance studied was the noise in the measurement for the feedback signal. To retrieve a feedback from a real system, some kind of sensor has to take measurement and output a signal. All signals have some kind of noise and how this noise affects the controller should be a concern. Qu and Zaheeruddin (2004) found the first-order-plus-dead-time (FOPDT) with the H1 loop-shaping tuning rules to be better at handling the presence of changes in parameters, disturbances and external noise acting on the system.

Wang, Cai et al.(2004) presents a technique for developing a simple and accurate Cooling Coil Unit model. Existing CCU models used for optimizing control strategies are normally complex or linear approximations that do not represent the real coil accurately. This was one problem experienced with trying to model the Psychometric Chamber, because of the cooling coils being one of the major components of the conditioning equipment. The Cooling Coils installed in the conditioning loops were custom-made for this chamber and there is not much manufactures or catalog performance data. Previous attempts at a detail model have shown inaccurate representation. If experimental data can be obtained and then a parameter estimation model constructed out of it, a more accurate control model of the psychometric chamber could be achieved. The modeling technique presented is based on an energy balance and heat transfer principles. Wang, Cai et al.(2004) actually breaks down the technique into three different models that can be chosen from, depending on the application and information available. The three techniques include a two parameter model, a two variable parameter model, and a three parameter model. All three techniques utilize the same equation (1) shown below.

$$Q = \frac{c_1 \dot{m}_{\mathrm{a}}^{e}}{1 + c_2 \left(\frac{\dot{m}_{\mathrm{a}}}{\dot{m}_{\mathrm{chw}}} \right)^{e}} \left(T_{\mathrm{a}} - T_{\mathrm{chw}} \right) \tag{1}$$

Where Q is heat transfer rate, $\dot{m}_a$ is mass flow rate of the air, $\dot{m}_{ch}$ mass flow rate of the chilled water, T_a is the entering air temperature, and T_{ch} is the entering chilled water temperature. The differences come into play with the initial assumption made before performing the parameter estimation. The two parameter model assume *e=0.8*. The variable two parameter model also assumes *e=0.8, but* breaks down the parameter estimation into multiple regions. By doing this, different parameters for each region can be found. Finally, in the three-parameter model *e* is not assumed and has to be estimated. A great attribute of Wang, Cai et al.(2004) work is all three modeling techniques where compared to experimental data. The comparison showed that all three methods give an excellent match to real performance over the entire operating range. Wang, Cai et al.(2004) even goes on to compared with existing methods in previous works and proves his method performed better over an entire operational range of coil. The sum of the errors from the model compared to the experimental data was less in Wang, Cai et al.(2004) model. This model is simple, easy to follow and could be useful in the development of the controls for the psychometric chamber.

Review of Pipe Insulation Test Apparatuses

Thermal performance of a wide range of pipe insulations is well known for hot pipe applications, where moisture regression is not a problem(Whitaker and Yarbrough 2002). Not only are these thermal performances well know, standards exist that specify how to test the pipe insulation and report it for "dry conditions" (no condensation) (ASTM 2003 (2006)). With cold pipes, there is insufficient thermal performance data in the range of conditions they operate in and a unified standard does not exist for testing cold pipes under wet conditions where moisture propagation can occur. The thermal performance of insulation differs in the presence of moisture and up until now the thermal performance found using the hot pipe operating conditions has been used to design and select insulation for cold pipe systems. The assumption that the insulation behavior does not change with the direction of heat transfer and presence of moisture has proven to give significant error in certain applications.

Recent works have begun to investigate the differences in thermal performance of pipe insulation on cold pipes. Wilkes, Desjarlais et al.(2002) at Oak Ridge National Lab developed a pipe insulation test

apparatus for use below room temperatures. The construction of the apparatus used an inch and three eights copper pipe to carry chilled water. The copper pipe was coated with Nextel paint with an emittance of 0.89. Three thermocouples were also attached to the copper surface before the coating was applied. The insulation to be tested was then applied around the copper pipe and on the outside of the test insulation a film heat was attached. Between the film heater and test insulation five thermocouples here inserted. On the outside of the film heater, more insulation was applied. This was not the insulation being test but applied to control the heat transfer. Finally, the outer most layer of the apparatus is what is called thermal guard. The thermal guard is pipe shaped slab of small tubes carrying a temperature-controlled fluid. By controlling, the temperature of the fluid flowing through the small tube allows the outer most layer to match the surface of the film heater. If temperature differences are absent between the two surfaces then it can be guaranteed that the heat transfer from the heater flows towards the chilled water. The total length of the apparatus is 60 inches (1.52m) and the heater power was measured using a calibrate voltmeter and a precision resistor placed in series with the heater. Some of the details of the construction are troublesome. One concern is that only a total of eight thermocouples were used through all of the layers in the apparatus. It is hard to believe that the temperature distribution was uniform with chilled water. It could be possible if the flow rate was high and the power from the heat was relatively low, but with the number of thermocouples available in the apparatus, it is significant to assess that uniform temperature exists within the test apparatus. Another concern with the setup is the use of Nextel paint. It is stated in the paper that the paint produces a better temperature distribution along the copper and eventually produces a better conductivity for the test insulation. The reasoning for the use of the paint is not clearly explained and definitely not validated. The apparatus was used to test three commonly used cold pipe insulation materials, where two of those materials have already been tested using ASTM Standards and where thermal performance for hot pipes is well known. The results for this new apparatus was compared to the known thermal performances and proved the apparatus has risible accuracy. The thermal performances produced by the test apparatus for all cases show a slightly low conductivity compared to the ASTM Standards. This could be a result of a systematic error from the test apparatus or a

physical property of heat transfer for pipe compared to flat slab; which was done for the results presented in ASTM Standard.

Work investigating the amount of moisture absorption with respect to time has also been recently done. Mumaw (2002) tested eight types of commonly used cold pipe insulations to see the amount of moisture that different insulations would absorb with time. A three month test used a controlled environment at an extreme condition to accelerate the moisture propagation and found that different materials have different absorption rates. The environment conditions were 90°F (32.2°C) at 90% RH. To maintain a constant temperature on the surface of the pipe that the insulation covers, chilled water at 35°F (1.6°C) is circulated through a tube in tube heat exchanger with an outside diameter of 1inch (25.4 mm). Both the inlet and outlet of the chilled water are on the same side allowing the chilled water to double back on itself. This allows for the pipe to have a more uniform temperature. This also allowed the insulation to be slid off one end quickly and easily because every seven days the insulation was removed and weighed to see how much water was absorbed. It was also found that cellular glass had no measurable moister gain over the testing period. It was found that if a vapor retard and PVC jacket is used on mineral fiber insulation that no measurable moister was gained. The result of the cellular glass is interesting to this project because this type of insulation is being used on the Pipe Insulation Test (PIT) apparatus to create an adiabatic boundary. Knowing that the cellular glass does not absorb moister is key to the construction of the PIT because it will be exposed to these same extreme conditions. If moisture were to propagate into the cellular glass then the adiabatic boundary assumption might become invalid.

Most work found has been done on small diameter pipe, less than 2 inches (50.8 mm). The assumption and effect on a small pipe relative to a large pipe should translate, but it is possible that some differences could accrue. Kimball (1974) investigate the thermal conductance of pipe insulation on a large scale. This large scale was a steel pipe 18 inches (457.2 mm) in diameter, that was 20 foot (6.1 m) long. The pipe was capped at both ends and filled with water where heaters were able to control the temperature of the water. The pipe was wrapped with the test insulation and placed into a chamber roughly eight feet high by eight feet wide by twenty nine feet long (2.4 m x 2.4 m x 8.34 m),

which was cooled using the expansion of liquid nitrogen. The pipe was heated to 160°F (71.1°C) and the chamber was cooled to -70°F (-56.6°C). This experiment looked at the heat transfer when the pipe was warmer than ambient and no moister was present. This is not directly related to the current project, but this work proves that the scale or size of the pipe should not affect the results for the insulation conductivity. The insulation conductivity matched well with the data collected with the same insulation on smaller pipes. The uncertainty of the experiment was stated to be plus or minus 4%, which was possible because of the large temperature difference between the pipe and ambient temperatures.

Not only has work been done were experiments were performed to find how moisture effects on the insulation, some modeling has been done to predict how it will change when experimental data is not available. Wijeysundera, Zheng et al.(1993) developed an analytical model that predicts the heat and vapor transfer in thermal insulation. It was found that the thermal conductivity of insulation with moisture present is dependent on seven variables. In this work a parametric study was performed to investigate the effects of these seven variables. The model predicts that the conductivity of the insulation could vary from about 1.5 to 15 times the dry-state value. Some observations that can be useful from this work are the trends the model predicts.

CHAPTER III

OBJECTIVE

The overall purpose of the work presented in this thesis was to complete the construction of a new psychrometric chamber at OSU and demonstrate that the chamber is capable of performing accurate and precise experiments on thermal systems. The experiments included ones with and without a live thermal load. Completion of the chamber involved the development and fabrication of the control system. The control system included both the hardware and software needed to adjust and maintain the conditions in both the indoor and outdoor rooms. The specific objectives of this thesis are to (1) develop and fabricate the control system for the chamber (2) design and construct the experimental setup needed to test HVAC rooftop units (3) design and construct test apparatus to measure the thermal conductivity of pipe insulation systems (4) run the chamber in order to produce conditions needed to perform the previous two experiments.

The outline of this thesis is meant to follow a style that it would be referred to as guidelines, which will give future chamber users insights into how the chamber operates and should be ran. The control system is a dynamic work and will continually be expanded, modified, and adjusted to meet the requirements of the experiments being performed inside the chamber. The two experiments presented here are referred to as proof of the chamber's capabilities as well as first examples and potential starting points for future experiments.

In my opinion, the chamber should be viewed as a tool and permanent structure. Any contributing aspect to the chamber's design, fabrication, and use should be done in a professional manner with the future expansion, experiments, and users kept in mind. The development of the controls as well as any

other work contributing or related to this thesis was approached with this idea in mind. The hope is that this idea will be carried throughout the evolution of the chamber in the future.

The design and construction of OSU Psychrometric Chamber was a collaborative effort among several students, faculties, staff, University research sponsors, and OSU Physical Plant. The work presented in this thesis is the result of this large collaboration. The following tasks emphasize my own contributions and my own tasks performed during the final stage of the construction of the chamber:

1. I installed the Heater Control Hardware
2. I mounted the Pump Flow Switch Hardware
3. I designed, constructed, and calibrated the Pipe Insulation Testing Apparatus Refrigeration Loop
4. I re-organized, cleaned, and structured the LabView Control Program and I designed specific control subroutines to operate the chamber safely
5. I developed the LabView Recording Program
6. I investigated and tuned the Chamber PID Control parameters and set up procedures to assist finding the PID parameters for cases other than the ones I specifically tested in the chamber
7. I developed an uncertainty analysis for both experimental work I conducted in the chamber: (1) the rating performance of an 11-tons rooftop unit at design, off-design, and transient conditions, and (2) the measurement of pipe insulation systems thermal conductivity at below-ambient temperatur

CHAPTER IV

METHODOLOGY

Controls of the OSU Psychrometric Chamber

The chamber currently has 384 sensor locations available that can used to determine the response, behavior, and adjustments needed to maintain the facility at the set points as well as monitor the experiments in the facility. Sensors currently include 256 thermocouples, 32 high accuracy RTDs, 4 relative humidity probes, 8 differential air pressure transducers, 1 barometer, 2 watt transducers and 81 analog inputs. The adjustments are done automatically using 192 analog outputs that control different components within the conditioning loops. The conditioning loops control the psychrometric state of each room and Figure 1 points out a few key features.

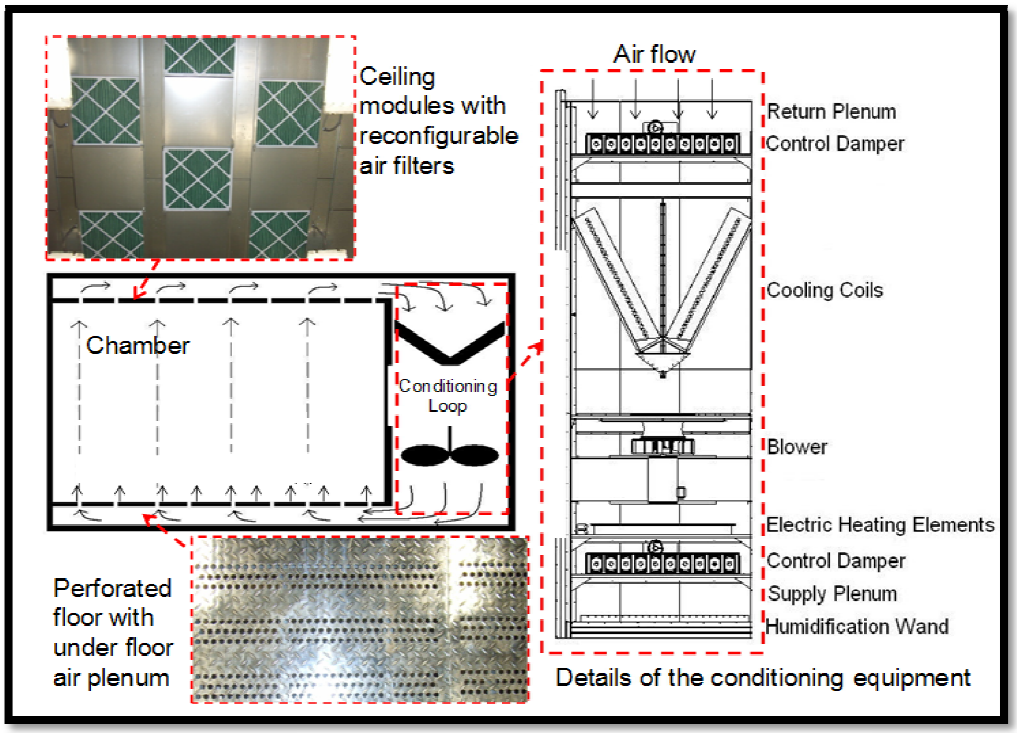

Figure 1: View of psychrometric chamber with details of the ceiling with reconfigurable air filters, of the perforated floor with under floor air plenum, and of the chamber conditioning loop

Air is circulated though the conditioning loop using variable speed fans. The airflow rate can be adjusted and electro-mechanical dampers can be altered for controlling the distribution of the air to and from the under floor air plenum and ceiling return plenum. Utilizing an under floor air plenum and a ceiling return allows uniform conditions to be obtained throughout the entire room. Some initial testing of the temperature distribution was performed by moving a sampling probe to different location in the room. The probe was installed at about 3 feet above the floor at each location. In these tests, only one conditioning loop was used to condition the room. This replicates the worst case where one conditioning loop would be performing a defrost cycle. An example of this type of test is shown in Figure 2. Other examples can be seen in the appendix (D).

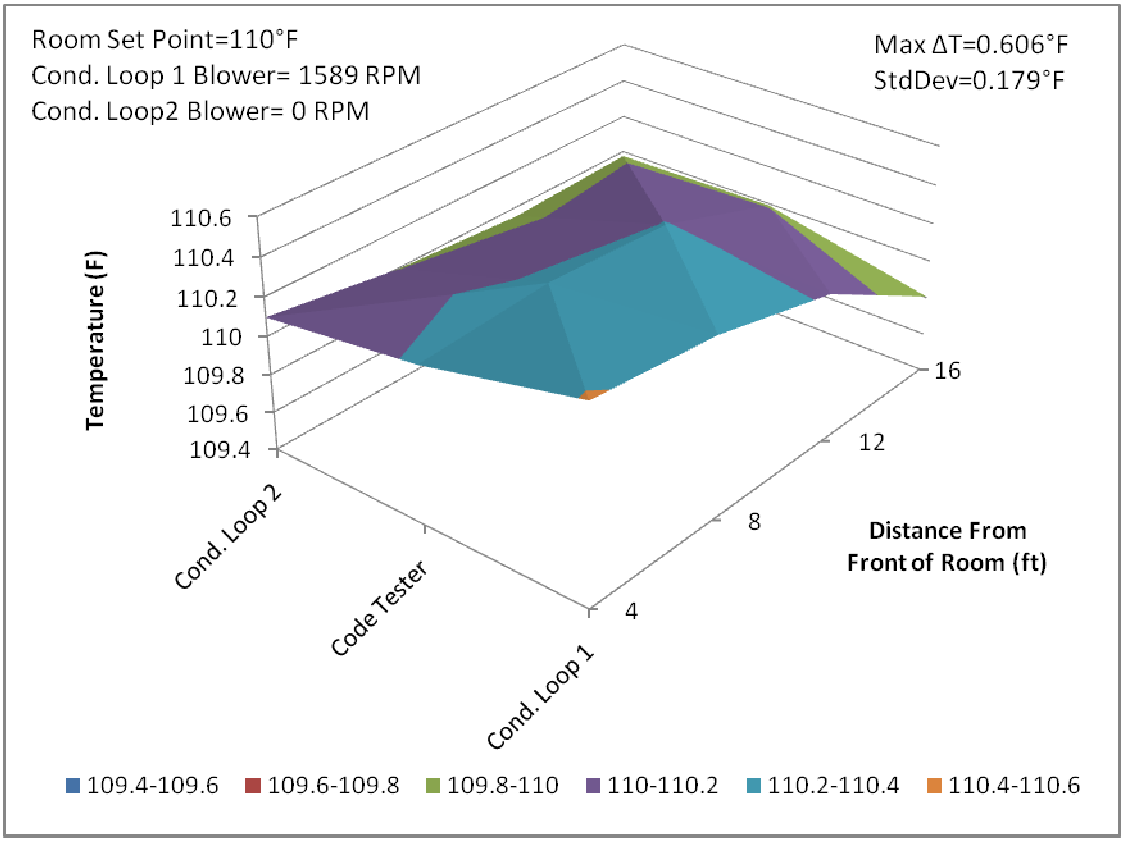

Figure 2 Air Temperature Distribution throughout the Outdoor Room of the chamber.

Figure 2 shows that at high blower speeds the temperature distribution in the room is within 0.6°F. However, it was found that as the blower speed is decreased the temperature distribution can reach up to 4.1 °F in difference between the two corners of the room. Future work should be done to improve

the air distribution for all blower speeds. The first process the air encounters inside the conditioning loops is being cooled and dehumidified by a set of cooling coils. The coils surface temperature and capacity are controlled by variable speed pumps, electronic mixing valves and electro-mechanical bypass valves. These parameters are adjusted so that the air is cooled and dehumidified below the desired room psychrometric state. After being cooled and dehumidified, the air passes over electric resistance heating coils, which raise the air temperature up to the desired room temperature. The electric resistance heaters allow for precise temperature control with an almost immediate response time. Rapid fine-tuning is performed accounting for variation in the chamber response to a live load; that is, to any variation of the load of the unitary equipment running inside the facility during the test. The power to these heaters is controlled by a PID control algorithm referencing the room dry bulb temperature. After passing over the electric heaters, air is passed over a steam wand where moisture is added to the air, raising the humidity to the desired state. The wand is connected to a steam generator that is also controlled by a PID control algorithm referencing the room wet blub temperature. The generator is capable of adding precise amounts of water vapor to the air. The control strategy is constructed so the cooling coils, having a large thermal inertia, are slowly changed while the heaters and steam generator are quickly adjusted to maintain desired conditions using the two PID algorithms working in parallel.

Labview Program

The control programming was done with LabView Real Time Software operating on a National Instruments PXI controller. The PXI performs all computations essential to operate the chamber, while a host computer is used as a graphical user interface, display, and plotting of the readings from the sensors. The Real Time software allows for data acquisition (DAQ) and processing as fast as 1 millisecond of sampling rate, while the Lab View is used for programming and tuning of the controls. Both the interface and control programming was designed and built in house to accommodate the chamber's unique features. The user interface incorporates graphical representation of the conditioning loops that illustrates sensors in their physical locations. Figure 3 illustrates the LabView interface for the outdoor room. This allows the user to quickly identify each sensor and help the user

to visualize the process involved in the controls of the conditioning loops. Due to the fact that there are two almost identical rooms, each room has its own graphical display. The interface also allows the user to interact with the facility in real time. The user can choose to operate the chamber in manual or automatic mode. In manual mode, the user is capable of controlling each component independently, while in automatic mode the chamber adjusts the components to maintain a user defined temperature and humidity. The process control program is also capable of a combination of both manual and automatic controls.

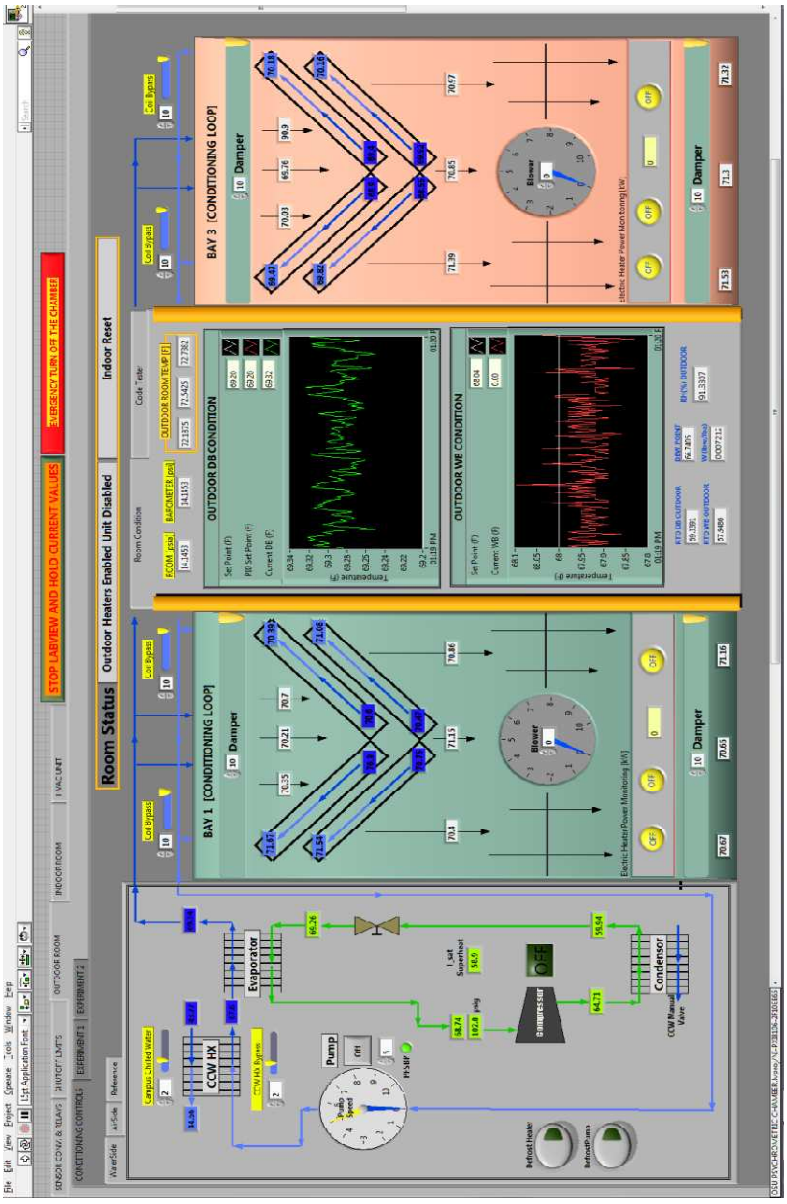

Figure 3 LabView Interface for the Outdoor Room

Safety Additions

When operated in automatic mode the user defines the desired dry and wet bulb temperatures and the chamber begins the process of obtaining and maintaining those conditions. The chamber has a large amount of thermal energy available to allow for rapid adjustments to internal loads, but rapid temperature changes in the chamber is normally not needed. When changing set points from a low temperature to a high temperature rapidly adds stress and ware to the equipment as well as causes instability to the controls. Therefore, in cases where rapid temperature adjustments are not needed it is ideal for the temperatures to be adjusted slowly from one extreme to the other, which could be done by the user. To help the user a Temperature Step Function was incorporated into the LabView program, which allows the user to define large set point changes, but the controls will slowly adjusts the conditions to match what the user wants. The temperature step function takes any set point changes larger than 2°F (1.1°C) and steps it in increments of 2°F (1.1°C) while waiting at each incremental change one minute to insure stable control. For example, if the user defined a set point change from 60°F (15.6°C) to 100°F (37.8°C) the controls would adjusts the set point from 60°F (15.6°C) to 62°F (16.7°C) and wait until the chamber reached 62°F (16.7°C) then wait an additional one minute. Next, it would adjust the set point from 62°F (16.7°C) to 64°F (17.8°C) and wait until the chamber reached 64°F (17.8°C) then wait an additional one minute. This would go on until the chamber reached the 100°F (37.8°C) defined by the user.

One of the fastest possible ways damage can accrue to the chamber is to operating the heater with little or no airflow. A secondary mechanical flow switch insures that the heater cannot operate at zero airflow rate but does not determine and insure the enough flow is present. To protect the heaters and reduce unnecessary ware, a LabView code was added to maintain sufficient airflow across the heating coils at any heater power despite the users specification. A correlation between heater power and airflow rate was developed and applied so at any time a minimum flow rate is maintain at a particular heater power. For example, if the heater power is 40 kw then the blower speed must be greater than or equal to 1250 RPM. If the user is calling for 1200 RPM the controls automatically adjust the speed to

1250 rpm, but if the user is calling for 1300 rpm then no adjustment is needed. Figure 4 shows the LabView interface when the blower speed/air flow rate is over taken by the LabView controls.

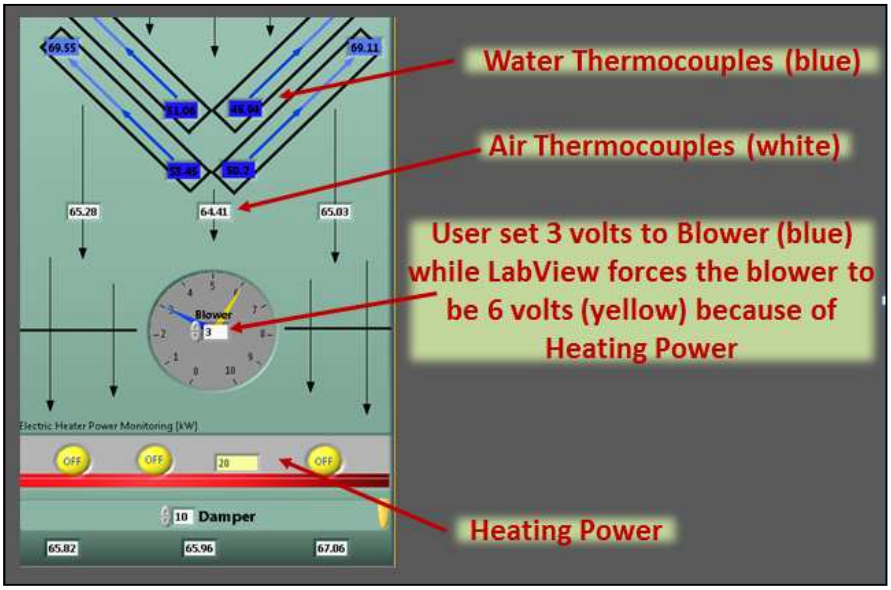

Figure 4 LabView Fan Speed Control

Beside user interface, the process control program is also equipped with safety control shutoff limits. These are the first preventive measures from potentially dangerous situations. The chamber will shut down by itself in a controlled and safe manner when potentially dangerous scenarios are estimated. The user can input the tolerance for the severity of the potential risk when drifting away from the specified test conditions during the experiments. This is accomplished by adjusting the parameters such as high and low temperatures of the room and conditioning loops, refrigerant high and low pressures, unit power consumption, as well as high and low room humidity limits.

New Experiments and Recording Data

Along with the controls part of the LabView, it was also developed to interact with the experiments being conducted inside the chamber. The host computer houses LabView code developed to easily add additional graphical displays to the interface to meet any unique requirements of experiment and/or taste of the user. The user can pull any data from the main data stream, which is assigned an index number, and manipulate, calculate, convert, etc. without affecting the control part of the

LabView program. The corresponding index number as well as other information for each channel/signal is documented in a Microsoft Excel database and is maintained and updated continuously. A key aspect of every experiment conducted in the chamber will be the need to recorded data so they can be analyzed. With the chamber, being cable of performing multiple experiments at once a recording program was added to the LabView. This recording program allows up to six recording to be simultaneously collected for any or all input and/or output signals occurring inside the chamber at sampling rates as fast as one millisecond. One can see that the data file could grow quite large as there are over five hundred input and output signals accruing in the chamber at any given time with room for further expansion. Therefore, to help with data analysis the chamber output and input signals where sub categorized to allow the user to reduce the amount of data recorded in their file. These six sub categories are called outdoor, indoor, DAQ Box #4, DAQ Box #5, DAQ Box #6, and DAQ Box #7. The user is able to chooses the sub categories desire and any signal being sent to or from the chosen selection will be recorded into a Tab delimited text tile. Figure 5 shows the chamber layout with respect to the DAQ Boxes, where Indoor and Outdoor sub categories are a combination of DAQ Boxes #1, 3 and 2, 3. DAQ box #3 holds signals both for the indoor and outdoor rooms.

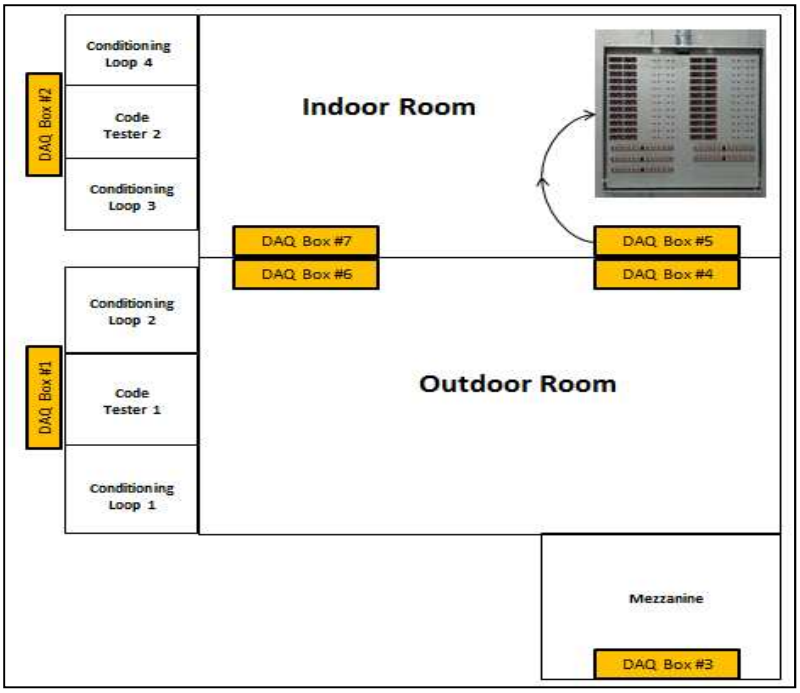

Figure 5 Layout for DAQ Boxes inside the Chamber

DAQ Boxes #1 ,2, and 3 located on top of the chamber and are utilized for more permanent instrumentation connection where the other boxes are located inside the chamber and allow for quick and easy experimental setup and the instrumentation connected to these boxes will be dependent on experimental be conducted. The use of speaker connectors and terminal strips in the boxes allows for this user-friendly experimental setup and are shown Figure 5. Once the chosen data is selected to be record, the user is prompted to answer a few questions before the recording program physical records data to a file. These questions include: what is desired file name and location, desired sampling rate, if the recording has specified duration and how long is that duration. Figure 6 show the interface the user encounters when recording data inside the chamber. The recording can be stop at any time by the user or it will stop automatically if duration time is specified and then file can be transfer and/or open to begin the needed data analysis.

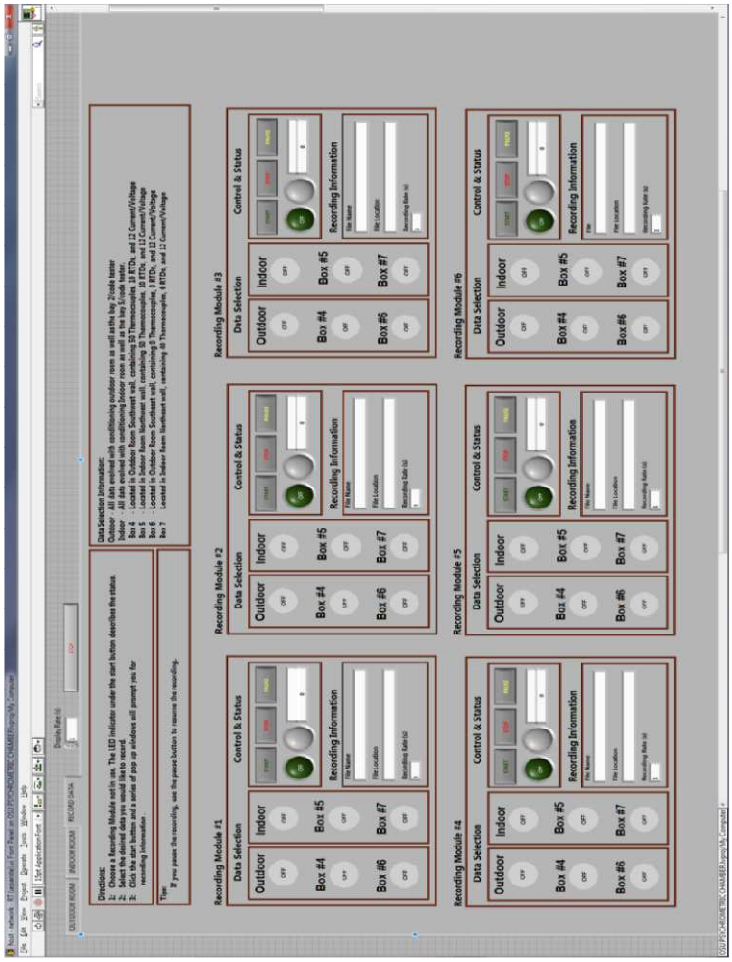

Figure 6 LabView Data Recording Interface

Code Usability/Readability

Both the LabVIEW Interface and the actual Labview code were developed with a user friendly perspective in my mind. Future user of this software will need to understand the program and its logic, and to achieve this understanding easily a clean, clear, and well-organized Labviewcode is necessary. A clean code also helps the user with further modifications , debugging, and future expansion of the code. LabVIEW is a graphical programing language that uses icons and wires to represent function and variables. Because of this graphical programming language and the need for clean code, care was taken to minimize the crossing of wires, aligning of icons, commenting of processes, as well as constructing the code in a modular fashion. The modular coding helps with organization as well as understanding of the code's logic. This modular code design is made up of sub routines called sub virtual instruments (Sub-VIs), which are called in a main program (main VI). This

allows all Sub-VIs to be and should be individually tested and debugged before being added to the Main-VI. This insures the Sub-VI is executing properly for all foreseen circumstances/cases before coupling it with main VI that controls an expensive and potential dangerous piece of mechanical equipment (Chamber). Figure 7 shows a small section of code that demonstrates the readability of the Chamber LabVIEW code, where the complete code can be found in the Appendix A.

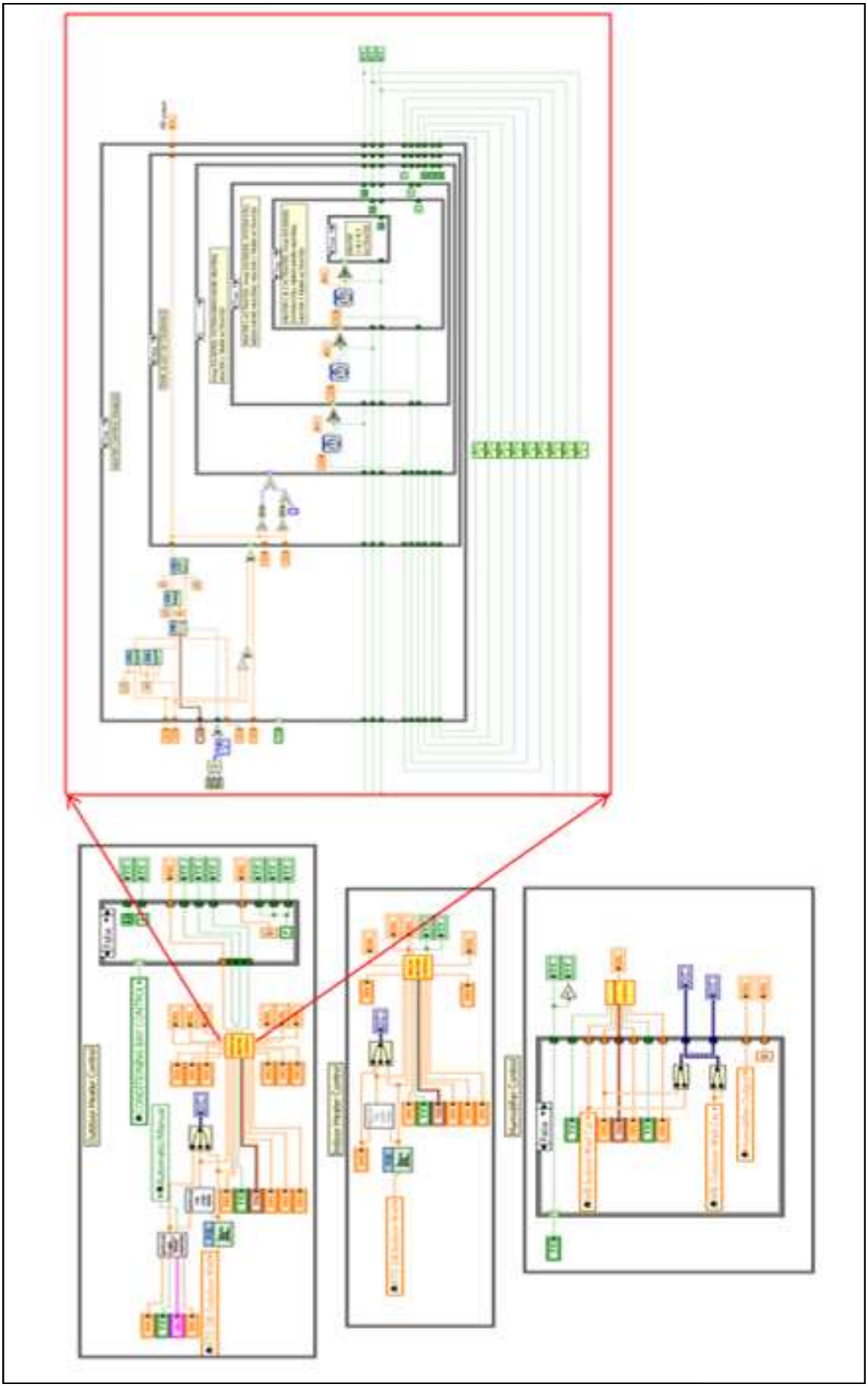

lular Layout.

Additional Chamber Control Information

Heater Control Scheme

Multiple heaters are available in the air stream of each conditioning loop and all of them are controlled by one PID control Signal. A LabView program was developed to transfer this single PID control signal into multiple, needed to control each heater individually. Each heater is approximately 20 kW where the outdoor loops are composed of four heaters having a heating power of 80 kW and the indoor loops are composed of two heaters having a heating power of 40 kW composed of two heaters. One heater in each loop is proportionally controlled while the remaining heaters are on/off control. Utilizing this setup allows for any incremental heating power needed, up to the maximum available, to be achievable. The proportional heater ramps up and down between the incremental steps of the on/off heaters. For example, when the capacity needed is 30 kW then one on/off heater will be on at 20 kW and the proportional heater will be supplying 10 kW. When the capacity reaches 40 kW then the proportional heater goes to zero and two on/off heaters will be on at 20 kW each. This configuration is for each conditioning loop and each room has two loops. Figure 8 shows the heater control box where the proportional controller and contactors are located.

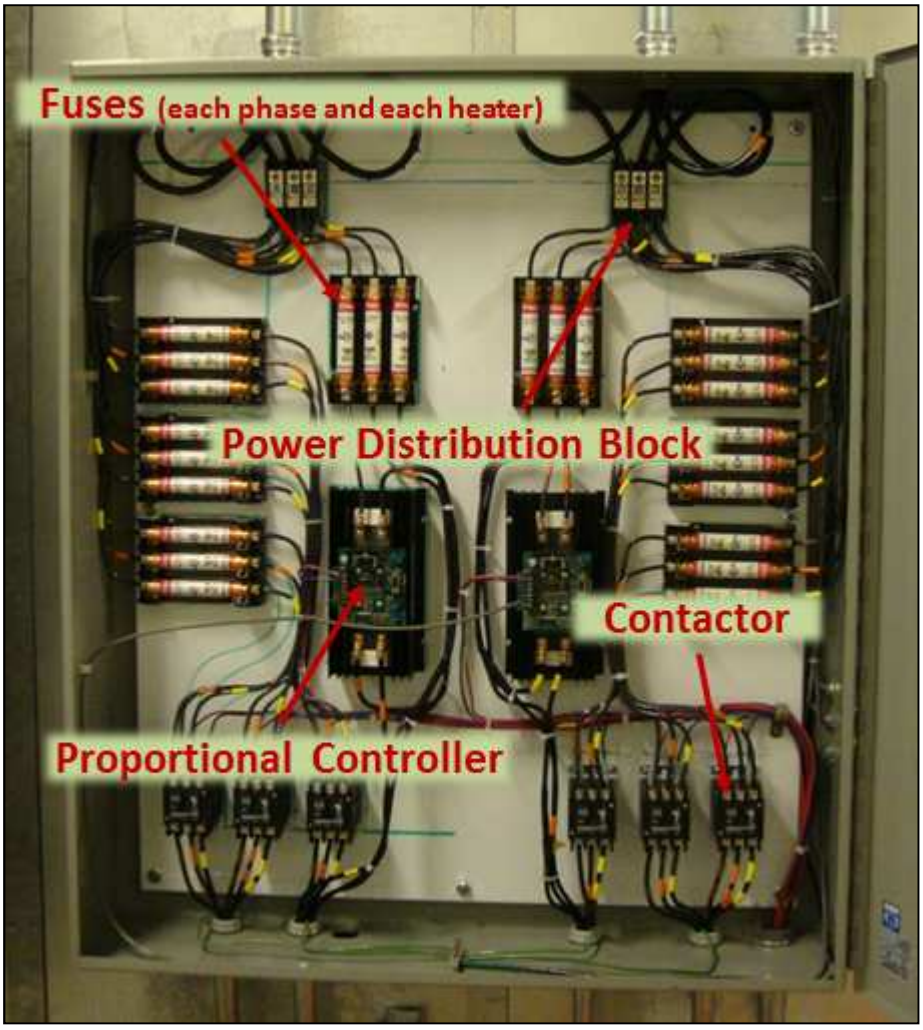

Figure 8 Chamber Heater Control Box

Not only does the chamber have a non-trivial way of utilizing a single PID control signal on numerous heaters, but also its electrical circuitry that physical turns on and off the heaters is also non-trivial. The heaters control signals are set up in double cascading configuration because the contactors and proportional controllers that regulate the power to each heater need a 24 VAC switching source, yet the National Interments DAQ hardware can only supply up to 10 VDC. Therefore, a solid-state relay (SSR) was introduced to convert the LabView signal to a 24 VAC signal. The 10 VDC signal form the hardware/LabView is sent to the SSR with switches the 24 VAC, which in turn switch the contactors and proportional controllers to power the heaters. Figure 9 shows the electrical circuitry involved with turn on and off the heater as well as how the safety switches are incorporated.

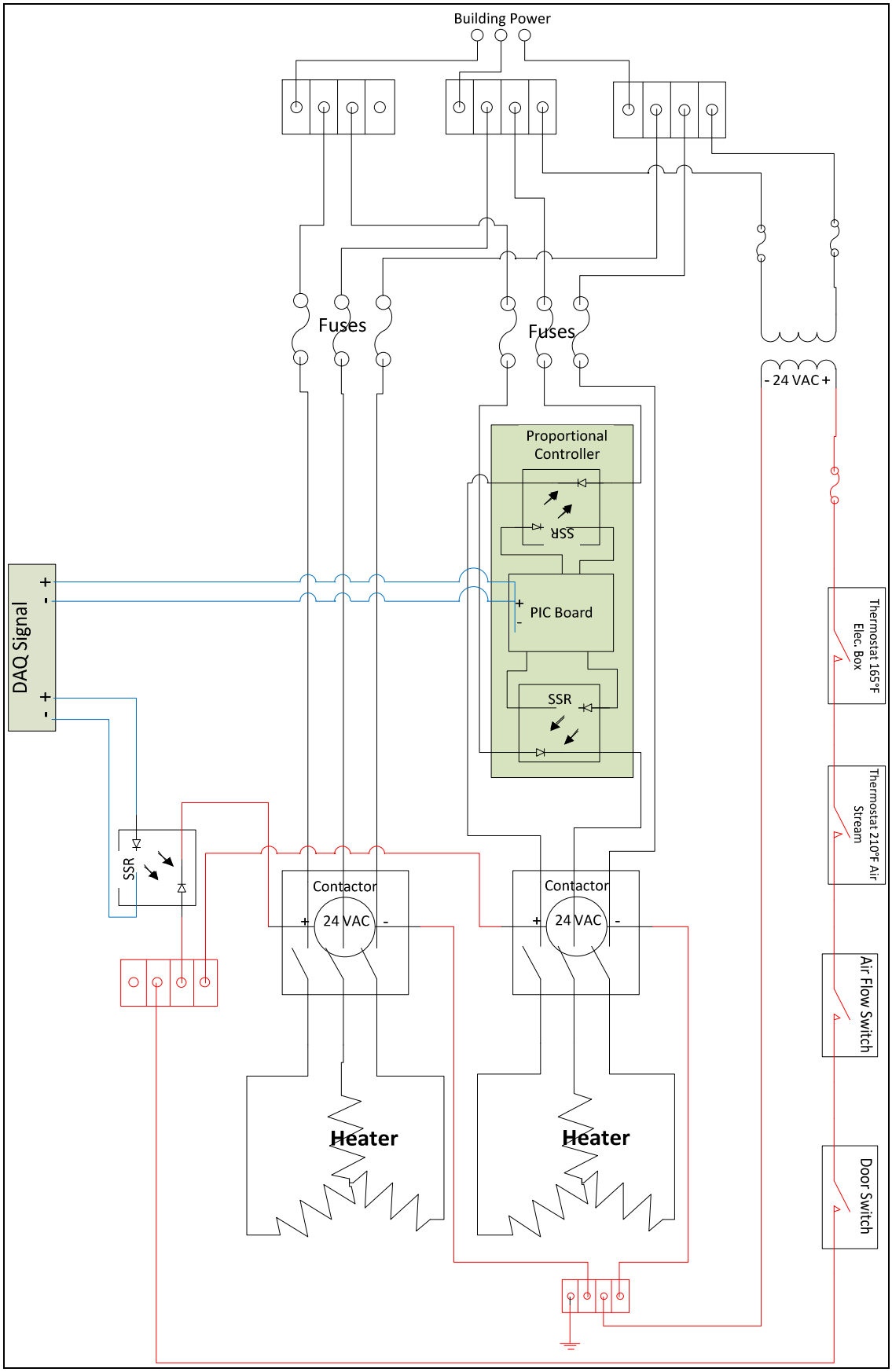

Figure 9 Wiring Diagram for Heater Control

The double cascading control signal loop was used to lower the cost of installation compared to price of using a device cable of switching the larger amount of power needed for the heater with a small 10 VDC signal. In addition, by using the cascaded control loop a secondary safety switches were easy implemented in case of software malfunction. These will shutdown the heater when there a potential danger is present such as fire, electrical shock, etc. These secondary safety switches include air stream thermostat, electrical junction thermostat, airflow switch, and conditioning loop door switch.

Pump flow switch bypass

A secondary safety switch was also implemented on the each room's chilled water pump. This safety was mainly designed to protect the pump from damage if no water flow is present. No water flow can be a caused by numerous scenarios, dry pump (piping system leak), blockage (PFHX clogged, wrong valve configuration, frozen water in pipe), damage pump or electric motor, etc. and in all, shutting down the pump can minimize the damage. The implantation consisted of a flow switches installed in the hydroinc loops to detect water flow. This flow switches were wired to the VFDs powering the pumps, which have internal contactors. The contactors need a 24VAC signals to maintain power to the pumps. The VFDs also have a 24 VAC power source, which is wire through the flow switches, and then back to the VFD. (Note: From the factory the 24 VAC power source is jumpered to the contactor simulate a flow switch that is continuous on.) This creates the scenario that if the flow switch detects no flow, no 24VAC signal will be present on the VFD; therefore, no power will be available at the pump. A problem arises when the pump needs to be turn on. With this setup no power is available at the pump when no flow is present, yet flow cannot be present unless the power is available at the pump. To correct the scenario a pump flow switch bypass was implemented. This bypass is an electrical circuitry bypass (jumper) simulating flow is present even when the pump is off. Once the pump is power on and flow is present the bypass can be turned off and the flow switch operates as previously stated. Another scenario arises now with the bypass set up. If the bypass never gets turned off and no flow is present, the VFD would still allow power to the pump and potential damage could occur. Therefore, a timer was added, so the bypass is only allowed to be on for 20

seconds, eliminating the potential of being left on. The bypass switch is a SSR controlled by LabVeiw where code was implemented to activate the bypass when the user starts the pump. The code starts a timer at the same time and turns off the bypass after 20 seconds. Twenty seconds is used to allow the hydronic loop time to stabilize and the potential for damage is small in 20 seconds. The pump flow switch bypass electrical circuitry is much the same as the heater control circuitry because the VFDs need to a 24VAC signal to activate the contactors (power). The SSR coverts the 10 VDC from the IN hardware to 24VAC. Figure 10 show the pump bypass box, which houses a SSR for each pump (room).

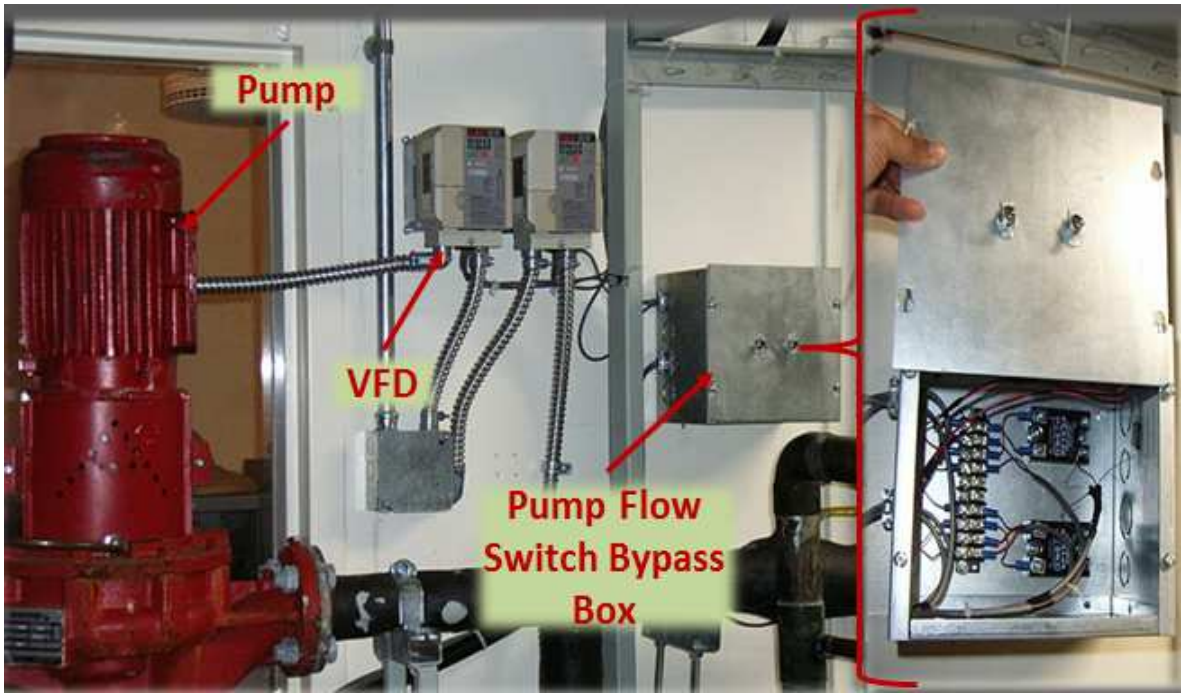

Figure 10 Pump Flow Switch Box

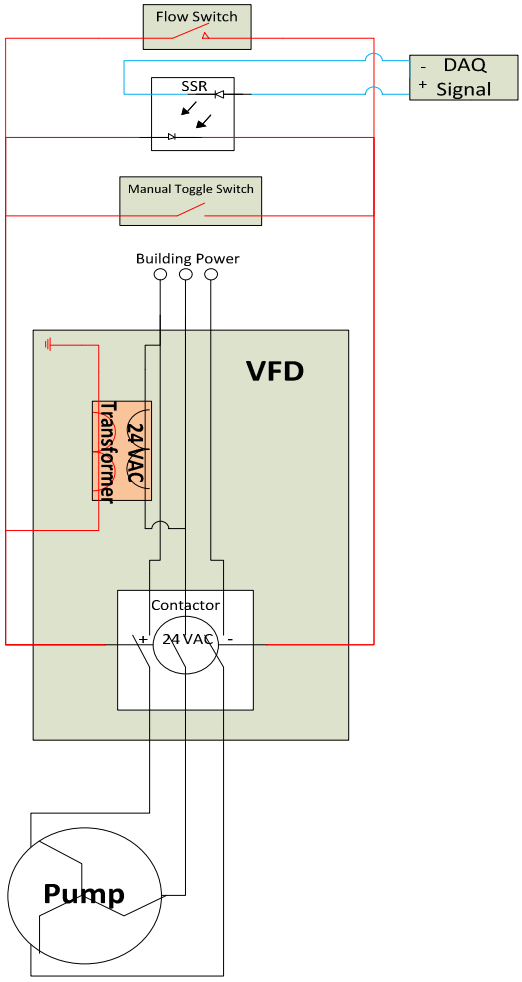

Figure 11 Pump Flow Switch Bypass Wiring Diagram

Determining the PID Gains

Determining the gains for a PID algorithm can be achieved in numerous ways. This is called tuning of the PID and in many peoples' eyes is considered an art. This is because the more experience and interaction one has with the system being controlled, drastically helps with achieving accurate and precise control. The user of the OSU Chamber may potentially need to tune these PID gains for different scenarios, conditions, and experiments. To help inexperienced users, a mathematical method was explored, so they could have a starting point. Numerous different mathematical methods have been developed and generalized for PID tuning. The Ziegler and Nichols' heuristic method was preliminarily tested on the OSU pychrometric chamber and was found to work well. The Ziegler and Nichols' method was used to find gains, which would achieve reasonably good control of

approximately ±2.5 ° F (±1.25 ° C), from the desired set point. Once this was achieved, the gains were tweaked to obtain the desired control with less than ±0.5°F (±.25°C) from the desired set point. This tuning of the gains was purely done with the knowledge gained from experience as well as trial and error. This process of using the Ziegler and Nichols' method to find the gains and then tweaking them to achieve better control was repeated for each condition needed for each experiment. The conditions were not limited to the chamber temperature, the water temperatures, airflow rates and conditions surrounding the chamber also effect the gains. It was found that at times the same gains could be utilized if the differences between conditions were not drastically different and minor tuning to those gains would allow for the desired control. The key to success when tuning the PID gains is the user needs to have extensive knowledge in how the software uses the gains and feedback signal to manipulate the output. For the OSU pychrometric chamber, PID algorithms available in LabView were utilized. The complete documentation for the algorithms are available from National Instruments in the PID Control Toolkit User Manual. It should be noted that all PID algorithms utilize the same basic concept, but different softwares sometimes use slightly different variations. The following is a description of how the Ziegler and Nichols' method explicitly pertaining to the OSU Chamber was used to determine the initial PID gains.

Both the derivative and integral time gains were set to zero, then slowly the proportional gain was increased until the process variable (PV) began a slight oscillation. The proportional gain that causes this slight oscillation is defined as the ultimate proportional gain (K_c), while the PV is either the dry or wet blub temperature (depends on which PID algorithm is being tuned). Once this was achieved the period between oscillations (T_u) in minutes was found. Once the K_c and $T_u$were found, the Ziegler and Nichols' equations were applied. The equations are summarized in the Table 1 below:

Table 1 Ziegler and Nichols Method for Tuning PID Gains

Controller	P gain	I gain	D gain
P	2.00 K_c/PB	0	0
PI	2.22 K_c/PB	0.83 T_u	0
PID	1.67 K_c/PB	0.50 T_u	0.125 T_u

The proportional band (PB) is the range, which the process variable (PV) can achieve. The PB is hard coded in the Chamber LabVeiw Program as 175. The 175 comes from the outdoor room dry bulb temperature that is designed to go from -40°F to 135°F giving a PB of 175°F. All PID proportional bands are defined as 175 in an effort to allow for gains that worked in one room to be translated into the other room experiencing the same conditions. It was found from experience that a good initial guess for the ultimate proportional gain is twice the PB, equaling 350. It was also found at the time of drafting this thesis, that PI controller worked better than PID controller. When the derivative gain was added, periodic instability was experienced. This was thought to be due to the noise occasionally experienced by the temperature readings. To utilize the derivative gain some signal processing/filtering needs to be developed to keep a stable control at all times. Since the PI controller achieved the needed control, it was unnecessary at the current time to add the derivative control.

CHAPTER V

CASE STUDIES AND EXPERIMENTS CONDUCTED IN THE OSU PSYCHROMETERIC CHAMBER

Testing for Performance Rating of Unitary Rooftop Units

Experimental Setup

For critical investigation of the comprehensive performance-rating figure of merit for unitary equipment, a set of sensors, probes, and flow nozzles were custom-made and installed in the facility. These measuring devices were in compliance with ANSI/ASHRAE Standard 116 (1995) and exceed the recommended accuracy tolerances. Figure 12 shows the locations of these measuring devices.

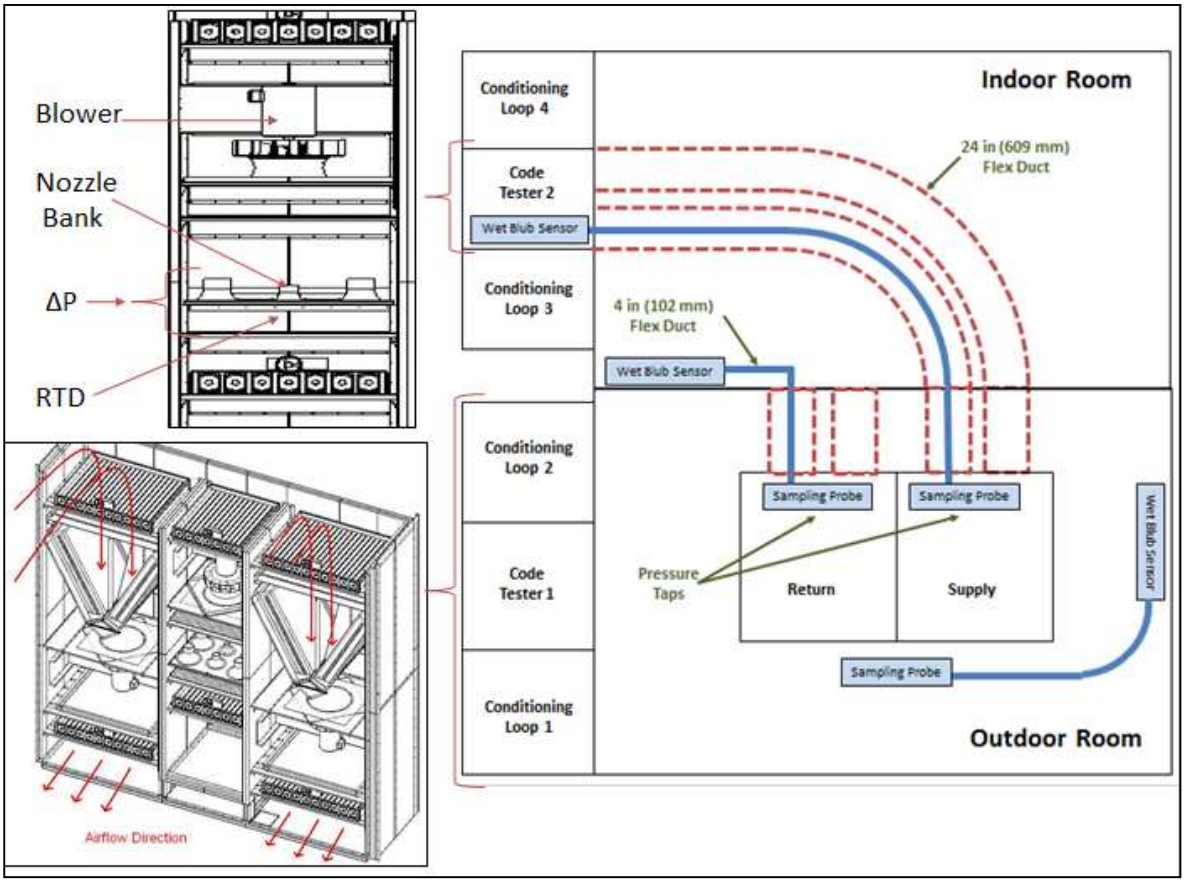

Figure 12 Experimental layout for testing a rooftop unit

The humidity, air temperature, and pressures are measured directly at the unit supply and return locations. This is achieved with sampling probes and pressure taps secured immediately at the beginning of the duct system that connects the unit to the indoor room. With this configuration, the pressure drop and heat transfer through the ducting system resulted to be negligible during the performance measurements. The sampling probes are designed to mechanically average the air in the duct. This is achieved by probing small samples of air at different locations in the duct cross section and mixing all the samples into one air stream. This mixed air stream is then transferred to remote wet bulb probes, which are in a fixed position and are connected to the sampling probe by using flexible air ducts. Having the wet bulb probes in a fixed remote position helped prevent any damage and inconsistencies during setup of the instrumentation for the unit; thus improving the repeatability of the measurements. Another added benefit to having this setup is that the sampling probes are capable of being easily moved and modified depending on what equipment is going to be tested. Therefore, allowing for quicker setup time. Along with the unit supply and return states being measured with a wet bulb and sampling probe setup, the outdoor conditions are measured using the same probe design, where the sampling probe is located at the condenser air intake.

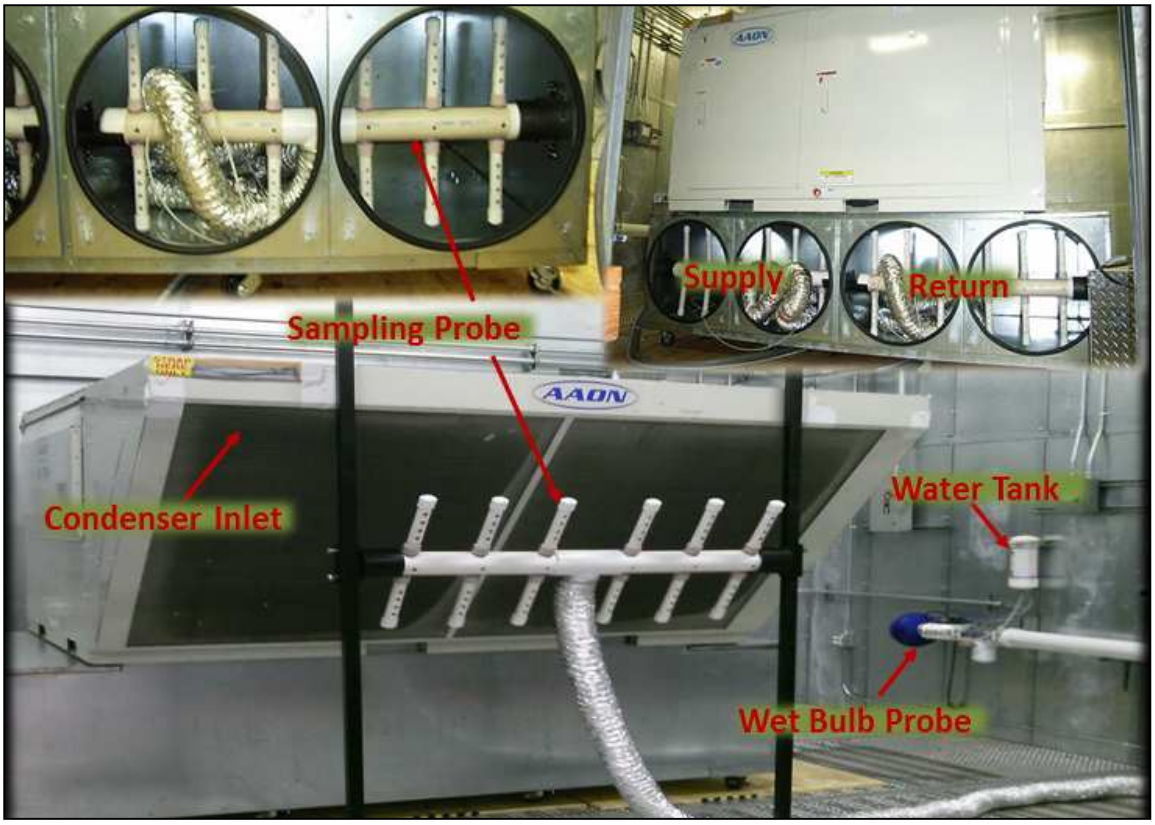

Figure 13 Sampling Probe and Wet Bulb Probe Setup

Before the air, which is conditioned by the unit, is supplied to the indoor space, it passes through an area of the chamber referred throughout this thesis as the "code tester". The code tester is a built in flow nozzle bench. A set of flow nozzles are activated to measure different airflow rates by simply plugging certain flow nozzles to form the best configuration for the airflow measurements. Recommendations for the best nozzle configuration for the range of flow rates can be found in the appendix. The pressure drop across the flow nozzles is directly measured to determine the airflow rate. Also inside the code tester, the air temperature and static pressure are measured so the density of the air can be calculated. Knowing the actual density of the air allows very accurate estimation of the airflow rate. A variable speed blower and a set of precision dampers were also installed inside the code tester. The blower is used to account for the pressure losses caused by all the measuring devices located in the duct system that connects the unit to the indoor space. With the variable speed blower the external static pressure experienced by the unit can be accurately controlled during the performance measurements. More details about the design and fabrication of code tester can be found

in Lifferth (Lifferth 2009). The code tester design is based on the same concept as the wet bulb probes where it is fixed in a remote location and it is connected to the unit using flexible 24-inch (609 mm) diameter circular neoprene ducts. Two 24 inch (609 mm) ducts where chosen to minimize the pressure drop and maintain a low air velocity inside the duct. At each end of all the flexible ducts an adapter was installed. This allows the ducts to be connected to any of the components (code tester, separation door, and unit cart), as well as insures good sealing between components and fast experimental setup time. The adapter converts the circular ducts to a flat plate with a bulb seal. It only takes four bolts to attach or disconnect an adapter and flex duct from a component. Photos for the flex connection to the cart and separation door are illustrated in Figure 14.

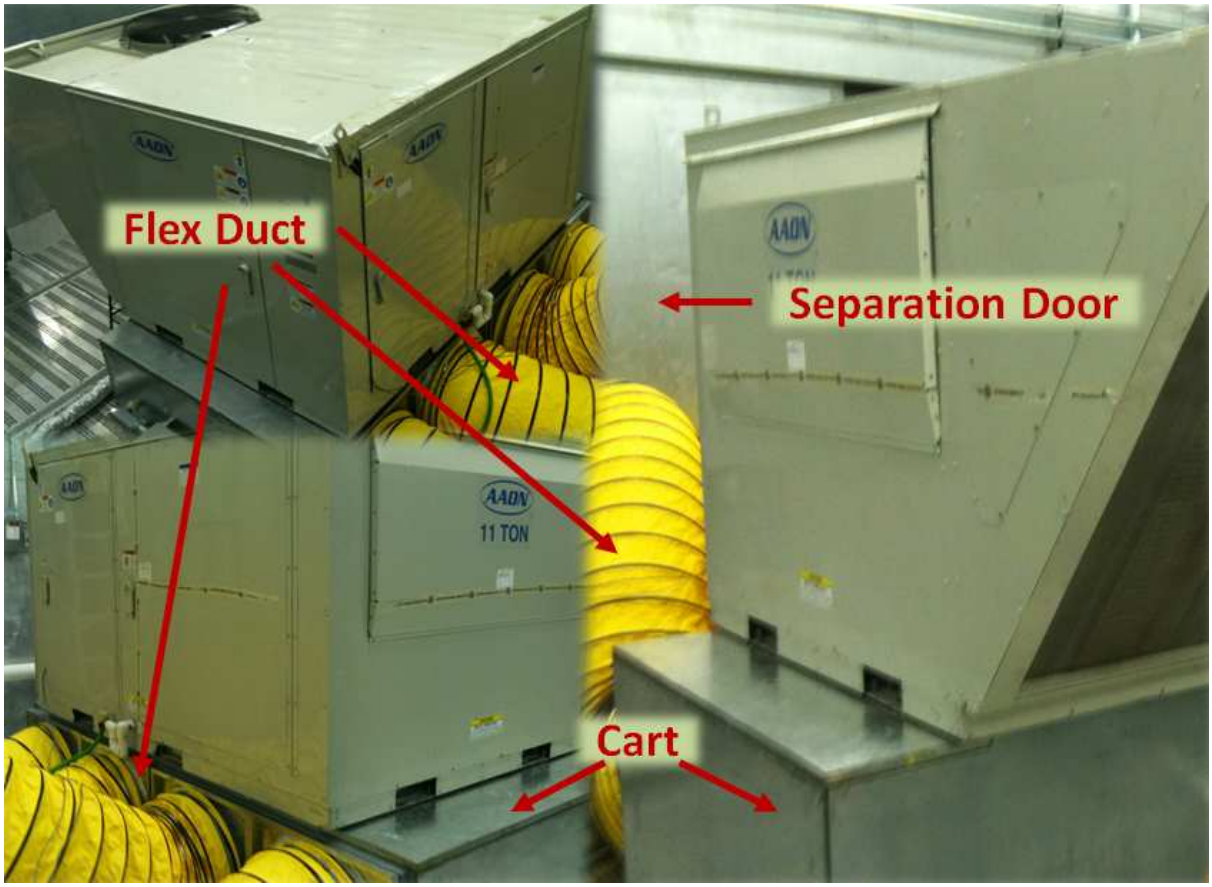

Figure 14 Flex Duct Connection to Unit Cart and Separation Door

The separation door and unit cart mentioned previously where constructed at AAON Inc. and assembled in house. These components are built like the chamber walls. Foam insulation is filled between sheet metal outer layers to form panels. The separation door is a large 4-inch (102 mm) panel

that fits in the doorway that separates the indoor and outdoor rooms of the chamber. The large panel has four 24 inch (609 mm) diameter holes that allow the supply and return air of the unit to past through. It also isolates the indoor and outdoor room from one another so they can operate at different conditions.

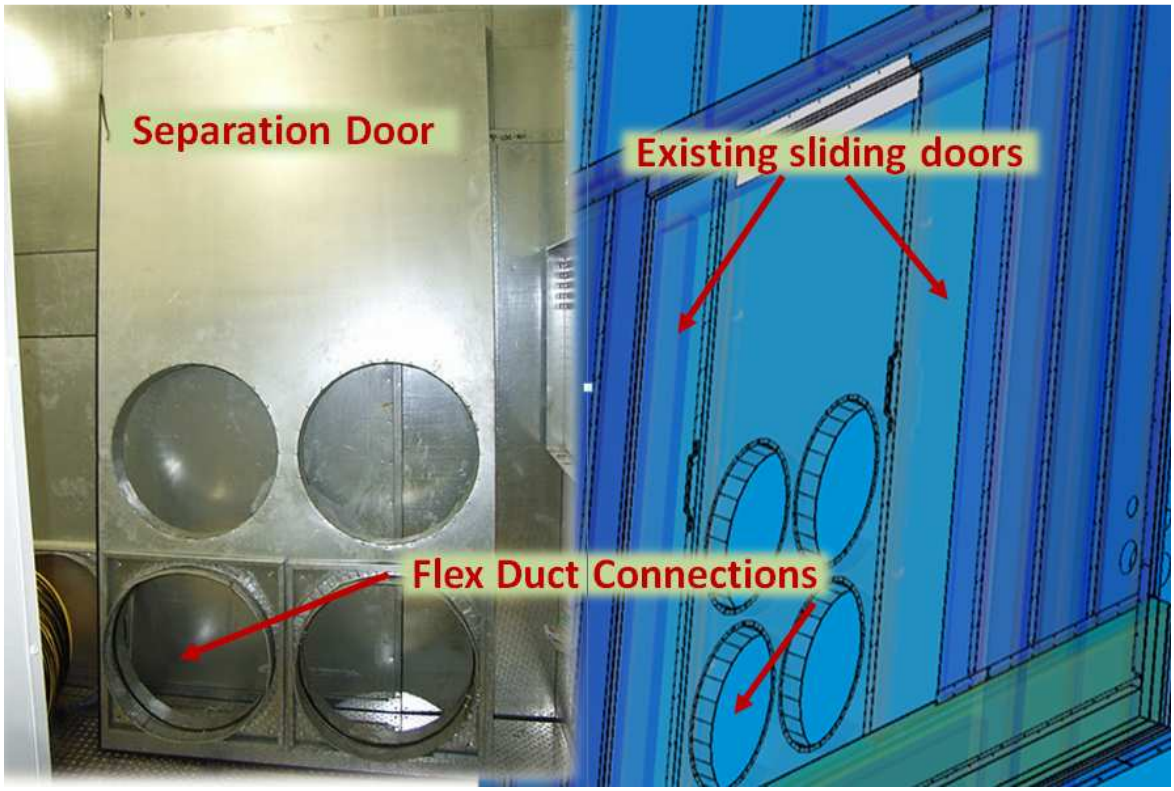

Figure 15 Chamber Separation Door Design

The unit cart is utilized to move the unit in out of the chamber as well as convert a typical rooftop unit with duct connect located at the bottom to be located on the side. This allows the flex duct to be connected to the cart, which carries the air to the conditioned space. The cart is built out of 2 inch (50.8 mm) foam panels to isolate the supply and return conditions from one another as well as isolated them from the conditions of the outdoor room. Twelve swivel casters are located on the bottom of the cart to distribute the load of the unit over a large area and allow agile movement of large units. The cart design can be seen in Figure 16.

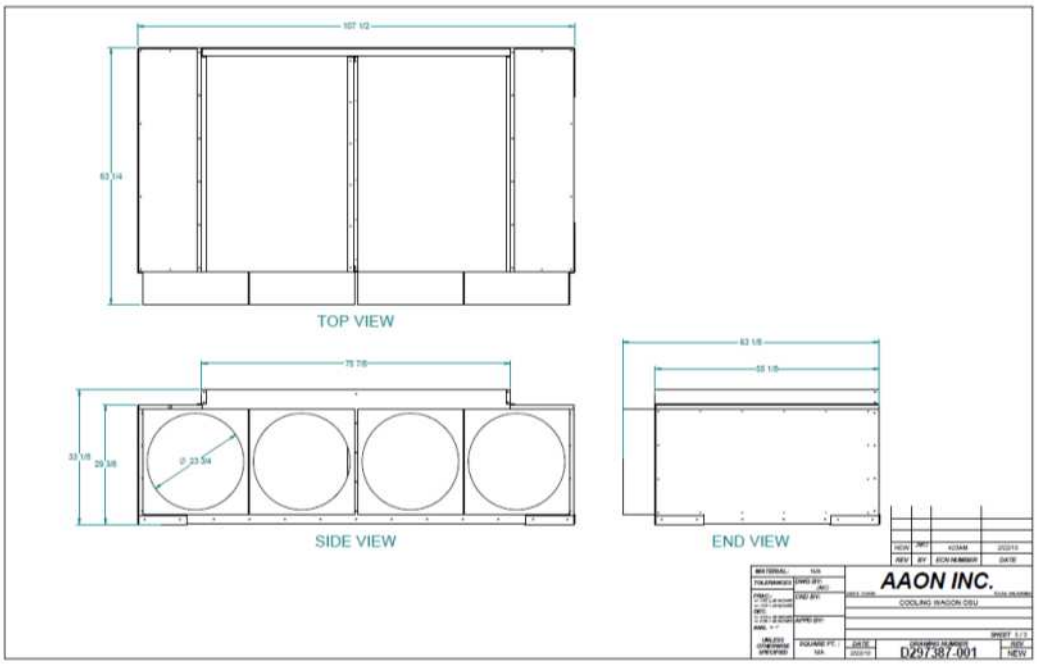

Figure 16 Rooftop Unit Cart Design

The electrical power of the unit is provided by a variable transformer, which allows the voltage and power configuration (single, two, or three phase) to be adjusted. At the power source, connection a watt transducer measures the current and voltage on all legs to allow the electrical power consumption of the unit to be directly measured. The watt transducer is located in a box with all the need connection and current transformation prewire to a plug and terminal strip. This power measurement box allows for quick and easy experimental setup as well as accurate and precise power measurement despite the equipment being tested. Figure 17 illustrates the connection between the power measurement box, unit, and power source connection.

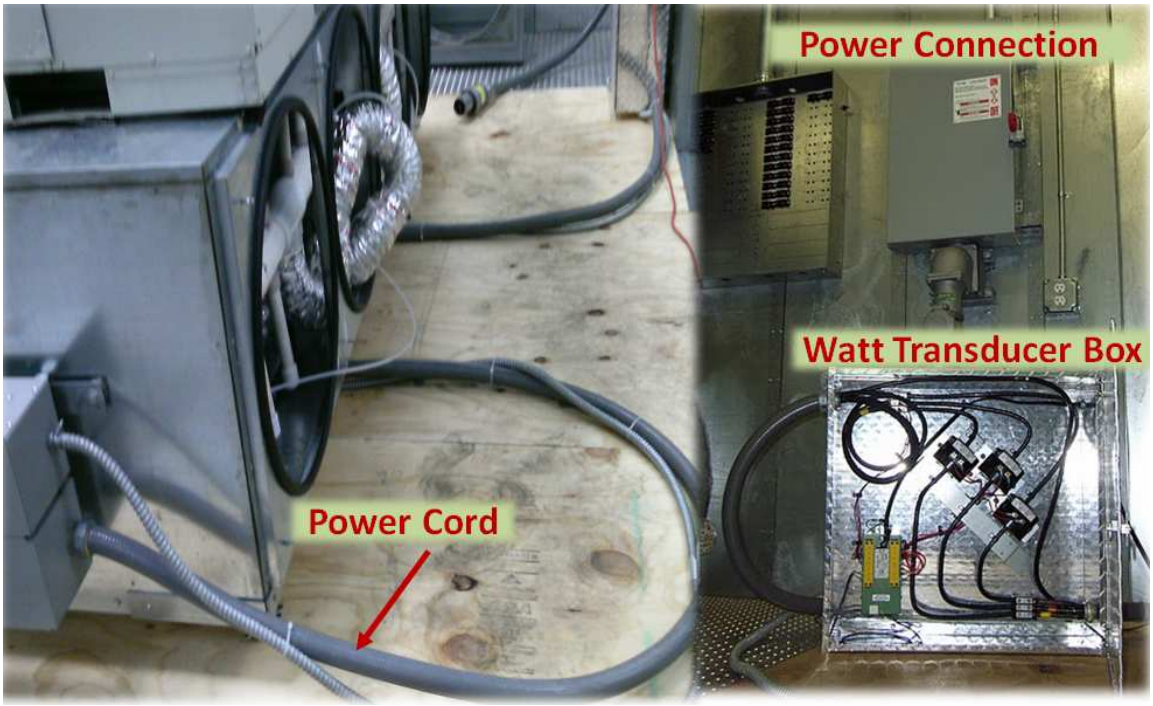

Figure 17 Watt Transducer Connection and Electric Circuitry

There are two power measurement boxes available. These boxes can be easily changed out for different electrical power measurement ranges. Having two ranges allows for a more accurate measurement of power over a larger range. In addition, two boxes allows for the potential for having two unit setup and ready for testing at once. The only needed input to switch from one unit to the other would be to change which power measurement box is plug in to the power source connection. This would resemble the act of one plugging in and unplugging a coffee maker. One box is design and constructed for up to 150 amps and 150 volts while the other box for up to 50 amps and 250 volts

Uncertainty Analysis

An uncertainty analysis on the testing for performance rating of the rooftop unit was performed to understand which measurements were the most sensitive to error propagation. To perform the analyses a model was developed in Engineering Equation Solver (EES) Software. The output for the model was Coefficient of Performance (COP) where the parameters are the measurements from the experiment. This model follows the indoor side air enthalpy method present in ASHARE Standard

37(2009) where the fundamental equations are below in (2) and (3). The complete EES code can be seen in appendix.

$$Q_{total} = \dot{m}\left(h_{supply} - h_{return}\right) \tag{2}$$

$$COP = \frac{Q_{total}}{W_{electrical} * 3.41} \tag{3}$$

EES is capable of performing an uncertainty propagation analysis using a Taylor's Series expansion approach that accounts for random errors in the measured variables . The accuracy of the measured variable is the only needed input to calculate the uncertainty on the derived quantities. The accuracy of the sensors is related to the nominal accuracies of the sensor from in-house and in-situ calibration or from the manufacturer specs, and to the variability of the measured quantities during the period of the test. The former factor is determined by how well the chamber is controlled within the operating tolerance specified by the test standards. . An example is shown below in equations ((4) and ((5) of how the Taylor's Series Uncertainty Propagation theory in EES for the uncertainty in the Heat Transfer Rate Q_{total}.

$$U_{\dot{Q}}^2 = \left(\frac{\partial \dot{Q}}{\partial \dot{m}}\right)^2 U_{\dot{m}}^2 + \left(\frac{\partial \dot{Q}}{\partial h_{supply}}\right)^2 U_{h_{supply}}^2 + \left(\frac{\partial \dot{Q}}{\partial h_{return}}\right)^2 U_{h_{return}}^2 \tag{4}$$

$$U_h^2 = \left(\frac{\partial h}{\partial T}\right)^2 U_T^2 + \left(\frac{\partial h}{\partial w}\right)^2 U_w^2 \tag{5}$$

In this case, the accuracies of readings for the measured variables was found from the sensors manufacture's specifications and were used to consider the theoretical uncertainty. These sensors' accuracies are summarized in Table 2 below. Also summarized in Table 2, are the accuracy of the

measurements that must be maintained to meet AHRI Standards as well as the accuracy available with the OSU Psychrometric Chamber at the time of testing the 11-ton (39 kW) rooftop unit. These accuracies proved to be of poorer quality than the theoretical as they account for the fluctuations from the desired conditions experienced during testing. The fluctuations are an inherent effect of the Psychrometric Chambers controls capability to keep the temperature from shifting within the room where the rooftop unit was being tested.

Table 2 Accuracy of Measurements used in Testing of Performance Rating of Unitary Equipment

Measurements Accuracy For Unit Performance Rating						
Parameter	Manufacture	Model	Nominal Value	Manufacture's (Theoretical)	AHRI Standard	OSU Chamber
Differential Pressure Across Nozzles	Setra	Model 264	0 to 3(747) InWC (Pa)	±0.25% full scale	2% Rdg	±.04(10) InWC(Pa)
Differential Pressure Across Unit	Setra	Model 265	0 to 3(747) InWC (Pa)	±0.25% full scale	±.05(12.5) InWC(Pa)	±.05(12.5) InWC(Pa)
Pressure at Nozzle Inlet	Setra	Model 266	-1.5(-374) to 1.5(374) InWC(Pa)	±0.25% full scale	±.05(12.5) InWC(Pa)	±.04(10) InWC(Pa)
Pressure Of Indoor Room	Setra	Model 267	-1.5(-374) to 1.5(374) InWC(Pa)	±0.25% full scale	±.05(12.5) InWC(Pa)	±.0075(1.9) InWC(Pa)
Unit Supply Dry Bulb RTD	Omega	PR-10	5(-15) to 140(60)°F(°C)	±0.1(0.2)°F(°C)	±1.0(2.0)°F(°C)	±0.31(0.62)°F(°C)
Unit Supply Wet Bulb RTD	Omega	PR-10	5(-15) to 140(60)°F(°C)	±0.1(0.2)°F(°C)	±0.5(1.0)°F(°C)	±0.37(0.74)°F(°C)
Unit Return Dry Bulb RTD	Omega	PR-10	5(-15) to 140(60)°F(°C)	±0.1(0.2)°F(°C)	±1.0(2.0)°F(°C)	±0.26(0.52)°F(°C)
Unit Return Wet Bulb RTD	Omega	PR-10	5(-15) to 140(60)°F(°C)	±0.1(0.2)°F(°C)	±0.5(1.0)°F(°C)	±0.43(0.86)°F(°C)
Nozzle Dry Bulb RTD	Omega	PR-10	5(-15) to 140(60)°F(°C)	±0.1(0.2)°F(°C)	±1.0(2.0)°F(°C)	±0.29(0.58)°F(°C)
Barometer	Vaisala	PTB110	0.002(500) to 0.004(1100) InWC(hPa)	±0.12(30) InWC(Pa)	n/a	±0.116(29) InWC(Pa)
Unit Power Watt Transducer	Flex Core	AGW	0 to 45,000 Watts	.2% Rdg	2% Rdg	2% Rdg
Refrigerant High Pressure	Setra	Model 206	0 to 500 (3447) psig (kPa)	±0.13% full scale	n/a	n/a
Refrigerant Low Pressure	Setra	Model 206	0 to 500 (3447) psig (kPa)	±0.13% full scale	n/a	n/a
Humidity Sensor	Omega	HX71-MA	15% to 85% RH	±3.5% RH	n/a	n/a

The first parametric study was done by altering three different pressure readings: pressure drop across the nozzle, pressure rise across the unit and the static pressure at the nozzle inlet. Due to the design of the chamber code tester and nozzle bank these pressures can be manipulated by the user independent of what equipment is being tested. Understanding how these pressure measurements affect the COP uncertainty can allow the user to make adjustments during the testing to produce results that are more precise. The pressure across the nozzles was varied from 0.5 to 3.0 InWC (125 to 374 Pa) to cover the pressure transducer nominal operational range (see Table 2). The pressure rise across the unit according to the AHRI Standards is to be maintained at 0.31 InWC (77 Pa) during testing with a tolerance of ±0.5 InWC (±125 Pa). Therefore, this pressure was varied from 0.25 to 0.35 InWC (62 to 87 Pa) to reach past the acceptable zone in an effort to extract the trend of the uncertainty. The final pressure varied was the static pressure at the nozzle inlet. Ideally, the equipment is tested independently from the air duct system attached to it. The chamber code tester is setup for this ideal test where the speed of a blower in the code tester is adjusted to make up for the obstruction to airflow

(pressure drop) caused by the duct and instrumentation setup. During this scenario the nominal operational static pressure at the nozzle inlet has proven to be approximately zero; therefore, it was varied from -0.16 to 0.14 InWC (-40 to 35 Pa).

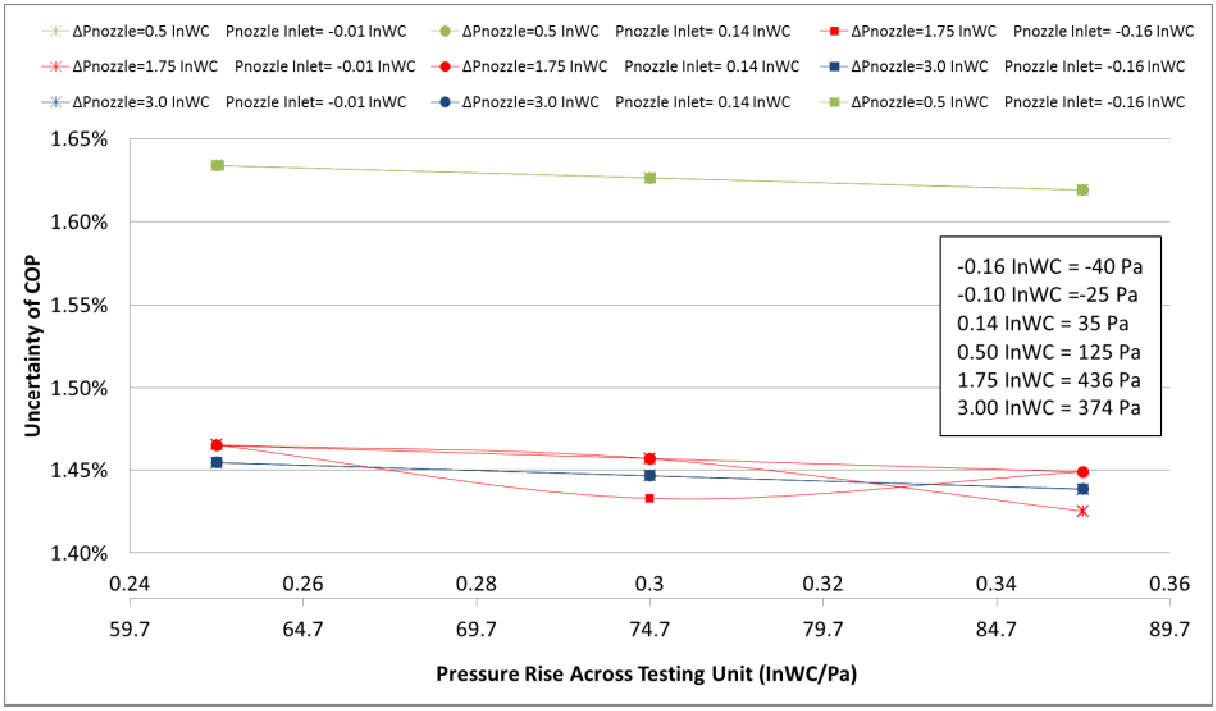

Figure 18 Uncertainty of COP with Varying Pressure Measurements

Figure 3 summarize the results found by varying the pressures for testing of performance rating on unitary equipment. The most obvious effect is the change in pressure drop across the nozzles. Operating the nozzles at low-pressure drop increased the COP uncertainty. This was expected and as a result all the recommended nozzle configurations were designed to keep the pressure drop larger than 1.0 InWC (250 Pa). Another effect seen from Figure 18 is as the pressure rise across the unit increased the uncertainty decreased slightly. This conveys the user to test with pressure rise across the unit at the higher tolerance range of 0.31 InWC (77.2 Pa) to decrease the uncertainty. This arguably would have a small effect on the uncertainty and should not be placed as a prority, but note to the user when trying to push for just a little more percion this measurement is a possible solution. The final bit of knowlegde that can be pulled from Figure 18 is the static pressure at the nozzle inlet has little or no

effect on the uncertianty of the COP. With all said the overall effect on the uncertianty, due to variation in the pressure measurements was only 0.25%.

A second parmetric study was done by varying the indoor dry bulb and wet bulb temperatures. This will allow the user to understand when testing at different indoor condtions how the uncertianty will be effected. The chosen ranges of both the dry bulb and wet bulb were done to cover ranges of realistic indoor conditions. The dry bulb was varied from 85°F to 75°F (29.4°C to 23.8°C) and the wet bulb was varied from 69°F to 65°F (20.5°F to 18.3°C). It is shown in Figure 19 that the dry bulb temperature of the indoor room has little to no effect on the uncertaintly while the wet bulb demonstrated a trend that as it dereased the uncertanty increased. The overall effect for the variation in indoor conditons on the COP uncertianty was only 0.30%.

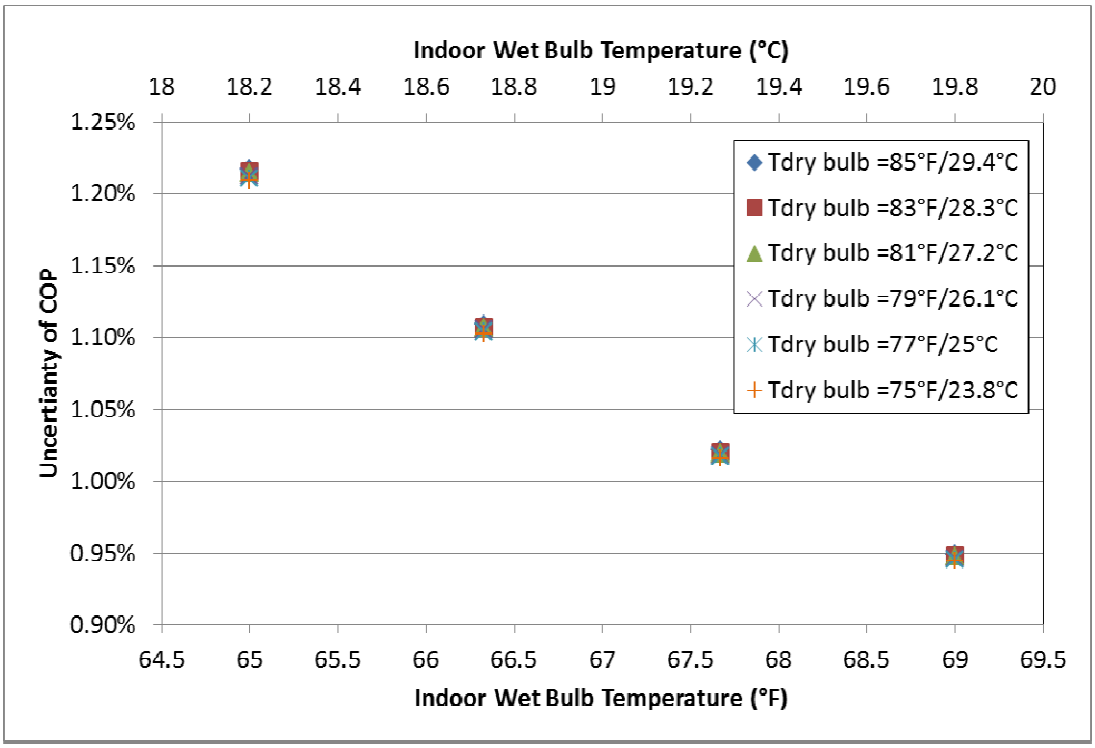

Figure 19 Uncertainty of the COP with Varying Indoor Conditions

The third parmetric study was done by varying the unit supply dry bulb and wet bulb temperatures. The supply temperatures are effected by numerious different parameters such as the air flow rate, refrigerant high temperature, refrigerant charge, unit type and manufacture, etc. Understanding how

the supply temperature effected the uncertianty of the COP may lead to changes in any or all of these parameters, if possible.

The chosen ranges of both the dry bulb and wet bulb were done to capture a typical air conditioner temperature range, operating in cooling mode. The dry bulb was varied from 75°F to 65°F (23.8°C to 18.3°C) and the wet bulb was varied from 54°F to 52°F (12.2°F to 11.1°C). It is shown in Figure 20 that the supply dry bulb temperature has the same effect as seen in Figure 19 with varying indoor conditions, which is little to no effect. The wet bulb demonstrated a trend opposite of what is seen in Figure 19, as it increased the uncertaitny increased. The overall effect for the variation in supply conditons on the COP uncertianty was only 0.15%.

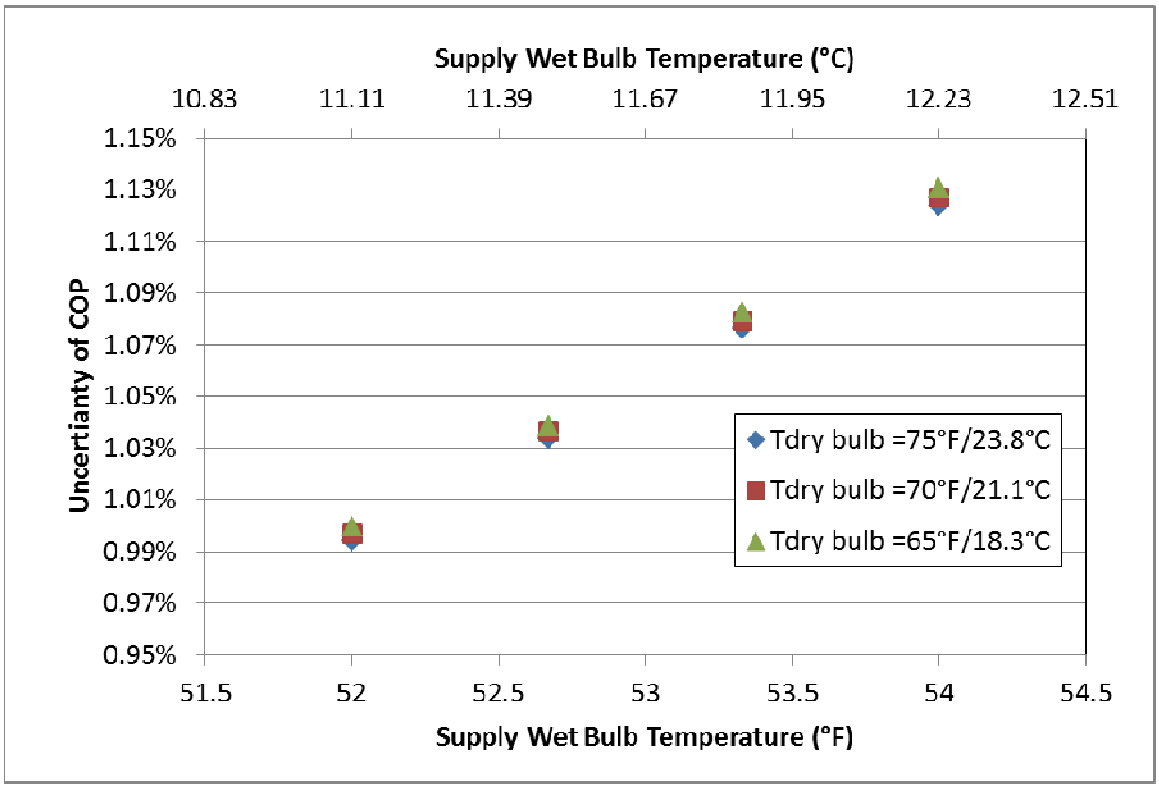

Figure 20 Uncertainty of the COP with Varying Supply Conditions

The uncertainty due to the variations in temperatures is small, but at close look, it can be seen as the indoor and supply temperatures approached each other the uncertainty increased. As these conditions become closer together it has an inherit effect of lowering the equipment capacity. Consequently another parametric study was done on the uncertainty of the COP by varying the two key parameters that determine the capacity, the airflow rate and enthalpy difference. The dry and wet bulbs for both

the supply and return were varied to decrease the enthalpy difference between the supply and return beyond a typical operational scenario from -1.25 to -6.5 Btu/lb. (-2.9 to -15.1 kJ/kg). This was done so the uncertainty could be exaggerated and produce a recognizable trend. Along with the varying enthalpy differences, the airflow rate was varied. This was done by changing the nozzle configuration of the code tester nozzle bank while holding a constant pressure drop across each configuration. Every recommended nozzle configuration was used in this study.

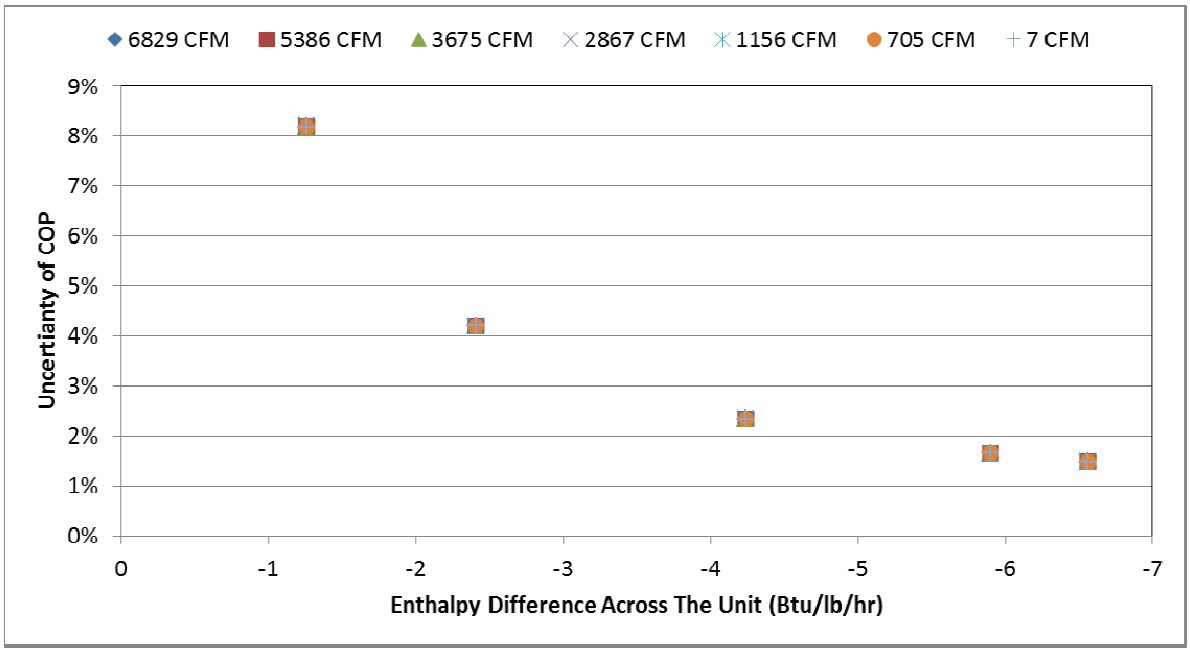

Figure 21 Uncertainty of the COP with Varying Enthalpy Differences and Airflow Rate

Figure 21 show the results from the study and it can be seen that the airflow rate or nozzle configurations has no effect on the uncertainty of the COP. The enthalpy difference shows an opposing story and has a drastic effect on the uncertainty. The uncertainty of the COP increased as the enthalpy differences decreased. The trend showed an exponential curve whereas when the enthalpy difference approached zero the uncertainty approached infinity and as the enthalpy difference approached infinity, the uncertainty reached an isotonic value of approximately one percent.

The previous parametric studies where done using the theoretical accuracy of the measuring sensors and it was found that the most dominating parameter on the uncertainty of the COP is the enthalpy difference. This is what can be considered as the theoretical uncertainty, which does not capture the

entire story. To see the effect of the room fluctuation on the uncertainty, the AHRI Standards and OSU Chamber operation tolerance limits where used with varying enthalpy difference and the results are shown in Figure 22.

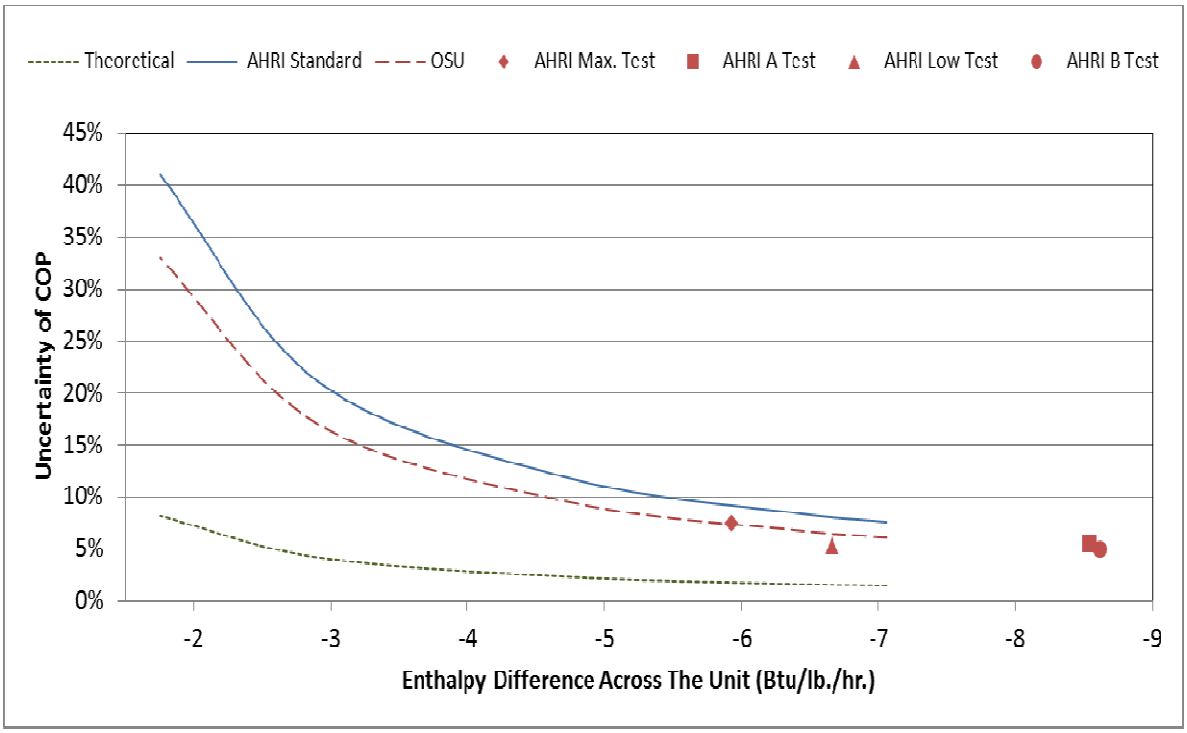

Figure 22 The AHRI Standard and OSU Uncertainties Compared with the Theoretical Uncertainty

The AHRI and OSU Uncertainties have the same trend as the theoretical uncertainty, but have drastically different values. It is shown that the ability to maintain the chamber at constant and uniform conditions is critical. It is also shown that by meeting the AHRI Standards during testing will allow the uncertainty during normal operation to be below 10%. The OSU Chamber exceeds the AHRI criteria and is capable of achieving less than 8% uncertainty. The enthalpy difference as stated previously is the most influential parameter, but the controls of the chamber are the largest most donating characteristic on the uncertainty of the COP. Therefore, the conclusion from this study is the dry bulb temperature should be controlled to within ±0.4°F (±0.2°C) of the dry bulb set point while the wet bulb temperature should be maintained within ±0.5°F (±0.25°C) of the wet bulb set point.

Fabrication of a Test Apparatus to Measure the Thermal Conductivity of Pipe Insulation Systems

Experimental Setup

The experimental setup for the measurements of pipe insulation thermal conductivity can be divided into three parts: the pipe insulation tester (PIT), the refrigeration system, and the psychrometric chamber, which was described previously.

Pipe insulation tester (PIT)

The pipe insulation tester (PIT) consists of a 4-foot (1.2 m) long, 3-inch (76.2 mm) nominal Aluminum pipe with a 10-foot (3.0 m) long 3/8-inch (9.5 mm) nominal Copper pipe concentrically placed and centered inside it. The space between the copper pipe and the Aluminum pipe was filled with pre-dried sand. Sand was selected because of its compact structure and appropriate thermal properties for this application (Tarnawski et al. 2009). To keep the sand dry, a sealed vapor barrier was utilized to isolate it from the ambient environment. The vapor barrier consisted of enclosing the sand in long cylindrical plastic bag/sock and then gluing plastic plugs at each end of the Aluminum pipe. The sock and plugs were constructed to allow the copper pipe to extend through them. Figure 23 illustrates these features and how the PIT was assembled.

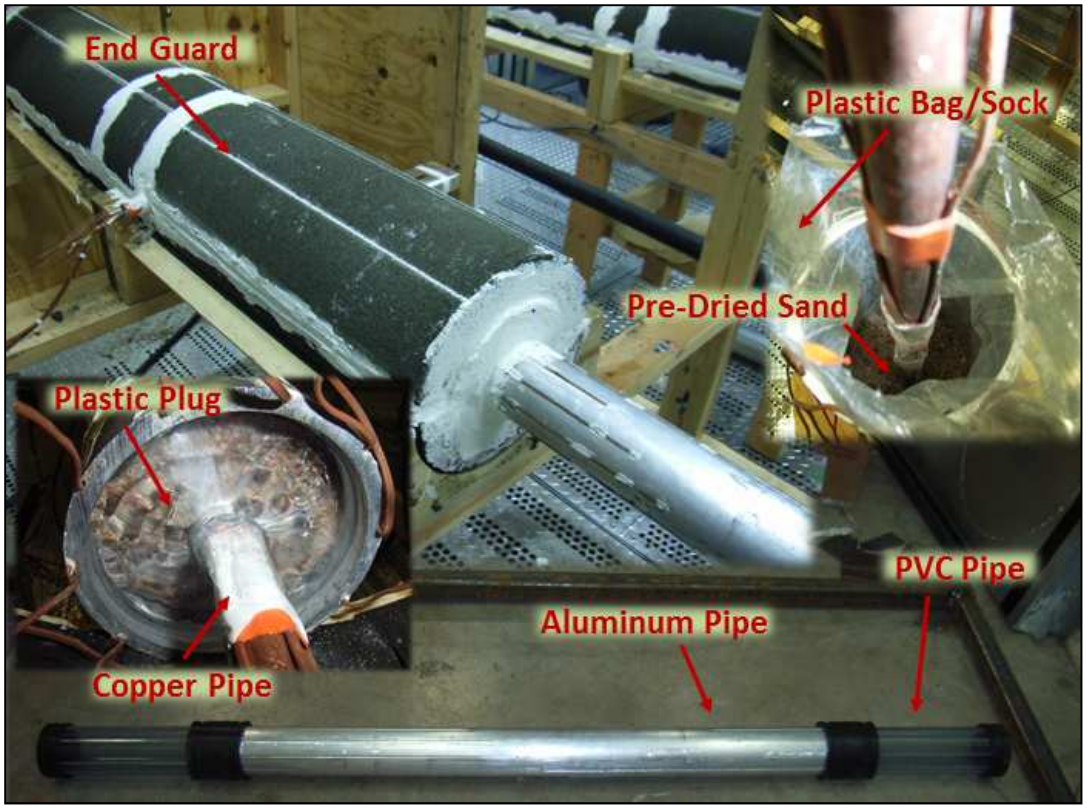

Figure 23 Construction of Pipe Insulation Test Apparatus

This is because the copper pipe is carrying the refrigerating fluid in a two-phase liquid-vapor state experiencing a slow evaporation process. This fluid needs a point to enter and exit the PIT apparatus. The pressure drop is minuscule through the PIT and utilizing the concept that a mixture in a two phase state at a constant pressure will result in a constant temperature, a uniform temperature is maintained along the copper pipe and inherently along the Aluminum pipe. To insure this behavior, twenty surface temperature sensors were distributed on Aluminum pipe surface, 6 surface temperature sensors along the surface copper pipe as well as 2 pressure sensors at the entrance and exit of the PIT were installed. The 20 thermocouples positioned around the Aluminum pipe exterior surface were installed inside longitudinal grooves of about 1/8 inch (~0.32 cm) depth. The grooves were cut out in the Aluminum pipe so that the thermocouple wires did not interfere with the installation of the pipe insulation around the Aluminum pipe. The fabrication of the grooves as well as the thermocouple attachment to the aluminum and copper pipes are shown in Figure 24.

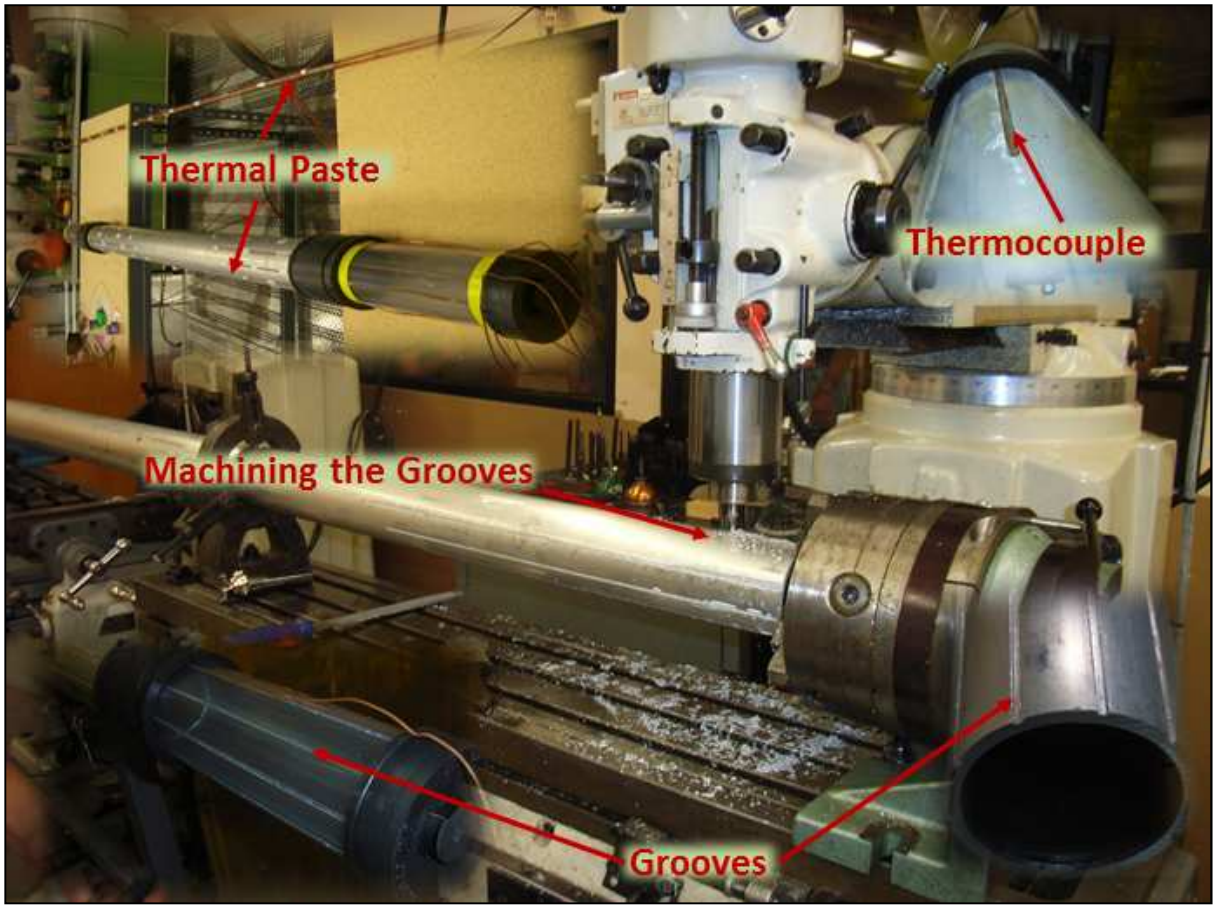

Figure 24 PIT Thermocouple Grooves and Attachment

The 6 thermocouples attached to the copper tube were glued on to outer surface with a highly thermal conductive yet low electrical conductive epoxy. The refrigerant saturation temperature inside the copper pipe was estimated from the 2nd refrigerant pressure at each end of the PIT device. The end sections, referred in this thesis as thermal end guards, were designed to minimize the axial heat transfer of the PIT apparatus, so only the radial heat transfer could be assumed. The two thermal end guards are 48 inch (1.2 m) long, with an outer diameter of 10½ inch (0.2667 m) sections place at the each end of the aluminum pipe composed of materials having large thermal resistance and are inherently vapor repellent. The construction of the thermal end guard is as follows and the complete PIT apparatus construction is illustrated in Figure 25: A 12 inch (0.3m) long section of nominal 3 inch (0.0762 m) plastic pipe was installed at the end edges of the Aluminum pipe. Rubber couplings were used to join the plastic pipes to the Aluminum pipe while maintaining about ½ inch (12.7 cm) of air gap between the pipes to minimize thermal bridges in the axial direction. Polyethylene foam rubber

was inserted inside the plastic pipe and rubber caps were installed at their ends. Cellular glass cylindrical inserts were placed in between the rubber caps and refrigerating cold copper pipe in order to eliminate any direct contact between the higher conductive materials such as rubber and the copper. All other material of the end guard is composed of cellular glass pipe insulation.

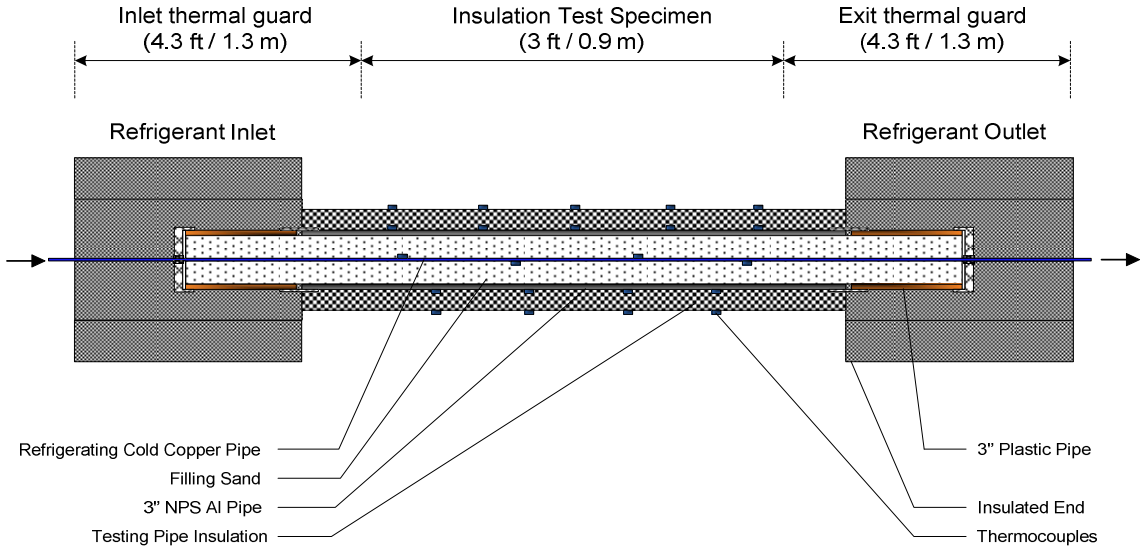

Figure 25: Schematic of the Pipe Insulation Tester (PIT)

The test insulation was precisely cut to fit the Aluminum pipe and a type of joint sealant was applied to the longitudinal butt joints to ensure the insulation to the pipe, similar to typical field applications. The type of joint sealant, if any, is dependent on the characteristics of the test insulations and on the manufacturer installation recommendations. The PIT apparatus is constructed in such a way to replicate a real chilled water insulation system application. An additional 20 thermocouples were placed around the exterior surface of the test insulation approximately following a spiral path. The tips of these thermocouples were place directly on insulation surface and the ambient side was covered by a low thermal conductivity silicone gel. This helped to prevent interference with the surrounding air and provide a more accurate measurement of the local pipe insulation surface temperature as well as temporary adhesion to insulation.

More than 50 temperature sensors were used to monitor the interior and exterior local surface temperature of the pipe insulation specimen. An example of the axial and angular temperature

measurements is shown in Figure 26. By blocking the air stream directly below the test apparatus with a panel of flexible elastomeric insulation, the temperature distribution of the pipe insulation exterior surface was within 2.1°F (~1.2°C). The local surface temperatures of the Aluminum pipe were within a maximum difference of 0.8°F (~0.45°C) when considering both axial and angular directions, as shown in the central plot of Figure 26. The thermocouples attached to the copper tube were within 1.5 °F (~0.8°C). This is shown in the bottom plot of the figure. The average copper surface temperature was slightly higher than the refrigerant saturation temperature inside the copper pipe.

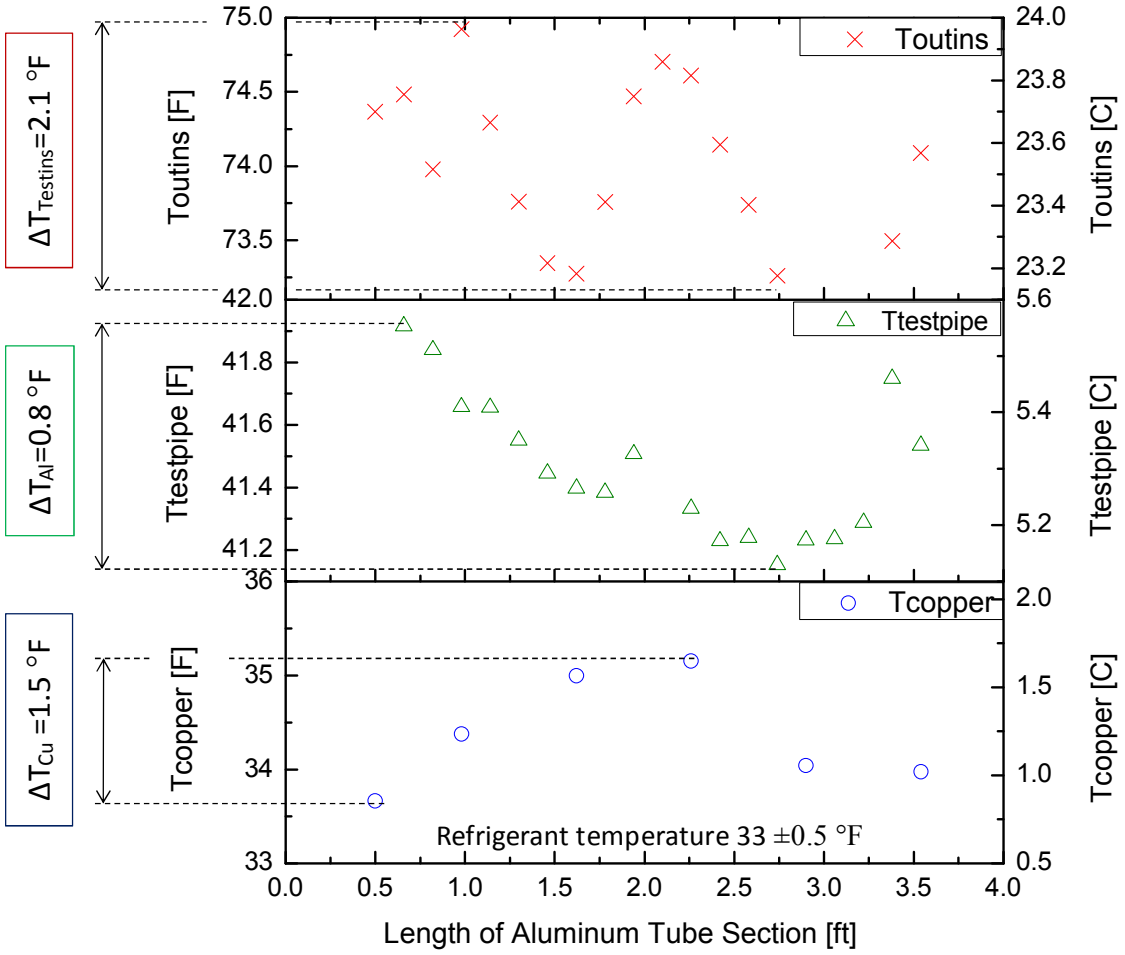

Figure 26: Example of surface temperature measurements during the experiments (note that thermocouples are positioned along the axial and angular direction according to a spiral configuration)

Refrigeration system used to achieve below ambient temperature of the pipe insulation

Two PITs apparatuses were connected in series. Just before the first PIT an expansion valve was placed to produce refrigerant in a two phase region throughout both PITs. The measurements on the first PIT aimed to determine directly the thermal conductivity of the pipe insulation specimen. The second PIT allows for constant monitoring of the apparatuses and test insulation's behavior during testing. The test insulation was applied to the 1st PIT and remained undisturbed during the duration of the test, while the 2nd PIT could be disturbed to see physical changes in real-time during the test. This allows for more accurate measurement of the thermal conductivity, but allows for studying and understanding of what happens during the test. The available refrigeration unit (compressor and condenser) did not produce the cooling capacity needed for the two PITs, if configured in the traditional vapor compression cycle. To increase the cooling capacity of the refrigeration unit, a tube-in-tube suction line heat exchanger (HX) was installed after the second PIT device. The suction line HX was made in house by welding a 48 inch (1.2m) long, 3/4 inch (19.05 mm) nominal copper pipe around 1/4 inch (6.35 mm) copper pipe and using tee and reducer fittings to keep the two fluid streams independent. Fabrication of the tube and tube heat exchangers are illustrated in Figure 27.

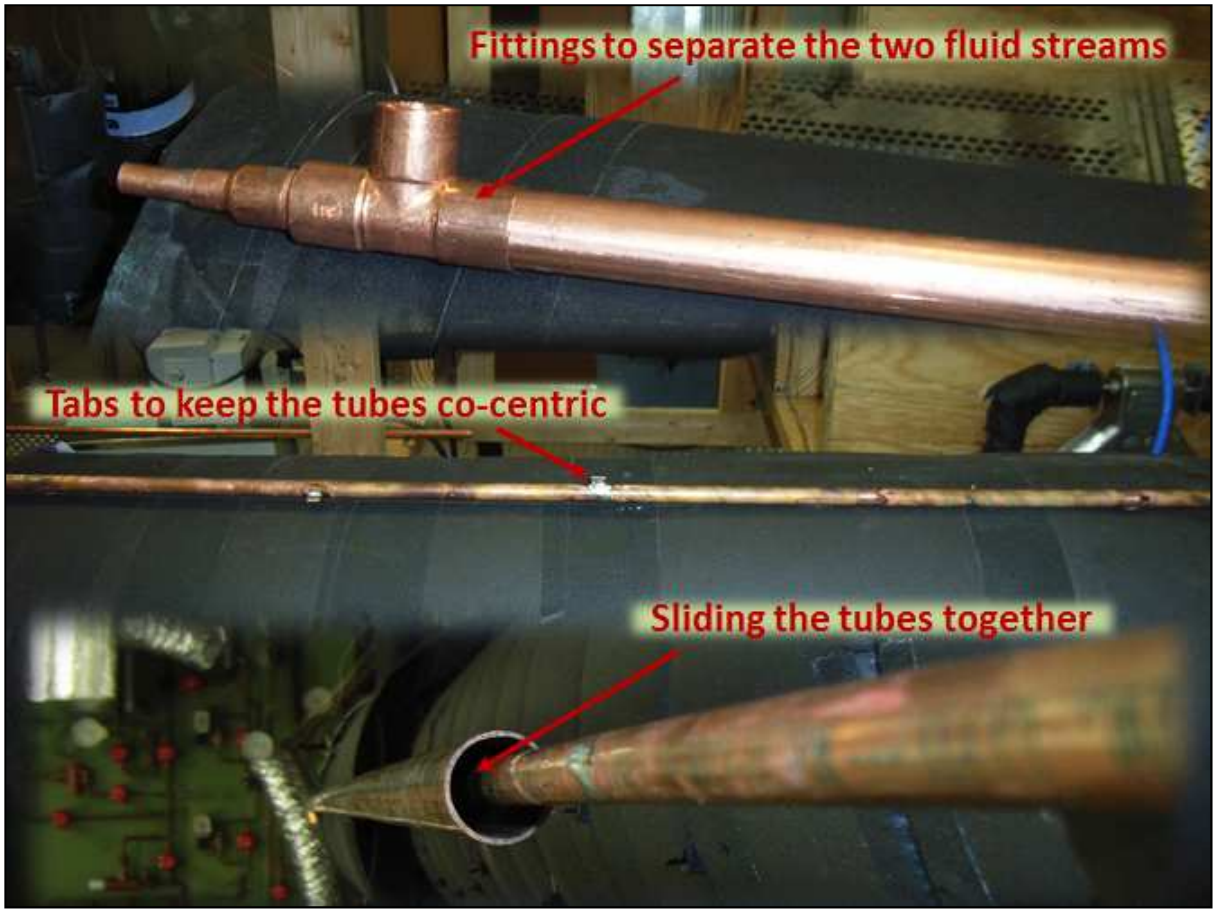

Figure 27 Construction of the Tube and Tube Heat Exchangers

To allow the experiment to operate at a range of ambient and refrigerant saturation temperatures another tube and tube heat exchanger was fabricated and installed just before returning the refrigerant back to the refrigeration unit (compressor). The superheat HX was made almost identical to the suction line HX, but instead a 72-inch (1.8m) long, 1 inch (25.4 mm) nominal copper pipe around 1/2 inch (12.7 mm) copper pipe was used. This tube and tube HX was utilized as auxiliary water-to-refrigerant HX to allow adjusted for the proper degree of superheat at the compressor suction despite the experiments operating conditions. Hot water was circulated in an auxiliary loop with an in-line heater, whose power is adjusted to guarantee proper suction conditions at the compressor. The configuration of the refrigeration loop is illustrated in Figure 28.

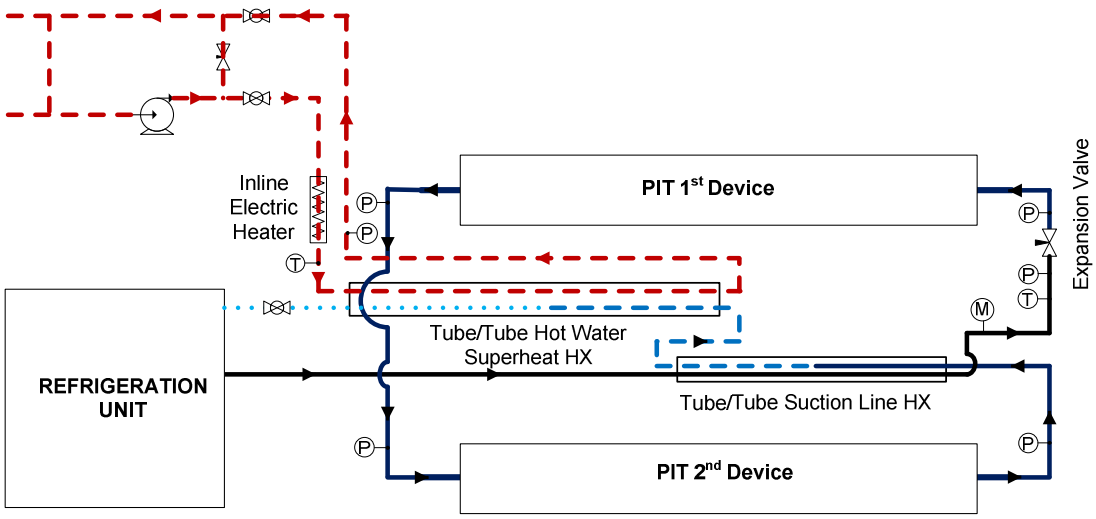

Figure 28: Schematic of the test apparatus with refrigeration unit to achieve cold pipe

It should be noted that electric heaters applied directly on the surface of the cold copper pipe were intentionally avoided in the test apparatus because they created large axial temperature gradients, reliable/durability issues, insufficient control, and instrumentation noise in the refrigeration loop and PIT devices. The large axial temperature gradients are the results of conduction across the walls of the pipes and they affected the uniformity of the surface temperature along the axial direction of the pipe insulation. The reliability/durability issues are a result of the experiment operating 24 hours a day and the economical surface heater available cannot withstand that type of duty cycle. The insufficient control is a result of how well the heat is in contact with the copper pipe and the instrumentation noise is the in electrical magnetic interference with measuring sensors used to collect data. All these results produce systematic errors during the calculation of pipe insulation thermal conductivity. Thus, electric heater directly in contact with any metal surface of the test apparatus was purposely avoided. Two types of refrigerant were used in the system, Refrigerant R134a and R404a. These were selected based on their interchangeability and boiling points. The choice of refrigerant to use at certain times was the result of the test insulation thermal conductivity so the PIT apparatus produces a measurable radial heat flux across the pipe insulation system. Both refrigerants were maintained in two-phase region during the tests, which as expressed earlier is the key to a uniform and stable temperature profile

along the center section of the PITs. The experimental setup for the pipe insulation test apparatus experiment is shown in Figure 29.

Figure 29 Pipe Insulation Tester Experimental Setup

Testing Procedures

Two types of test were performed on the PIT apparatus. The insulation thickness ranged from 1 to 2 inches (25 to 51 mm) in wall thickness and were applied the 3 inch (76.2 mm) NPS aluminum pipe, whose surface temperature is controlled at approximately 40°F (4.5°C). All the measurements of the insulation are in accordance to ASTM C585 Standard (ASTM, 2009). First, a set of Dry non-condensing tests were performed on a variation of pipe insulation materials to compare manufacture, literature and our data. The Dry Test validated the PIT apparatus and methodology produced accurate results and also expanded the already existing pipe insulation conductivity data base. Dry non-condensing conditions were achieved by operating the chamber room with very low ambient humidity. In these conditions, water vapor did not condensate on the Aluminum pipe surface and the tests are referred throughout this paper as Dry Tests. The second sets of test are referred to as Wet Tests. These

tests were done to investigate the moisture propagation effect on select types of pipe insulation materials. This was achieved by operating the chamber at a very high ambient temperature and humidity. In these conditions the moisture propagation into the insulation was exaggerated to accelerate a process that typically takes year into only weeks or months.

Calibration tests were conducted at the beginning of each experiment to determine the actual thermal conductivity of the sand filling the 3 inch NPS Aluminum pipe. In the calibration tests, a tape resistor-type heater was applied uniformly around the exterior surface of the Aluminum pipe and a large volume of rubber elastomeric insulation was installed around the heater creating a thermal barrier from the ambient. When the electric heater was energized, the electric power was carefully measured using a precision watt meter. The total heat transfer into the Aluminum pipe, $Q_{Al,pipe}$, was estimated by considering both the electric power of tape resistor heater, Q_{heater}, and a small amount of heat transfer leaking in from the surrounding ambient, $Q_{leak,in}$, as given in (6):

$$Q_{Al,pipe} = Q_{heater} + Q_{leak,in} \tag{6}$$

The heat transfer leaking in was a combined effect of heat transfer through the thick rubber insulation layer and from the axial heat conduction from the end sections of the test apparatus. To minimize these effects during the calibration tests the ambient temperature was adjusted such that the temperature difference across the outer thermal insulation barrier resulted in less than 5.4°F (~3°C) and the axial temperature gradient along the Aluminum pipe was less than 0.43% of the radial temperature gradient. Therefore, it was reasonable to assume that these effects were minimal compared to the magnitude of the radial heat flow from the electric heater. However, even though the resulting $Q_{leak,in}$ was small it was accounted for during the calibration tests to eliminate a systematic error on the actual thermal conductivity of the sand inside the Aluminum pipe. It should be noted that the actual thermal conductivity of the sand inside the Aluminum pipe was slightly different as expected from the thermal conductivity of pure dry sand found in Whitaker and Yarbrough (2002). This is because the measured values during the calibration test account for the end effects of the thermal guards, axial heat flow, and for the non-uniformity and non-homogenous properties of the

sand inside the Aluminum pipe. Calibrating the Aluminum pipe at the same thermal conditions, which occurs during the actual measurements of the insulation thermal conductivity, allows all of these non-ideal effects to be accounted for in the sand conductivity. This sand thermal conductivity approximates the 3D geometry and non-homogeneity of the PIT device as a 1D heat conduction model that follows Fourier law for heat conduction.

Once the effective conductivity of the sand filling the Aluminum pipe, k_{sand}, was known from the calibration test, a 1-D heat transfer balance equation along the radial direction was applied to the PIT device, as shown in the schematic of Figure 30 . As a result, the pipe insulation thermal conductivity, k_{ins}, was determined directly by the following expression (7):

$$k_{ins} = k_{sand} \times \frac{(T_{Al,pipe} - T_{cold,copper,pipe})}{(T_{exterior,ins,specimen} - T_{Al,pipe})} \times \frac{\ln\left(\frac{D_4}{D_3}\right)}{\ln\left(\frac{D_2}{D_1}\right)} \quad (7)$$

Where D1, D2, D3, and D4 are the pipe insulation exterior diameter, cold Aluminum pipe inner and outer diameters, as well as refrigerating copper pipe outer diameter, as shown in Figure 30. The diameters of the pipe insulation were measured according to the standard ASTM C585(ASTM 2009).

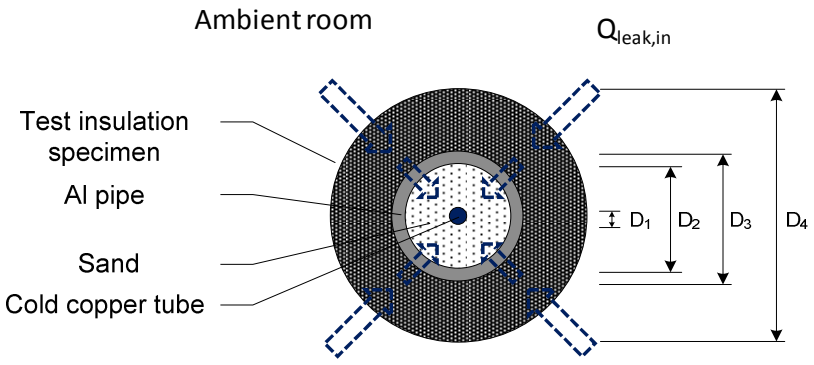

Figure 30: Schematic of the 1D model of the Pipe Insulation Tester (PIT) and corresponding diameters

The average temperature of the test insulation specimen was calculated from the measurements of the surface temperature sensors as follows:

$$T_{avg,ins,specimen} = (T_{Al,pipe} + T_{exterior,ins,specimen}) / 2 \quad (8)$$

Dry Test

In order to reach conditions needed for the Dry Tests, a solid desiccant silica gel material was installed in the air stream inside the conditioning loop. The desiccant was needed due to the current limitations of the chamber. As mentioned previously, the chamber was designed to achieve desired conditions but a lack of funding resulted in a missing component (auxiliary Chiller). The chamber was capable at the time of testing to reaching as low as 30% RH and the desiccant was implemented to further lower the relative humidity. This solid silica gel material was replaced periodically to insure that the room humidity was maintained low enough throughout the experiments such that non-condensing conditions were achieved. The 1st PIT apparatus measured the thermal conductivity of the pipe insulation for average insulation temperature ranging from 56°F to 73°F(13°C to 23°C), where at all times the cold surface side was maintained at 40°F (4.5°C) and hot surface side ranged from 70°F to 104°F (22°C to 40°C). The hot surface temperature was controlled by varying the ambient temperature of the surrounding air from 77°F to 110°F (25°C to 43.4°C). The changing of the ambient air temperature and precisely maintaining a desired set point for any duration was done with the use of the chamber. The 2nd PIT apparatus, also experiencing the ambient temperature changes, monitored the thermal conductivity of the sand. This was achieved by continuously performing a calibration to the 2nd PIT to detect any change of the sand thermal conductivity due to failure of the joints or due to moisture ingress inside the Aluminum pipe. The electric heater was adjusted to obtain a similar Aluminum surface temperature occurring on both PIT devices during the tests. Since the two PITs were of identical geometry, constructed at the same time, and maintained at the same temperature and humidity boundary conditions, the assumption was that any variation in the sand conductivity measured with the second PIT device could be translated in a proportional variation of the sand conductivity inside the first main PIT device.

Wet Test

For the wet tests, the operating condition needed inside the chamber was 95°F (35°C) at 95% RH. This caused condensation to occur on the aluminum surface and boost moisture propagation through the test insulation. Common operation conditions for a chilled water piping system are not typically this high in temperature and humidity, but this exaggeration was done to accelerate moisture propagation and shorten the needed time to saturate the test insulation. These conditions are easily achieved with the chamber and controls previously described. Before the chamber was set to this exaggerated condition, it was first dehumidified. This process is the same as defined in the dry test. At the dry non-condensation conditions, the test insulation thermal conductive was determined. This thermal conductive is the initial or base line thermal conductivity for the particular insulation type and specimen. Once the base line was determined, the room was set to the wet test condition. The chamber continued to maintain the wet test condition until the test insulation became completely saturated and was removed from the PIT. The time needed for the insulation to reach saturation was very dependent upon the insulation material being tested. Some took days, while others took months to reach complete saturation. Throughout this time, the thermal conductivity was determined twice a day for both PITs. The 1st PIT was fitted with insulation exactly the way it would be applied out in the field, while the 2nd PIT was fitted with the same insulation but it was pre-cut into 6 inch (152.5 mm) long segments. There was a total of 16 segments (8 top and 8 bottom), which were weighed before being applied to the PIT. These segments were periodically removed and weighed to determine the amount of moisture that had propagated into the test insulation. Having the two PITs allowed for the comparison between thermal conductive, time, and amount of moisture to be made while the 1st PIT was left undisturbed throughout the entire test insuring accurate measurements.

Uncertainty Analysis

A uncertainty analysis for the measurements of the sand conductivity and test insulation conductivity was performed to understand which measurements are the most sensitive and critical to error propagation. To perform the analyses two models were developed in Engineering Equation Solver (EES) Software. The outputs for the two models were: the sand conductivity and test insulation

conductivity where the parameters are the measurements from the experiment. These models follow Fourier law for heat conduction, which is similar to equation (7). The complete EES code can be seen in appendix (miss Letter which one???). EES is capable of performing an uncertainty analysis using a Taylor's Series expansion approach to account for measurement error propagation.. An example is shown below in equations ((9) and ((10) of how the Taylor's Series Uncertainty Propagation theory in EES for the uncertainty in the Thermal Conductivity calculation $k_{insulation}$.

$$k_{ins} = \dot{Q} \times \frac{\ln\left(\frac{D_4}{D_3}\right)}{(T_{exterior,ins,specimen} - T_{Al,pipe})} \tag{9}$$

$$U_k^2 = \left(\frac{\partial k}{\partial \dot{Q}}\right)^2 U_{\dot{Q}}^2 + \left(\frac{\partial k}{\partial D_4}\right)^2 U_{D_4}^2 + \left(\frac{\partial k}{\partial D_3}\right)^2 U_{D_3}^2 + \left(\frac{\partial k}{\partial T_{exterior,ins,specimen}}\right)^2 U_{T_{exterior,ins,specimen}}^2 + \left(\frac{\partial k}{\partial T_{Al,pipe}}\right)^2 U_{T_{Al,pipe}}^2 \tag{10}$$

Accuracies from the measured variables was obtained from the sensors manufacture's specifications and were used to consider the theoretical uncertainty.These sensors accuracies are summarized in Table 3 below.

Table 3 Uncertainty of Pipe Insulation Tester Measurements

Pipe Insulation Tester Uncertainty Table				
Parameter	**Manufacture**	**Model**	**Nominal Value**	**Accuracy**
Mass Flow Meter	Micromotion	CFM025 Elite	0.066 (0.03) to 1.32 (0.6) lb/s (kg/s)	±0.011 lb/s (0.005 kg/s) of flow
High Pressure	Setra	Model 264	0 to 250 (1723) psig (kPa)	±0.25% full scale
Low Pressure	Setra	Model 265	0 to 50 (345) psig (kPa)	±0.25% full scale
Hummidy Senors	Honneywell	HIH-4000	0% to 99% RH	±3% of reading
Aluminum Thermocouples	Omega	T-type	32°F (0°C) to 77°F (25°C)	±0.4°F (0.2°C)
Outer Insulation Thermocouples	Omega	T-type	32°F (0°C) to 113°F (45°C)	±0.4°F (0.2°C)
Copper Thermocouples	Omega	T-type	-13°F (-25°C) to 50°F (10°C)	±0.8°F (0.4°C)
RTDs	Omega	Pt-100	-13°F (-25°C) to 50°F (10°C)	±0.2°F (0.1°C)
Aluminum Pipe Diameter	n/a	n/a	3 in (76.2 mm)	±0.015 in (0.381 mm)
Copper Pipe Diameter	n/a	n/a	3/8 in (9.5 mm)	±0.010 in (0.254 mm)
Insulation Thickness	n/a	n/a	0.5 (12.7) to 1.5 (38.1) in (mm)	±0.125 in (3.17 mm)
Length	n/a	n/a	3 ft (914.4 mm)	±0.25 in (6.35 mm)

The only accuracy that was not obtained from the manufacturer was the thermocouples, where extensive in-house and in-situ calibration was done to increase the accuracy. The stated accuracy in the

Table 3 for thermocouples came from a bias uncertainty analysis that took into account the temperature distribution and profile. This allowed one temperature value to represent multiple thermocouples in calculations, yet the accuracy related to these problems was accounted for. The uncertainty of the thermocouples was calculated as follows in equations (11), (12), and (13) using the worst case scenario.

$$B_{T,distribution} = \frac{T_{max} - T_{min}}{n} \tag{11}$$

$$B_{T,uniform} = \frac{\Delta T_{uniform}}{n} \tag{12}$$

$$U_T = \sqrt{B_{T,uniform}^2 + B_{T,distribution}^2} \tag{13}$$

Sand Conductivity

A parametric study was run to see the effects each parameter had on the sensitivity of the sand conductivity uncertainty. The first set of parameters varied was the temperatures of the copper surface from -40°F (-40°C) to 32°F (0°C), aluminum surface from 4 to 6, and ambient from 20 to 38. Figure 31 shows the result for the temperature variations. The uncertainty was largely sensitive to the ambient temperature variation. The higher the ambient temperature was the higher the uncertainty was. Next was the aluminum, where the higher the aluminum temperature the better the uncertainty. The smallest sensitivity on uncertainty was the copper surface temperature, but as the copper surface temperature decreased the better the uncertainty. The sensitivity on uncertainty for copper and aluminum temperature variations was within 4% , which was not drastic. The results present an understanding that the larger the temperatures difference between the copper and aluminum surface the better the uncertainty for the sand conductivity becomes. Also, because the controlled heat source

is from the electric heater, the more uncontrolled heat gain from the ambient, caused by a higher ambient temperature results in a higher uncertainty. The optimal scenario is to maximize the temperature difference between the copper and aluminum while minimizing the temperature difference between the aluminum and ambient.

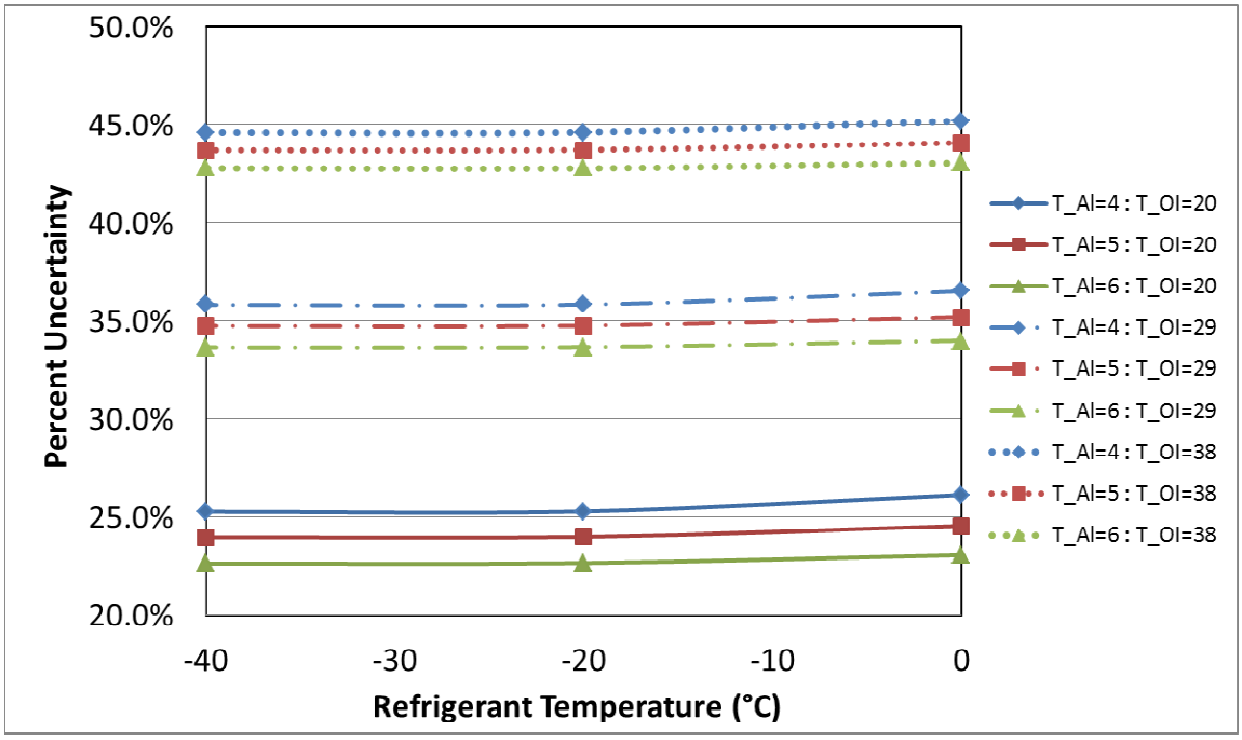

Figure 31 Uncertainty in the Sand Conductivity with Varying Temperatures

Because the rubber insulation around the heater during the calibration tests did not provide an adiabatic boundary and the uncertainty of the sand conductivity being sensitivity to variation in ambient temperature demonstrated in Figure 31, the 2nd parameter varied was the rubber insulation conductivity accuracy. The conductivity of this insulation was stated by the manufacture as 0.00004 kW/m-k and its accuracy was unspecified, so it was varied in parametric study from 0.000001 kW/m-k to 0.0001 kW/m-k. As expected a decrease in the accuracy of the insulation conductivity increased the uncertainty for the sand thermal conductivity. The trend coincided with the temperature variation results, as the heat transfer from the ambient increases the uncertainty increases, i.e. the possibility of

the rubber insulation being more conductive allows for an increased potential for more heat transfer. Figure 32 demonstrates this trend.

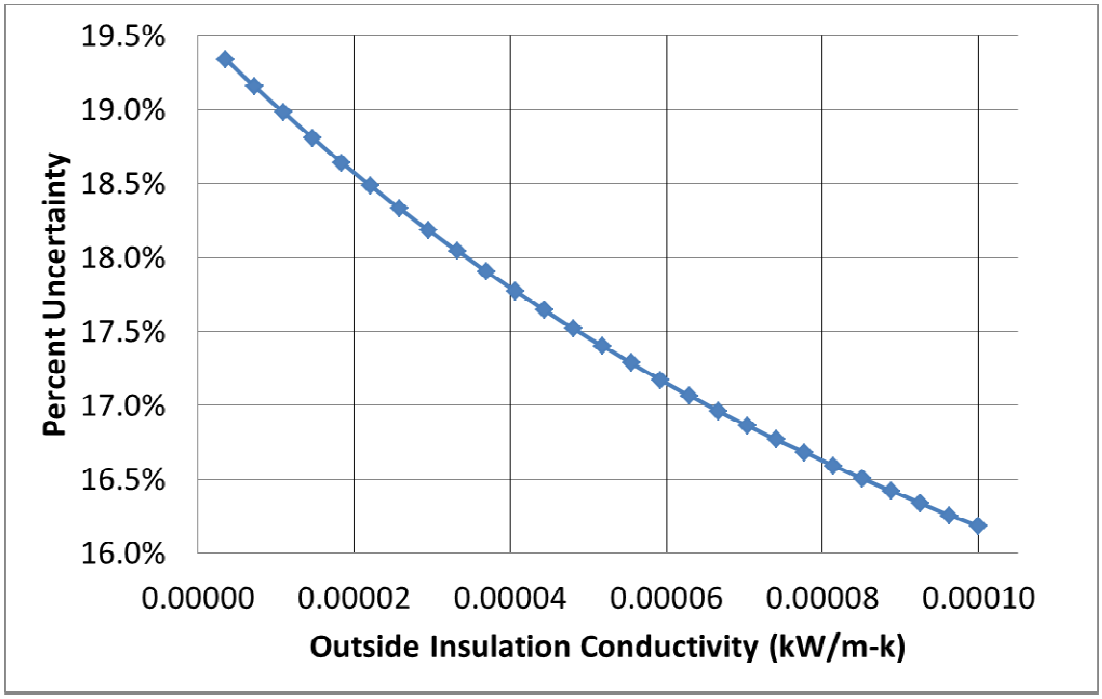

Figure 32 Uncertainty in the Sand Conductivity with Varying Rubber Insulation Conductivity

Since, the copper, sand, and aluminum conductivity are all lumped into one conductivity, considered as the sand conductivity; the last parameter checked was the addition of heat to the aluminum by the electric heater. It was found that the uncertainty due to the variation in the heater power was enormous compared to all other parameters. As demonstrated in Figure 33, the heater power increased the sand conductivity uncertainty decreased. When the heater applied no heat the uncertainty is almost 140%, at 10 watts it reduces to 40% and at the maximum heat considered of 40 watts the uncertainty drops to approximately 15%. The trend demonstrates an exponential decay.

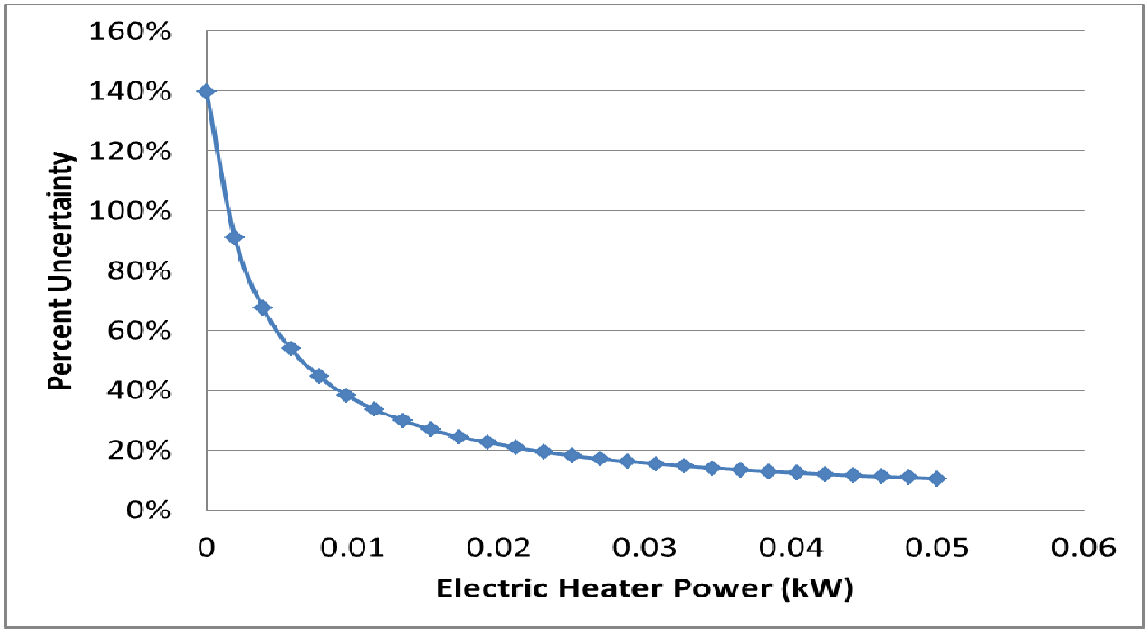

Figure 33 Uncertainty in the Sand Conductivity with Varying Heater Power

There are two reasons why the uncertainty of the sand conductivity was drastically sensitive to the heat applied by the heater. First, the watt transducer used to measure the power of the heater had a measuring range of 0 to 500 watts. Since maximum watt the experiment could possibly achieve is 40 watts, the results from using the transducer are at the low end of its operating range. Second, at low heater power, the heat gained from the ambient became a higher fraction of the total heat gain and as shown in Figure 31 caused an increase in the uncertainty.

Test Insulation

Once the uncertainty in the sand conductivity is known, a second parametric study was run to find the sensitivity of parameter variation to the uncertainty in the test insulation's thermal conductivity. The first parameter varied was the copper surface temperature. It was found and is shown in Figure 34, as the copper surface temperature was decreased the uncertainty decreased. This relates to a trend seen earlier for the uncertainty in the sand conductivity; as temperature difference increased between the copper and aluminum surface, the uncertainty decreased.

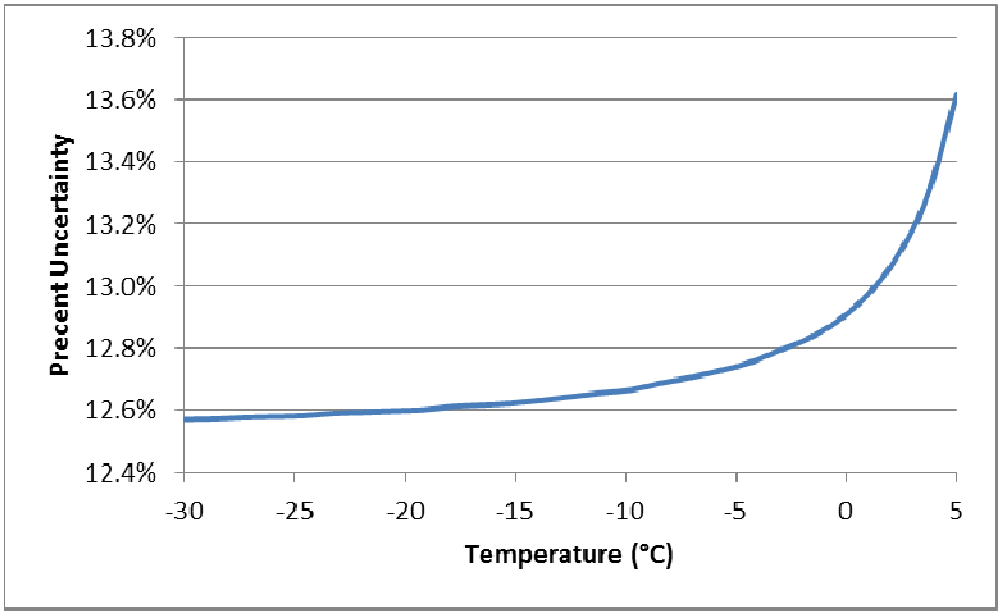

Figure 34 Uncertainty in the Test Insulation Conductivity with Varying Copper Surface Temperature

The next parameter varied was the ambient temperature. This produced a trend opposite compared to the effect of ambient temperature on the sand conductivity uncertainty. The reason this is counter intuitive compared to previous, was because before an electric heat was being used to apply heat and any extra heat from the ambient caused more uncertainty in the experiment. Now the ambient was acting much in the same way as the heater did in the previous experiment. The increase in ambient increased the temperature difference across the insulation and sand which decreased the uncertainty. Increase in temperature difference across the sand was caused by lowering the copper surface temperature to maintain the desire constant condition on the aluminum surface at 40°F (4.55°C). The overall sensitivity of varying the ambient only resulted in uncertainty deviation of only1%. This trend is demonstrated in Figure 35.

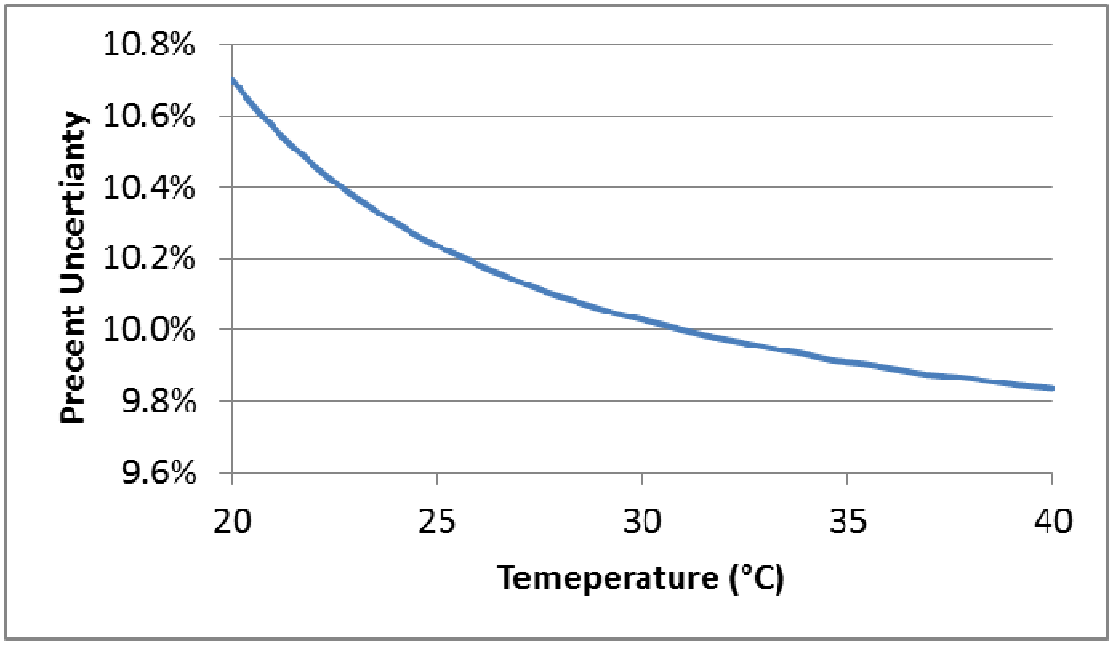

Figure 35 Uncertainty in Test Insulation Conductivity with Varying Ambient Temperature

Two insulation thicknesses were tested and the thickness sensitivity on the uncertainty of test insulation conductivity was of great interest. Figure 36 shows that as the insulation thickness increased the uncertainty decreased. The overall effect of the uncertainty due to thickness is small, less than 0.3% changes over the entire range of variations. Some of the effects of increasing the thickness not captured, as the thickness increased the heat transfer across the insulation decreased resulting in a large uncertainty change of 0.3%.

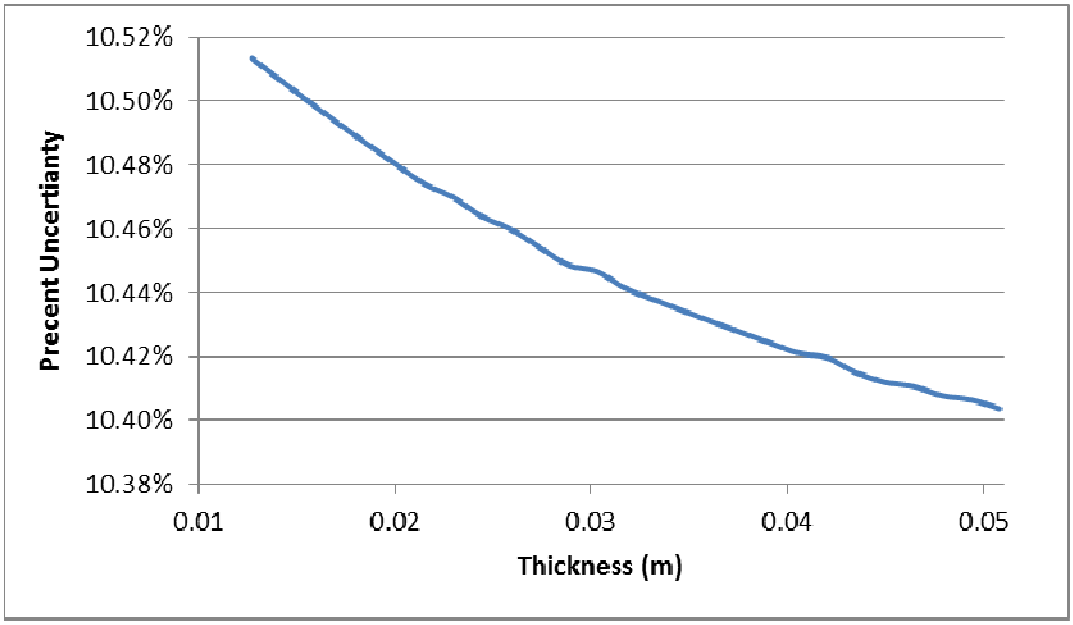

Figure 36 Uncertainty of the Test Insulation Conductivity with Varying Insulation Thickness

A lot of work went into finding the uncertainty of the sand conductivity and as demonstrated earlier the uncertainty varied drastically with power of electric heater. Therefore, the last parameter varied in the study was the uncertainty of the sand conductivity. It was found and is demonstrated in *Figure 37* that the uncertainty of the test insulation conductivity was drastically sensitive to the uncertainty of the sand conductivity. As the uncertainty of the sand conductivity decreased the uncertainty for the test insulation conductivity decreased. Basically it had a one to one relationship until the uncertainty of the sand conductivity dropped below 5%.

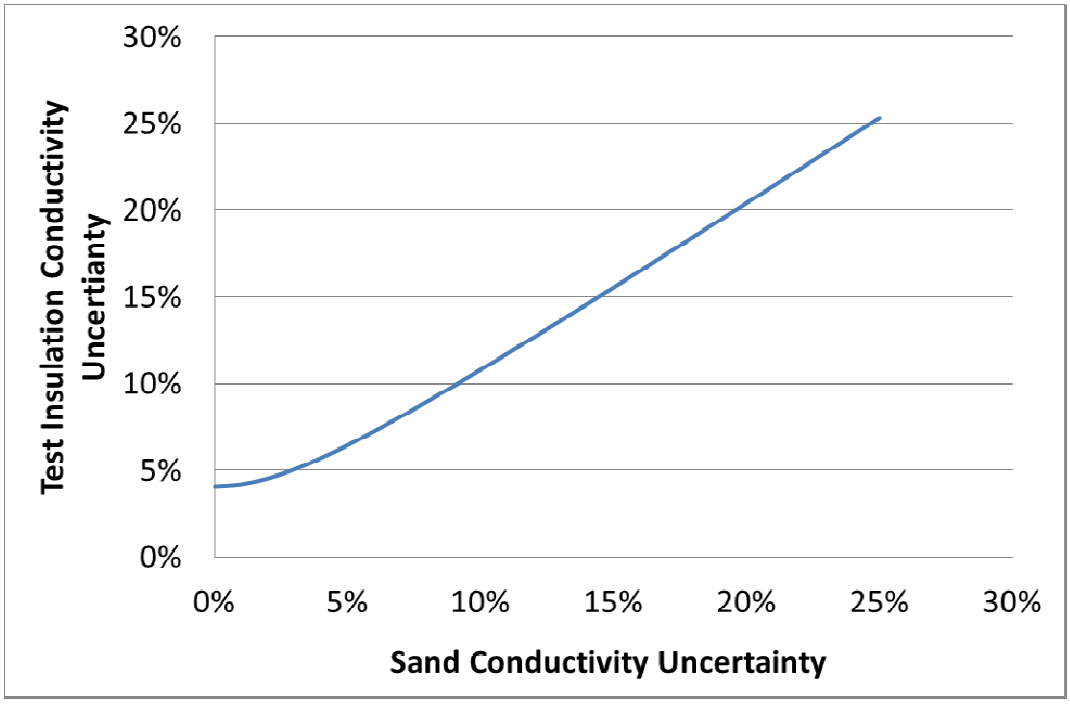

Figure 37 Uncertainty of the Test Insulation Conductivity with Varying Uncertainty of the Sand Conductivity

In turn, the uncertainty of the sand conductivity had a huge contribution and was the dominating parameter on the uncertainty of the test insulation conductivity. This falls back on the power applied during calibration test and insuring extra care is taken in determining the sand conductivity. The extra care will result in minimizing sand conductivity uncertainty, which will eventually produce more accurate results for the test insulation conductivity.

CHAPTER VI

FINDINGS

Testing for Performance Rating of Unitary Rooftop Units

Calibration

The energy performance, capacity, flow rates, and external static pressure of a 11 tons (39 kW) of refrigeration rooftop two stage cooling air conditioner was experimentally measured by two different outside laboratories: one was from a certified agency for energy performance rating of rooftop units and the other was the in-house laboratory of the unit manufacturer. The unit was tested in these laboratories at an outdoor temperature of 95°F (35°C) and indoor conditions of 80°F (26.7°C) and 67°F (19.4°C) dry and wet bulb temperatures, respectively. The unit was operated with both cooling stages activated and the unit blower was set to supply maximum air flow rate with an external static pressure drop across the unit indoor coil maintained at ~0.3 inch H_20 (71.2 Pa). This rooftop unit was placed in our new facility and this test was replicated to verify and calibrate our sensors and signals processing. These test conditions are considered the AHRI "A Test" and unit designed operating condition by the manufacturer. The test procedure in our facility consisted of setting the indoor and outdoor room to a desired ambient condition with the unit operating at a steady state. Once the set point conditions were met and maintained for a period of sixty minutes, data recording started at a sampling rate of two seconds for an additional sixty minutes. During this two hour period the dry bulbs in each room were maintained within ±0.4°F (±0.2°C) of the set points, and the indoor wet bulb was maintained within ±0.8°F (±0.4°C) of the set point. The results obtained from our measurement were within 5% of the same capacity and 2% of the air flow rate with respect to the measurement obtained by the outside laboratories. These findings confirmed that our facility was operating properly and we were able to accurately measure the capacity of the rooftop unit with respect to the technical

information from other external sources. We used these measurements as benchmark for our facility and to configure the position of the sensors, to fine tuning our operational procedures, and to take corrective actions that avoid potential sources of systematic errors during the energy and capacity measurements of the rooftop unit.

Steady State Test

After testing the rooftop unit at the design conditions and after validating the measurements for our new facility, a series of steady state experiments were conducted at different ambient outdoor temperatures and at selected indoor conditions. The ambient outdoor temperature varied from 67°F to 115°F (19.4°C to 46.1°C) capturing the unit real life service exposure. The indoor conditions were altered to investigate the unit thermal energy characteristics when subjected to different internal loads and different sensible to latent heat capacity factors with respect to the one at design conditions. A series of five tests were performed using the same test procedure described in the section above with the blower adjusted to maintain the same supply dry bulb temperature as the one measured at the design conditions. For both design and off design conditions, the COP was calculated at each data sample using the Air Enthalpy Method (ASHRAE 2009), and the instantaneous COPs were then averaged for the sixty minute period to obtain a single value. From these full load steady state tests a few observations can be drawn and the test results are summarized in Figure 38. The COP and capacity are considerably different as both outdoor and indoor conditions deviates from the design conditions. Some of these trends were expected. For example as the ambient outdoor temperature increases then the COP of the unit decreases.

An interesting outcome from these tests, also shown in Figure 38, is the result of the different ratio between sensible and latent capacities of the unit. One could observe a 12% degradation in the COP when only the humidity in the indoor room is decreased from 67°F to 63°F (19.4°C to 17.1°C) wet bulb temperature, that is, from 50% to 40% R.H in the indoor return air. This is represented by the data points at the outdoor temperature of 95°F (35°C). At the outdoor temperature of 67°F (19.4°C) we observed a

similar degradation in the COP from about 4.5 to 3.8, that is, more than 15% due to both lower indoor sensible and latent loads. These variations in the performances might be due to the variation of the sensible heat factor (SHF). The design SHF at 80°F/67°F (26.7°C/19.4°C) DB/WB indoor temperature and at 95°F 35°C outdoor temperatures was measured and it was about 0.66. At 67°F (19.4°C) outdoor temperature, if the indoor conditions were 80°F/63°F (26.7°C/17.1°C) DB/WB then the SHF increased to about 0.84 while if the indoor conditions are reduced to 67°F/53°F (19.4°C/11.6°C) DB/WB the SHF resulted of about 0.95. The latter SHF was further away from the SHF calculated at design conditions and as the SHF departed from the one at design conditions both COP and capacity was significantly penalized. This phenomenon could be observed by the data series at 67°F (19.4°C) and at 95°F (35°C) outdoor temperatures of Figure 38. When the unit operates at off-design conditions both capacity and COP deviated from the ones at design conditions.

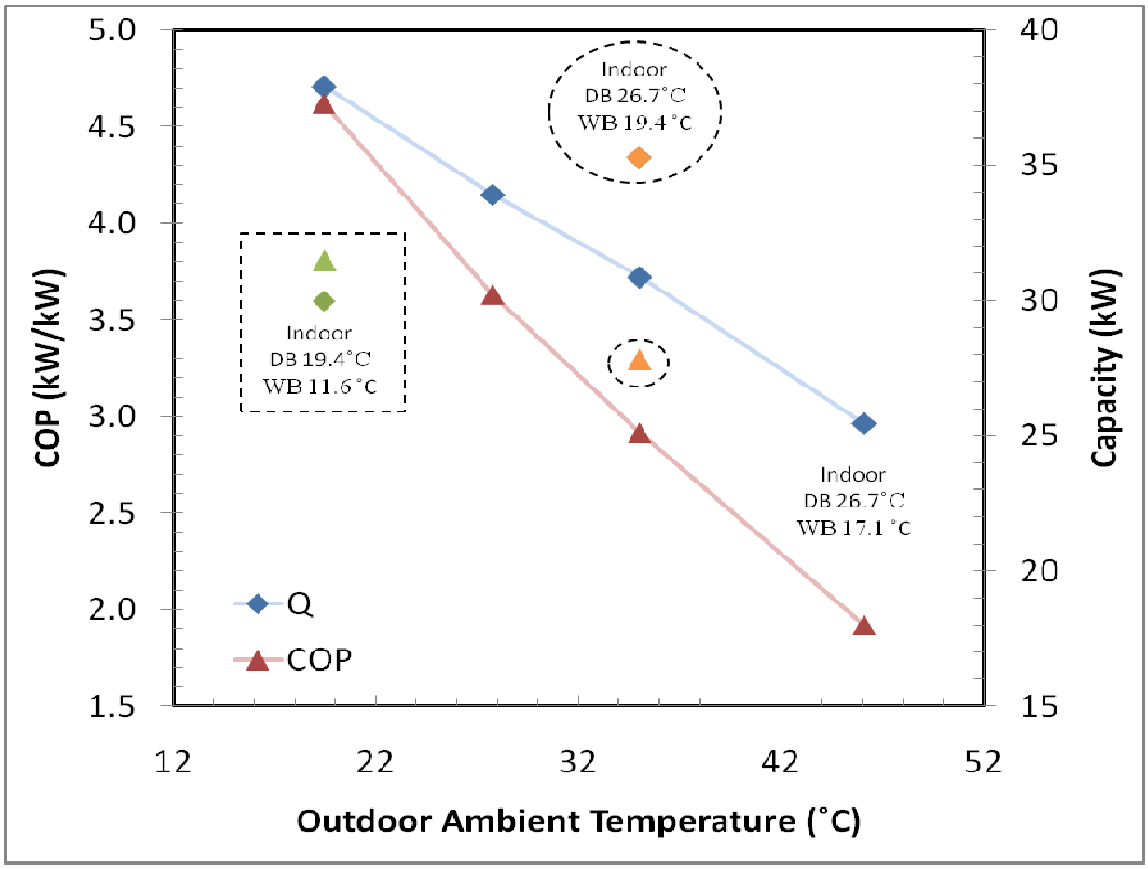

Figure 38 Effects of full load COP if both ambient outdoor temperature and indoor thermal loads vary.

Most testing facilities do not have the full ability to test at partial load due to the fact that the unit must be cycled on and off to meet partial loads conditions. To determine the partial load COP, standardize tests that involve multiple steady state tests at different ambient conditions, are commonly adopted. These tests are outlined in details in the ANSI/AHRI 340/360-2007 [3]

From the measurements during these tests, the integrated coefficient of performance (ICOP) is calculated as indicated in Equation (14) below.

$$ICOP = \frac{0.20*COP_{100\%}+0.617*COP_{75\%}+0.238*COP_{50\%}+0.125*COP_{25\%}}{3.41} \quad (14)$$

In our facility the steady state tests were performed as described next and the ICOP was determined for this rooftop unit. The rooftop unit had two refrigeration circuitries in parallel and this configuration resulted in an operational mode of about 50% or 100% loads without cycling. To find the COP at 75% part load, a full load test at 95°F (35°C) and a test operating only a single compressor at approximately 57% load were performed at an outdoor ambient temperature adjusted to 71°F (21.7°C), as specified by the standards. Interpolation between these two sets of data was used to determine the adjusted COP for 75% part load conditions.

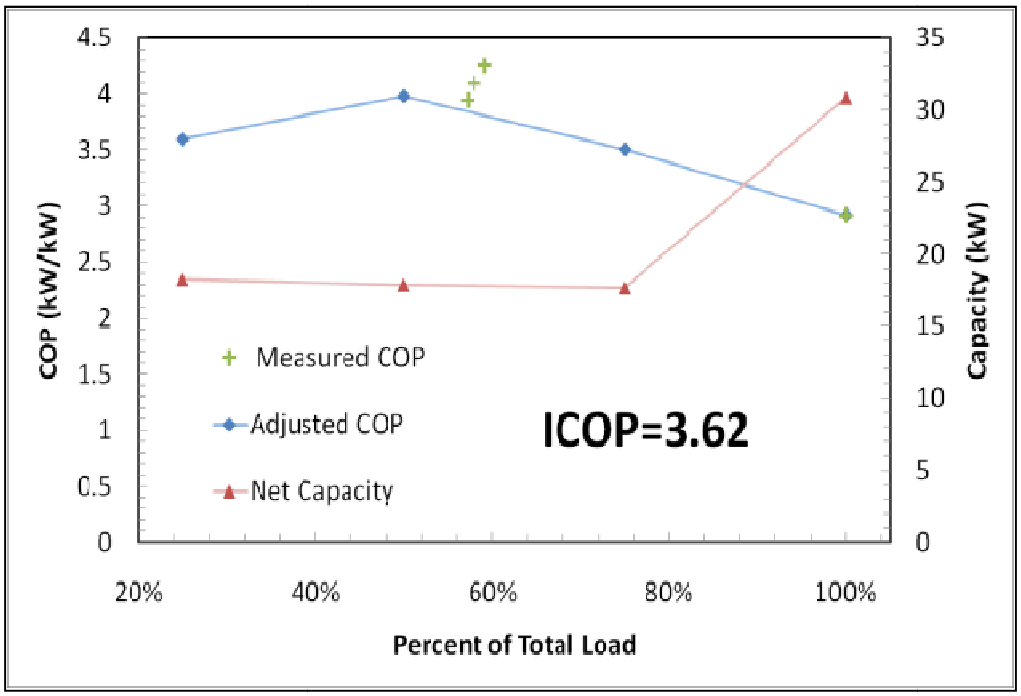

Figure 39 Measured COPs, Adjusted COPs, Net capacities, and ICOP for a rooftop unit operating at different load conditions

The adjusted COP accounted for the cycling of compressors for loads that were not equal to the unit incremental steps of capacities. Two more additional tests were performed to determine the ICOP. These tests were operated with only a single compressor at 68°F (20°C) and 65°F (18.3°C) ambient outdoor temperatures for 50% and 25% part load conditions, respectively. The actual single stage capacity was approximately 57% of the full load capacity, which causes the 50% and 25% COPs to be more complicated to determine.

Table 4 Matrix to estimate the Integrated Coefficient of Performance (ICOP)

Integrated Coefficient Of Performance											
Cooling Stages	Ambient	Theoretical Load	Actual Load	Net Capacity	Total Power	Power (P_{IF}+P_{CT})	Power (P_{IF}+P_{CT})	COP	LF	C_d	Adjusted COP
[-]	[C]	[%]	[%]	[kW]	[W]	[W]	[W]	[-]	[-]	[-]	[-]
2	35.03	100.00	100.00	30.86	10587	750.00	9837.94	2.92	1.00	1.00	2.92
1	21.67	75.00	57.25	17.67	4484	361.16	4123.19	3.94	Interpolated		3.50
1	20.00	50.00	57.93	17.88	4369	361.16	4007.89	4.10	0.86	1.02	3.98
1	18.33	25.00	59.18	18.27	4297	361.16	3936.00	4.25	0.42	1.08	3.59

From these two sets of data the Load Factor (LF) and the Degradation Coefficient (C_d) were calculated and are shown in Table 4. These coefficients allow the measured COPs to be corrected to adjusted COPs, which were then used to calculate the unit ICOP as shown in Figure 3. The peak efficiency at part load for this unit was estimated to be at about 50% part load conditions.

Cycling Test

A unique capability of our new psychrometric facility is that the rooftop unit can be studied when the compressor cycles on/off, during cyclic test conditions. Facilities that are capable of testing in cycling conditions are limited to only maintaining the dry bulb temperature during these tests. The main reason is because the wet blub has a large thermal inertia and cannot be adjusted quickly enough to counteract the compressor cycling. As preliminary tests, we considered same testing procedures as adopted by other facilities in USA and only the dry bulb temperature was maintained during our cycling tests despite the chamber potentials to also maintain the wet bulb temperature in cycling conditions. A relationship between ratio of COP during cycling tests (COP_{cyc}) and corresponding COP at steady state (COP_{ss}) proposed by Didion (Didion 1979) was used in this work to calculate the COP during cycling operating

conditions. The Equation (15) below states that the ratio of the COPs during dry and wet tests is maintained, that is,

$$\left|\frac{COP_{cyc}}{COP_{ss}}\right|_{Dry} = \left|\frac{COP_{cyc}}{COP_{ss}}\right|_{Wet} \qquad (15)$$

This approach provides an alternative way to calculate the COP of a unit at different part load conditions and we used this approach to verify the ICOP. Three tests were performed to determine the COP at a 25% part load conditions by allowing the unit to cycles on and off. This was done according to the standards by using only one stage of the compressor and at 82°F (27.8°C) and 80°F (26.7°C) for the outdoor and indoor temperatures, respectively. The indoor room was maintained at 63°F (17.2°C) and 57°F (13.9°C) wet bulb temperature for steady state wet and dry tests, respectively. Only the sensible capacity of the coil was used to estimate the COP_{ss} in dry conditions. A different test procedure was needed for the cycling tests, which were performed by bringing the unit to steady state for an hour using only one stage of the compressor and then cycling that stage for another hour. The compressor was cycled on and off at 15 minute intervals and Figure 40 shows the conditions the unit experienced while cycling.

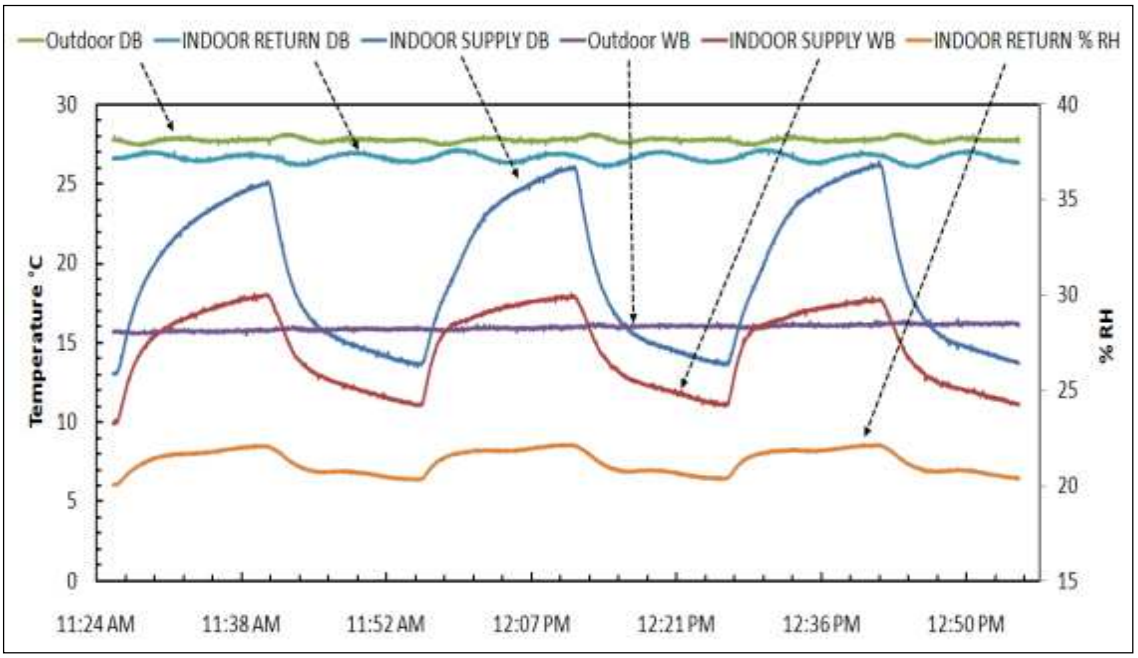

Figure 40 Temperatures during a cycling test

Data were continuously recorded at a sampling rate of two seconds for at least one hour during the cycling period. To determine the COP_{cyc} the total power and cooling capacity were averaged over the entire test. The COPs for all three tests were used to determine the COP for cycling the unit under wet coil conditions, according to Equation (16) below:

$$\left|\frac{3.19}{3.03}\right|_{Dry} = \left|\frac{COP_{cyc}}{3.38}\right|_{Wet} \quad \Rightarrow \quad COP_{cyc} = 3.55 \tag{16}$$

It should be noticed that COP_{cyc} calculated according to this approach was within 1% difference with respect to the adjusted COP calculated for the 25% part load conditions as indicated in Table 1 (~3.59). This comparison is a further verification of the accuracy of our measurements during the cycling tests.

Transient Test

The new psychometric chamber is capable of simulating and virtually reproducing any temperature profile for the outdoor climate and thermal load profiles for the indoor environments automatically. This might be useful for estimating a comprehensive figure of merit, referred in this paper as to comprehensive COP, of the rooftop unit. This figure of merit should provide a realistic measure of the average energy performance and cooling capacity of the rooftop unit subjected to regional climatic conditions. To explore this concept we applied a temperature profile for a typical day based on the design temperature for Fort Riley, Kansas (USA) and the daily variation recommended in the climatic design information in the chapter of the ASHRAE Handbook Fundamental (ASHRAE 2001).

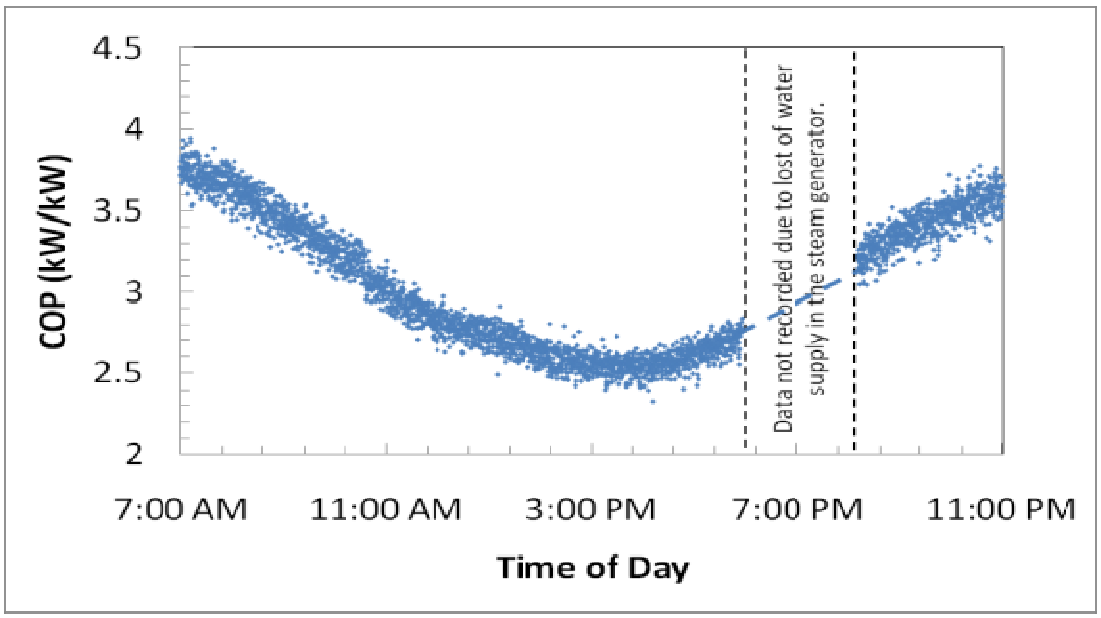

Figure 41 COP for a Fort Riley, (Kansas, USA) summer day simulated inside our psychrometric chamber

The indoor environmental temperature and humidity were kept constant during this test. The rooms were pre-conditioned to the initial set points for sixty minutes then a sinusoidal temperature profile was applied to the outdoor room to replicate a summer day in Kansas. Data were recorded at a sampling rate of fifteen seconds for a total of a sixteen hour period. The unit was run at maximum blower speed and with two compressors enabled while maintaining an external static pressure of 71.2 Pa. The temperature profiles are shown in

Figure 42. As expected an increase of the outdoor temperature throughout the day resulted in a decrease of the COP, which was the lowest when the climatic conditions were around the design energy performance rating conditions of the unit.

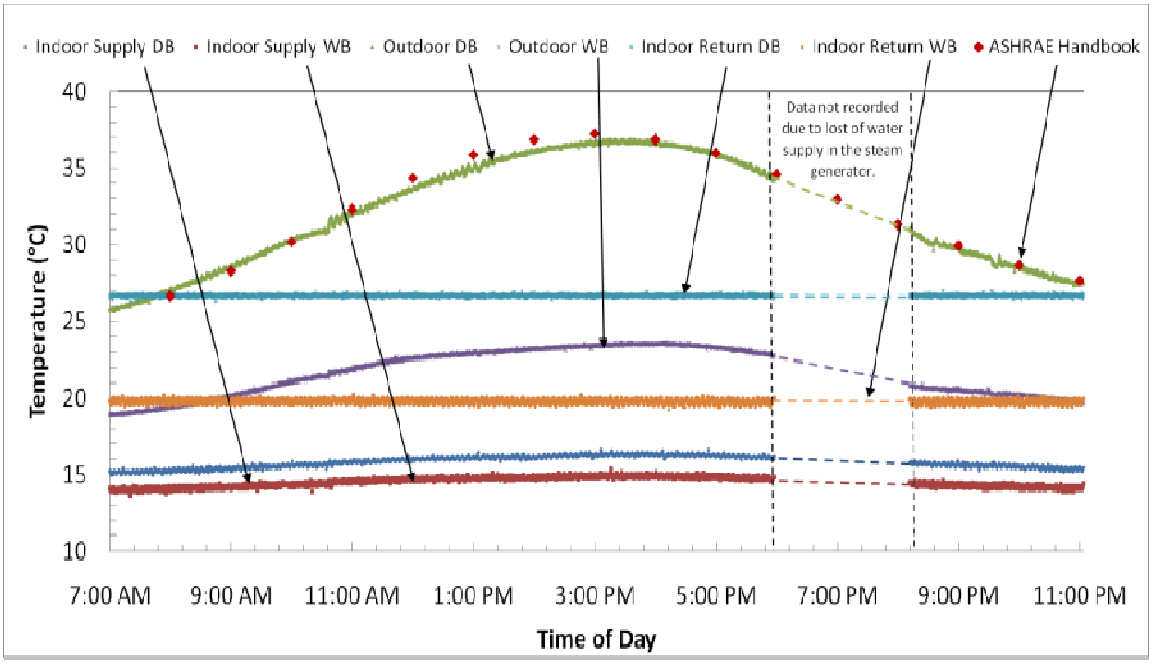

Figure 42 Temperatures during a test with variable outdoor climate

Lessons Learned

The Coefficient of Performance (COP) is a useful way of relating the energy efficiency of HVAC unitary equipment. A challenge with the next generation of air conditioning systems and unitary equipment arise because COP depends on numerous factors. This thesis describes some approaches available in the literature to evaluate the actual energy performance and capacity of a rooftop unit when operating at design, off-design, part load, and variable climatic conditions. Using a new low temperature psychrometric facility with 20 tons (70 kW) of refrigeration this paper introduces an example for which these methods were applied. An integrated COP was used to quantify the unit energy performance at part load conditions from 25% to 100%. Finally, a comprehensive performance figure of merit was introduced to estimate an average COP of the rooftop unit when subjected to regional, variable, and periodic climatic conditions.

Pipe Insulation Tester

Validation

The PIT apparatus was validated with two pipe insulation systems, cellular glass and Polyisocyanurate (PIR), to benchmark the measurements against data available in the public domain The measurements were taken at several insulations average temperatures to allow extrapolation of the thermal conductivity for temperatures slightly above room ambient. This was done because the data available in the public domain these two materials is at above room ambient temperature. The extrapolated estimates from the measurements for above ambient temperatures were compared with the measured thermal conductivity of flat blocks of the same material (public domain data). Also for the Polyisocyanurate, the same batch of insulation material in flat slab from was tested at another laboratory for comparison. (Oak Ridge National Labs). The comparison was done to verify that the thermal conductivities measured with the new apparatus presented were of the same order of magnitude as the data obtained from flat blocks. It was expected some deviations of the thermal conductivities would be present due to the radial configuration and split joints.

Cellular glass pipe insulation

Three thicknesses of cellular glass pipe insulation were selected for validation of the test apparatus: 1 inch (25.4 mm), 1 ½ inch (38.1 mm) and 2 inch (50.8 mm) wall thicknesses. The insulation samples were provided in length of 2 ft (609.6 mm) section (ASTM 2007), this is due to manufacturing constraints. Test specimens were machined to fit and staggered when installed on the Aluminum pipe, preventing air circulation through the gaps. All the joints were sealed with joint butyl rubber sealant (BOSS 368), which provides excellent adhesion in between the C-shells of the pipe insulation.

Since cellular glass material is practically not subjected to aging effect, the three samples were tested at different time and with two techniques for measuring the surface temperature of the insulation as listed in Table 5. Figure 43 compares the measured thermal conductivity versus insulation average temperature

and at different thickness of cellular glass pipe insulation systems. The error bar in the data represents the maximum deviation of experimental data from a linear fit correlating all the data. The experimental data from the new test apparatus agreed within ± 3% compared to the manufacturer's data, whose value of thermal conductivity was obtained for flat block configuration. The plots in Figure 43 were obtained by attaching the thermocouples on the exterior insulation surface using small neoprene adhesive square strips and by using droplets of silicone gel covering the tips of the thermocouples. These two techniques produced quite different results as shown in Figure 43. Due to the open-cell structure of neoprene, the local thermocouples on the exterior of the pipe insulation surface measured an average temperature between local ambient air temperature and local surface temperature of the material. From comparisons with measurements without any neoprene strips on the top of the thermocouple it was concluded that the local temperature was weighted toward the ambient temperature rather than the pipe surface temperature. On the contrary, the measurements obtained using silicone gel droplets as surface adhesive covering the tips of the thermocouples seemed to be more accurate because the local surface temperature of the exterior of the insulation was lower than the ambient temperature of the surrounding air. Silicone gel used in these tests had a low thermal conductivity and thus act as an adhesive and as a large thermal barrier between the tip of the thermocouple and its immediate air film around the insulation. The measurements of the thermal conductivity of the 1 inch (25.4 mm) wall thickness cellular glass insulation specimen were repeated four months later using the silicone gel method and the average thermal conductivity was observed to be about 4.5% higher than the previous tests in which neoprene was used. This was explained because of the effect of the thermocouple attachment method and of the joint sealant thickness, which slightly increased the inner diameter of the insulation creating air pockets for the second tests. It is concluded that the silicon method produced more accurate and more repeatable results. Thus, for all other insulation materials the measurements adopt silicone gel for attaching the thermocouples to the exterior surface of the pipe insulation.

Table 5: Validation Experiment Results of Cellular Glass

Cellular glass thickness Inch (mm)	Days after calibration of PIT	Thermocouple attachment	$k_{pipe,insulation} = a \cdot T + b$ Btu-in/hr- ft^2-F (W/m-K)	
			a	*b*
1 (25.4)	39	Neoprene	0.0003 (0.00005)	0.2695 (0.041)
1.5 (38.1)	78	Neoprene	0.0017 (0.0004)	0.1909 (0.0353)
2 (50.8)	140	Silicone	0.003 (0.0008)	0.0946 (0.0273)
1 (25.4)	154	Silicone	0.001 (0.0003)	0.2425 (0.0394)
Manufacturer	-	-	0.0006 (0.0001)	0.2498 (0.0386)

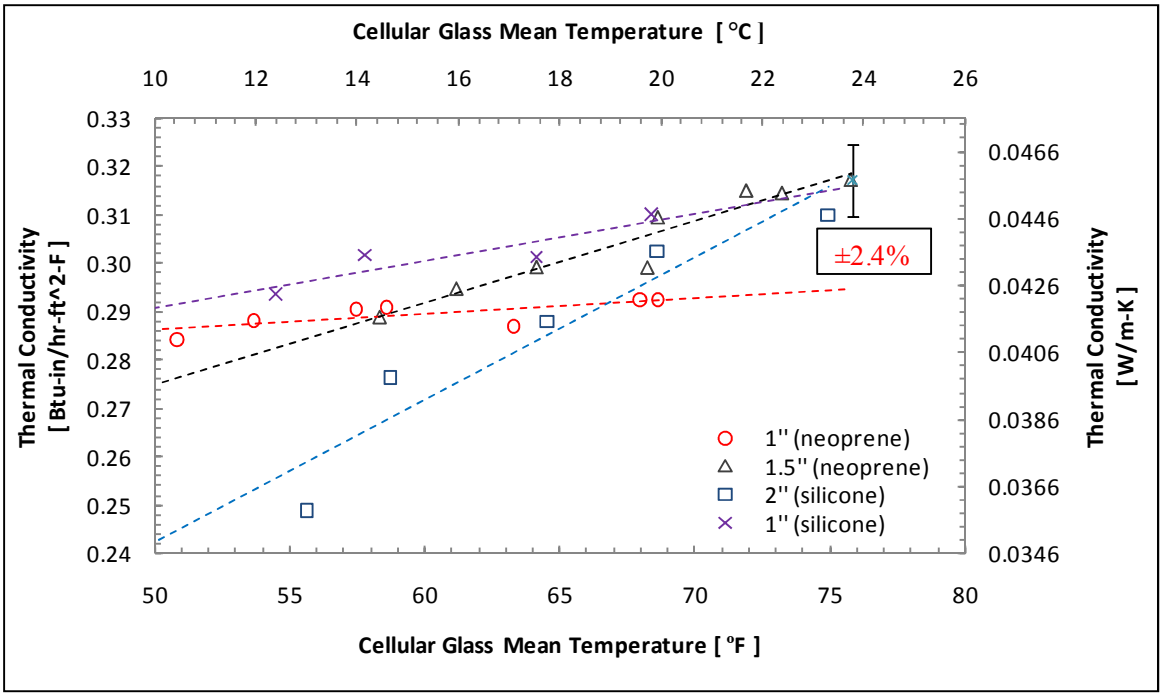

Figure 43: Thermal conductivity of cellular glass pipe insulation

Polyisocyanurate (PIR) pipe insulation

A 1 inch (25.4 mm) and a 2 inch (50.8 mm) wall thickness of Polyisocyanurate (PIR) pipe insulation systems were used in the second series of tests to validate the PIT apparatus. Unfortunately, PIR is subjected to aging phenomena and the thermal conductivity is also function of time. To obtain a fair comparison, radial C-shells and flat blocks were taken from the same batch at the same time and were tested at approximately the same time. The flat blocks were tested at Oak Ridge National Laboratory. The results of the experiments are given in Figure 44 and the correlations for the pipe insulation thermal conductivity are given in Table 6. The 2 inch (50.8 mm) wall thickness insulation specimen was very sensitive to the temperature when compared to the 1 inch (25.4 mm) wall thickness PIR insulation specimen. A possible reason might be due to the fact the PIR had extremely low thermal conductivity and the radial heat flux for the 2 inch wall thickness was too low to be accurately measured with the current PIT device were the Aluminum pipe surface temperature must be maintained at 40°F (4.5°C). In order to increase the accuracy of the measurements a larger radial temperature gradient would be necessary but changing the Aluminum pipe surface temperature would introduce more complexity for the comparison and it was outside the scope of this work. As shown in Figure 44 there is some difference between the measured value of thermal conductivity of the 1 inch wall thickness PIR pipe insulation and the value obtained with the flat block configuration. The difference was up to 8.8%. The edge effects of the C-shell longitudinal split joints and the presence of joint sealants along longitudinal joints of the C-shells could cause this difference.

Table 6: Validation Experiment Results of PIR

Cellular glass thickness (inch)	Days from calibration test	Thermocouple attachment	$k_{pipe,insulation} = a \cdot T + b$ Btu-in/hr- ft^2-F (W/m-K)	
			a	*b*
1	108	Silicone	0.0004 (0.0001)	0.1748 (0.0269)
2	120	Silicone	0.0032 (0.0008)	-0.0284 (0.0107)

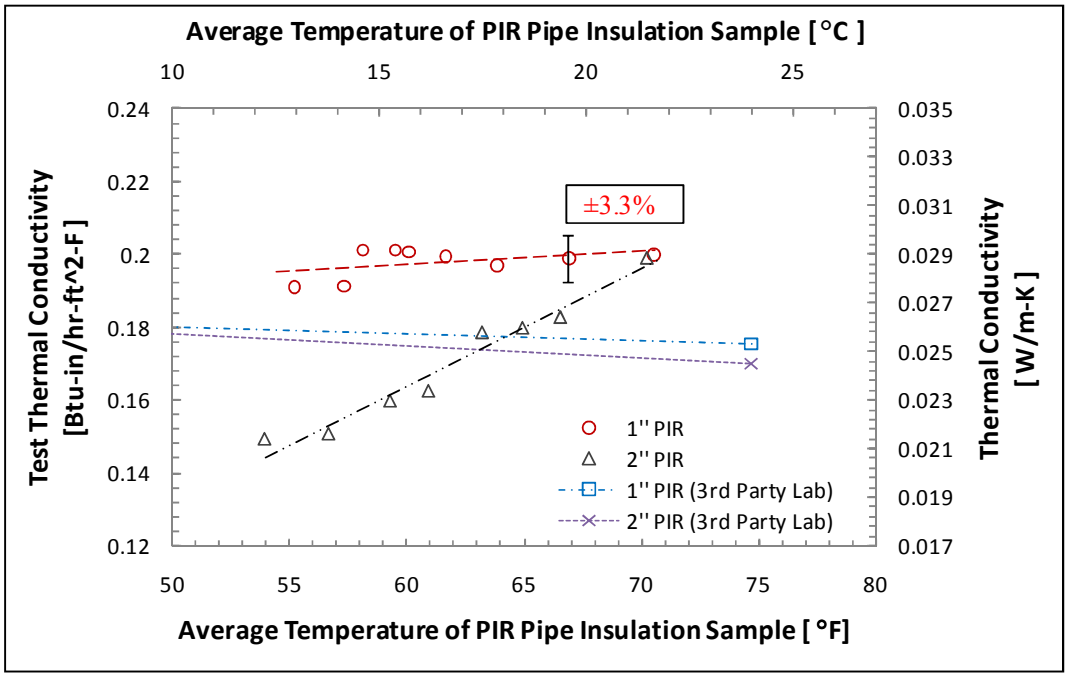

Figure 44: Thermal conductivity of PIR pipe insulation

Dry Test

The thermal conductivity of fiberglass, flexible elastomeric and phenolic pipe insulation systems was measured in dry non-condensing ambient conditions. The nominal insulation wall thickness was 2 inch (50.8 mm) for all three specimens and the average insulation temperature was varied from 57° to 74 °F (14° to 23 °C). Correlations of the pipe insulation thermal conductivity were developed based on insulation specimen average temperature and wall thicknesses. The thermal conductivity of these three insulation systems varied linearly as shown in Figure 45 and the coefficients of the linear correlations are given in Table 7. All three sets of experimental data fit well a linear interpolation curve fit with a maximum deviation of less than ±2.2%. Increasing thermal conductivity was observed if the temperature increases. Compared to ASTM standards and manufacturer or catalog data presented for fiberglass, flexible elastomeric and phenolic pipe insulation, we observed some differences which could be explained with radial configuration, aging effects, and the presence of joint sealant on the longitudinal butt joints.

Table 7: Thermal Conductivities of Pipe Insulations under Dry Condition

Test Samples	$k_{pipe,insulation} = a \cdot T + b$ Btu-in/hr-ft^2-F (W/m-K)	
	a	*b*
Fiberglass	0.0004 (0.00009)	0.2125 (0.0323)
Flexible Elastomeric	0.0005 (0.0001)	0.2144 (0.0334)
Phenolic	0.0012 (0.0003)	0.1217 (0.0233)

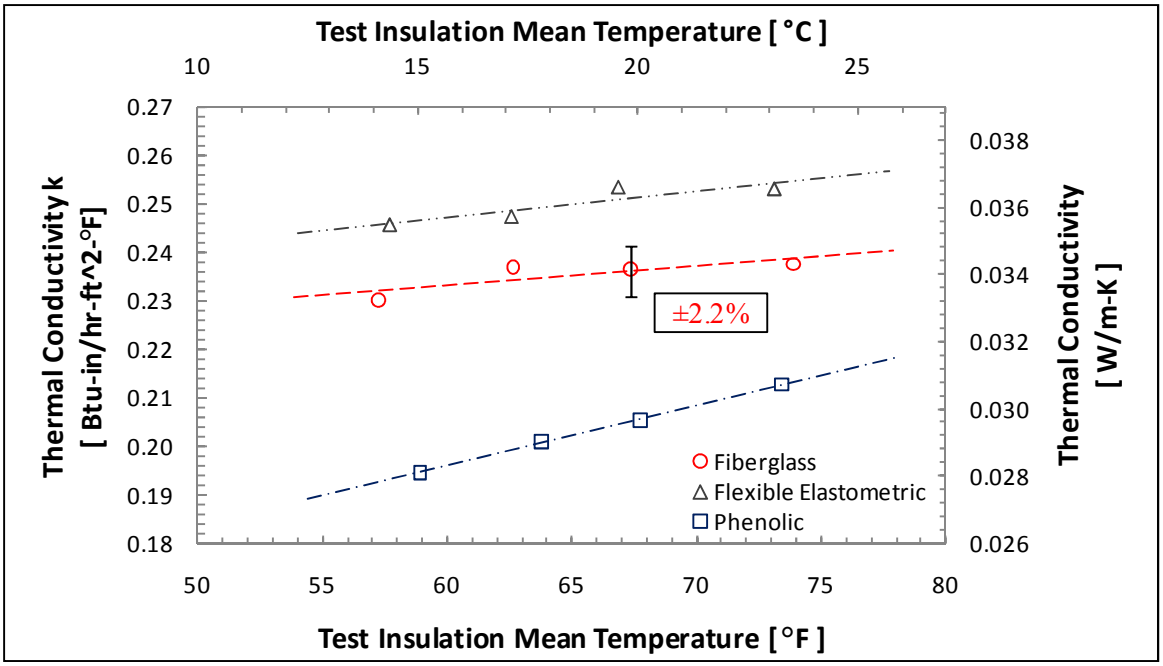

Figure 45: Thermal conductivities of fiberglass, flexible elastomeric and phenolic pipe insulation systems

Wet Test

The thermal conductivity of phenolic pipe insulation systems was measured in condensing ambient condition for a period of 24 days. The nominal insulation wall thickness was 2 inch (50.8 mm) and the average insulation temperature was 67.5°F (19.7 °C). Presented in Figure 46 and Figure 47 are the comparisons between thermal conductivity for phenolic pipe insulation with time and amount of moisture ingression. It is shown, an increase in moisture inside the insulation causes an increase in thermal conductivity. It is also shown; the moisture ingression is generally an exponential trend reaching an isotonic value over time. The thermal conductivity of phenolic pipe insulation exposed to 95°F (35°C) and 95% RH for 24 day increased by 1.6 times the dry thermal conductivity.

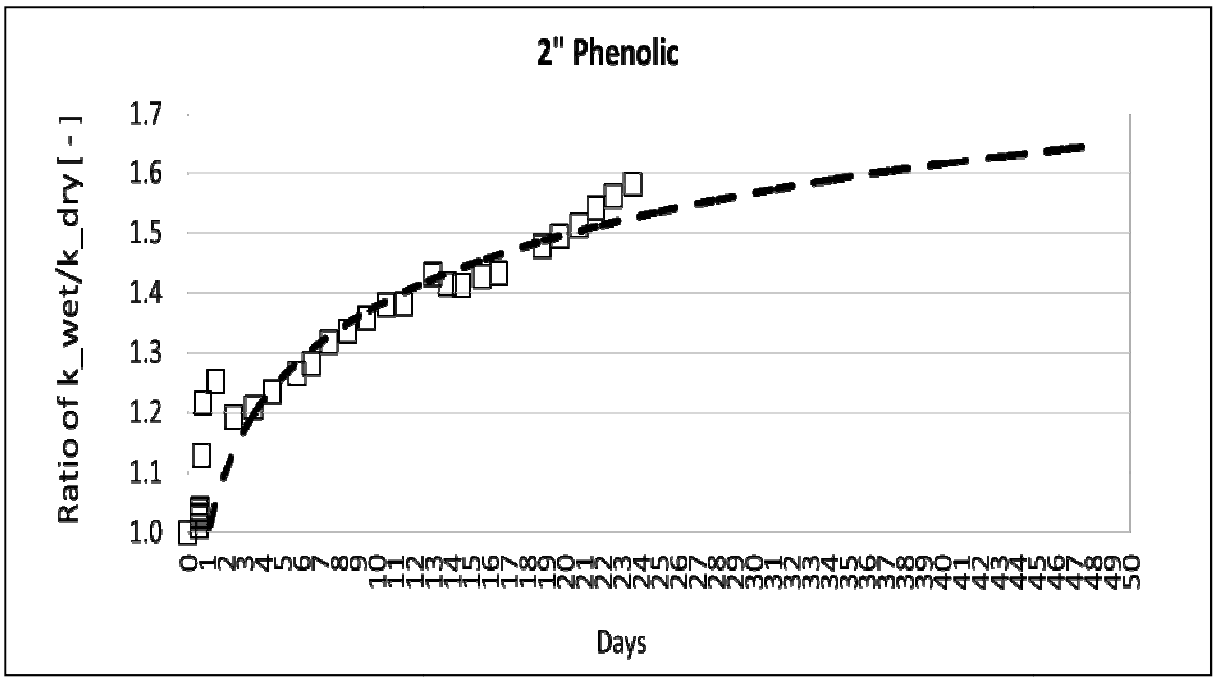

Figure 46 Thermal Conductivity of Phenolic Exposed to High Temperature and Humidity for 24 Days

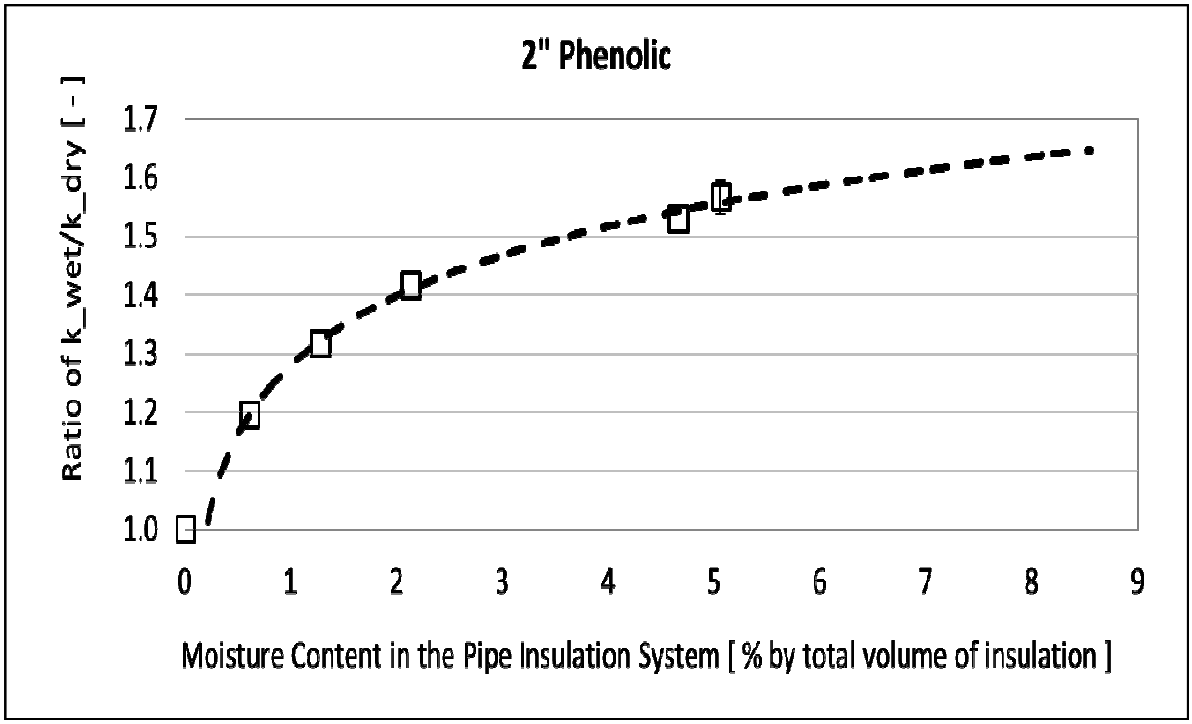

Figure 47 Thermal Conductivity of Phenolic with Moisture Ingress

Lessons Learned

A PIT apparatus to measure the thermal conductivity of mechanical pipe insulation systems at below ambient temperatures was developed. The test set up was validated by using two types of pipe insulation systems as benchmark and the thermal conductivity was measured for average pipe insulation temperature varying from 50 to 75°F (10 to 24°C). Through a series of extensive calibration procedures the uncertainty on the pipe insulation thermal conductivity was estimated to be within ±6% and the measured thermal conductivity was within 15% with respect to the data available in the public domain. The deviation was mainly due to radial configuration, edge effects, and the presence of joint sealants along the longitudinal butt joints of the pipe insulation systems. The thermal conductivity of pipe insulation systems with 2-inch nominal wall thickness was also presented for the case of fiberglass, flexible elastomeric and phenolic pipe insulation. Results were reported in dry non-condensing ambient conditions and linear trends of the thermal conductivity were observed with respect to the average insulation temperature.

Preliminary test have begun using the PIT apparatus in ambient conditions that accelerate moisture propagation into the test insulation. It was found that the correlation for moisture entering into the insulation follows generally an exponential trend. Further testing is plan and will need to be done to fully understand the nature of moisture propagation, but preliminary results prove the PIT work for determining the thermal conductivity in both non-condensing and condensing conditions.

CHAPTER VII

CONCLUSION

A control system was developed and fabricated for the chamber including: the hardware such as the contactors, relays, terminal strips, electrical wire, sensors, PXI, etc. and software utilizing labview code such as PID algorithms, safety shutoffs, temperature step functions, signal conversions, data recording, etc. The new controls were used to perform two experiments, one with and one without a live load inside the chamber. Not only were these two experiments performed, but the design, construction and fabrications for both experimental setups was completed.

An 11-ton (39 kW) rooftop air-conditioning unit was used to verify the design focus of the chamber for testing HVAC unitary equipment. These findings confirmed that the OSU Psychrometric Chamber was operating properly and was able to accurately measure the capacity of the rooftop unit with respective outside laboratories' results on the same unit. The findings were within 5% of the same capacity and 2% of the airflow rate of the two outside laboratories' results. This was used as a benchmark to calibrate the chamber and ensure the correct energy and capacity measurements of the unit could be obtained. Further evaluation of the actual energy performance and capacity of an 11-ton rooftop unit was done when the unit was operating at design, off-design, part load, and variable climatic conditions. The testing conditions during these tests range from 67°F (19.4°C) and 52°F (11.1°C) to 115°F (46.1°C) & 67°F (19.4°C) dry bulb and wet bulb respectively. This allowed for approaches and methods available in the literature to evaluate the actual energy performance and capacity of the rooftop unit to be introduced as examples and guidance on how the chamber's ability can be applied. It was shown that during the testing of the 11-ton

unit that the chamber can easily exceed both AHRI and ASHRAE standards to obtain certification for unitary equipment.

An experimental apparatus to measure the thermal conductivity of mechanical pipe insulation systems at below ambient temperatures was developed to prove the chamber could be used for experiments other than HVAC unitary equipment testing. The test setup for the PIT, which includes the chamber's ability to supply uniform and constant conditions, was validated by comparing the thermal conductivity found for two types of pipe insulation systems with respect to the data available in the public domain. The comparison was within 15% proving the chamber produces the desired conditions and the PIT is capable of measuring the thermal conductivity of pipe insulation accurately. The relatively large 15% difference was due to radial configuration, edge effects, and the presence of joint sealants along the longitudinal butt joints of the pipe insulation systems compared to flat plate data available in the public domain. Further testing was done with the apparatus and chamber to find the thermal conductivity of pipe insulation systems for fiberglass, flexible elastomeric and phenolic pipe insulation material. These tests as well as the validation tests were done in dry non-condensing ambient conditions where the room was capable of achieving low humidity, below 20% RH, throughout a temperature range of 70°F (21.1°C) to 110°F (43.3°C). At the time of drafting this thesis, initial testing had begun investigating the effects of moisture ingress on the actual thermal conductivity of pipe insulation systems under wet ambient conditions. The PIT apparatus operated in conditions of 95°F (35°C) and above 90% RH for an extended period, up to one month (324 days), to accelerate the moister ingression into the insulation. It was proven that the chamber could achieve this condition and maintain the condition for test duration. In addition, the PIT setup was capable of operating in the extreme conditions and measure a change in thermal conductivity due to the moister ingress present in the insulation system.

The validation of the chamber control system was proven proficient to perform these two different experiments. These two experiments were different in nature; in both experiments a range of conditions were used to further validate the chamber and control system's capability. The chamber has proven to be

a useful tool to conduct experiments in a wide range of conditions which has been shown in this thesis, but the entire operational range of the chamber is far from completely validated. As the chamber approaches its design limits of -40°F (-40°C) an 135°F (57.2°C) as well as when different experiments are involved, more work will be needed on the controls system. Even if every possible scenario could be validated, there should always be an endless quest to perfect the controls system. This is because as the control system becomes better the uncertainty, accuracy, and precision of the experiment being conducted inside chamber will also become better.

REFERENCES

ASHRAE (1995). Methods of Testing for Rating Seasonal Efficiency of Unitary Air Conditioners and Heat Pumps. ANSI/ASHRAE 116

ASHRAE (2001). ASHRAE Handbook Fundamentals. New York**:** p. cm.

ASHRAE (2009). Methods of Testing for Rating Electrically Driven Unitary Air-Conditioning and Heat Pump Equipment. ASHRAE Standard 37-2009.

ASTM (2003 (2006)). Standard Test Method for Steady-State Heat Transfer Properites of Pipe Insulation. Standard C335. West Conshohocken, PA, ASTM International.

ASTM (2007). ASTM C 552 - 07, Standard Specification for Cellular Glass Thermal Insulation. Philadelphia, ASTM International.

ASTM (2009). *ASTM C 585 - 09, Standard Practice for Inner and Outer Diameters of Thermal Insulation for Normal Sizes of Pipe and Tubing*. West Conshohocken, PA, ASTM International.

Bai, J., S. Wang, et al. (2008). Development of an adaptive Smith predictor-based self-tuning PI controller for an HVAC system in a test room. **40:** 2244-2252.

Cremaschi, L. and E. Lee (2008). "Design and Heat Transfer Analysis of a New Psychrometric Environmental Chamber for Heat Pump and Refrigeration Systems Testing." ASHRAE Transactions **114**(2): 619-631.

Didion, D. A. (1979). "New Testing and Rating Procedures for Seasonal Performance of Heat Pumps." ASHRAE **21**(9): 40-44.

Kimball, L. R. (1974). "THERMAL CONDUCTANCE OF PIPE INSULATION: A LARGE-SCALE TEST APPARATUS." American Society of Mechanical Engineers (Paper)(Compendex).

Lifferth, S. (2009). Design and construction of a new psychrometric chamber. United States -- Oklahoma, Oklahoma State University. **M.S.:** 174.

Mumaw, J. R. (2002). A test protocol for comparison of the moisture absorption behavior of below-ambient piping insulation systems operating in hot-humid environments. Insulation Materials: Testing and Applications: 4th Volume, October 21, 2002 - October 22, 2002, Charleston, SC, United states, American Society for Testing and Materials.

Qu, G. and M. Zaheeruddin (2004). Real-time tuning of PI controllers in HVAC systems. **28:** 1313-1327.

Rentel-Gomez, C. and M. Velez-Reyes (2001). Decoupled control of temperature and relative humidity using a variable-air-volume HVAC system and non-interacting control**:** 1147.

Tarnawski, V. R., T. Momose, et al. (2009). "Thermal conductivity of standard sands. Part I. dry-state conditions." International Journal of Thermophysics **30**(3): 949-968.

Wang, Y.-W., W.-J. Cai, et al. (2004). A simplified modeling of cooling coils for control and optimization of HVAC systems. **45:** 2915-2930.

Whitaker, T. E. and D. W. Yarbrough (2002). Review of thermal properties of a variety of commercial and industrial pipe insulation materials. Insulation Materials: Testing and Applications: 4th Volume, October 21, 2002 - October 22, 2002, Charleston, SC, United states, American Society for Testing and Materials.

Wijeysundera, N. E., B. F. Zheng, et al. (1993). "Effective thermal conductivity of flat-slab and round-pipe insulations in the presence of condensation." Journal of Thermal Insulation and Building Envelopes **17**(Compendex): 55-76.

Wilkes, K. E., A. O. Desjarlais, et al. (2002). A pipe insulation test apparatus for use below room temperature. Insulation Materials: Testing and Applications: 4th Volume, October 21, 2002 - October 22, 2002, Charleston, SC, United states, American Society for Testing and Materials.

Wong, J. K. W. and H. Li (2010). Construction, application and validation of selection evaluation model (SEM) for intelligent HVAC control system. **19:** 261-269.

APPENDICES

Appendix A - LabView Chamber Control Program

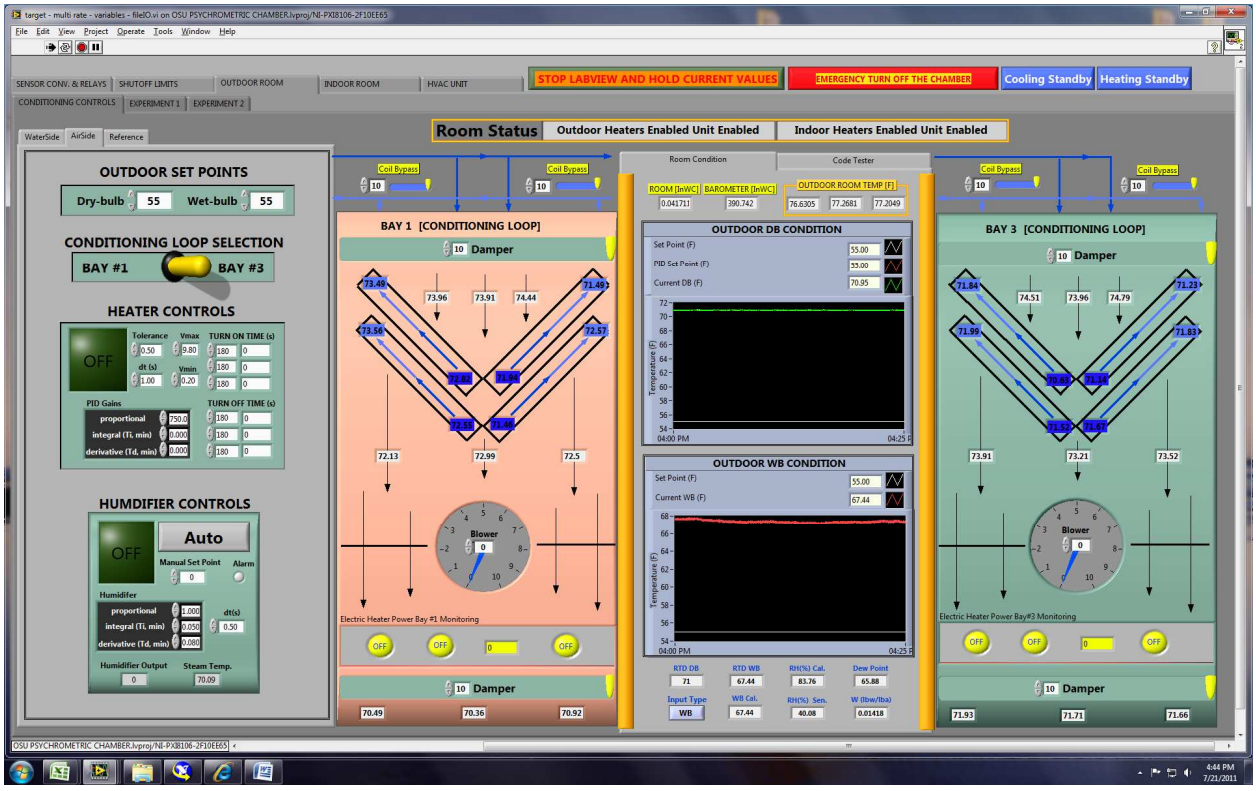

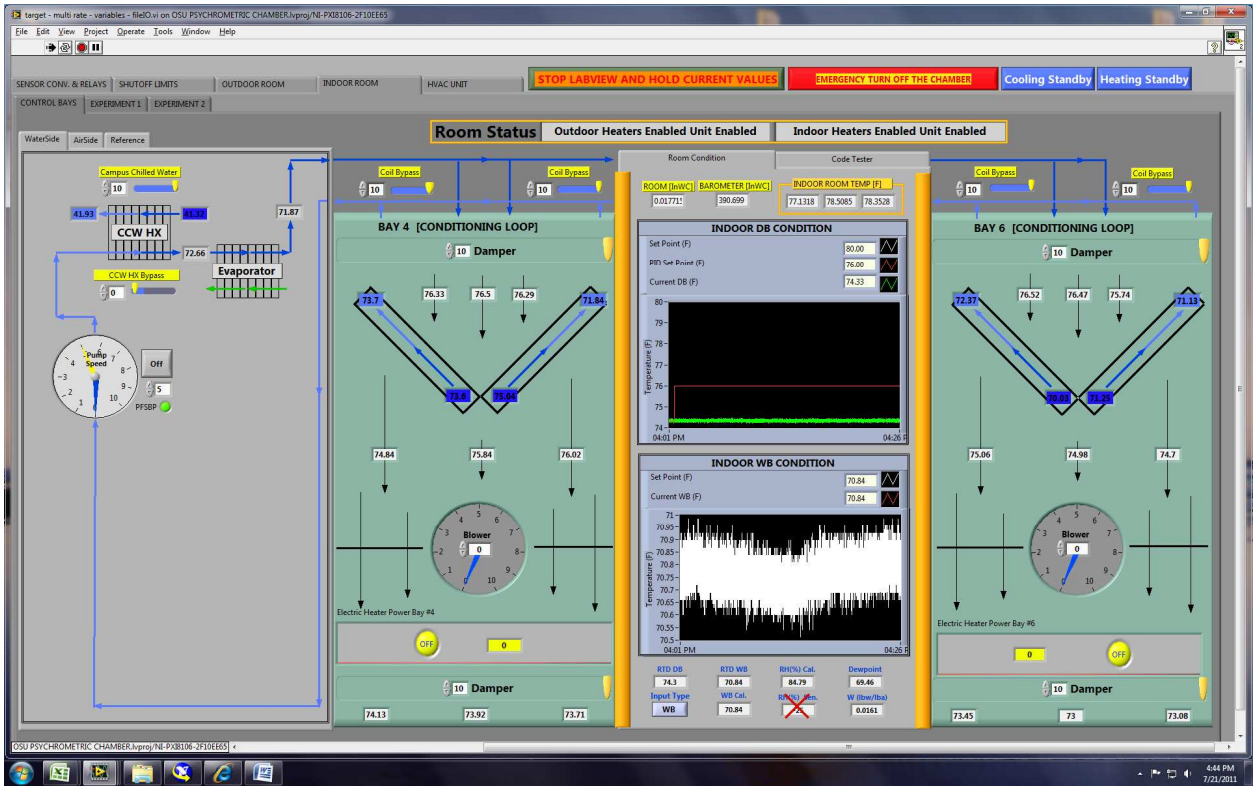
STOP LABVIEW AND HOLD CURRENT VALUES
EMERGENCY TURN OFF THE CHAMBER
Cooling Standby
Heating Standby
Room Status
Outdoor Heaters Enabled Unit Enabled
Indoor Heaters Enabled Unit Enabled
CCW HX
Evaporator
BAY 4 [CONDITIONING LOOP]
BAY 6 [CONDITIONING LOOP]
INDOOR DB CONDITION
INDOOR WB CONDITION
Blower
Damper

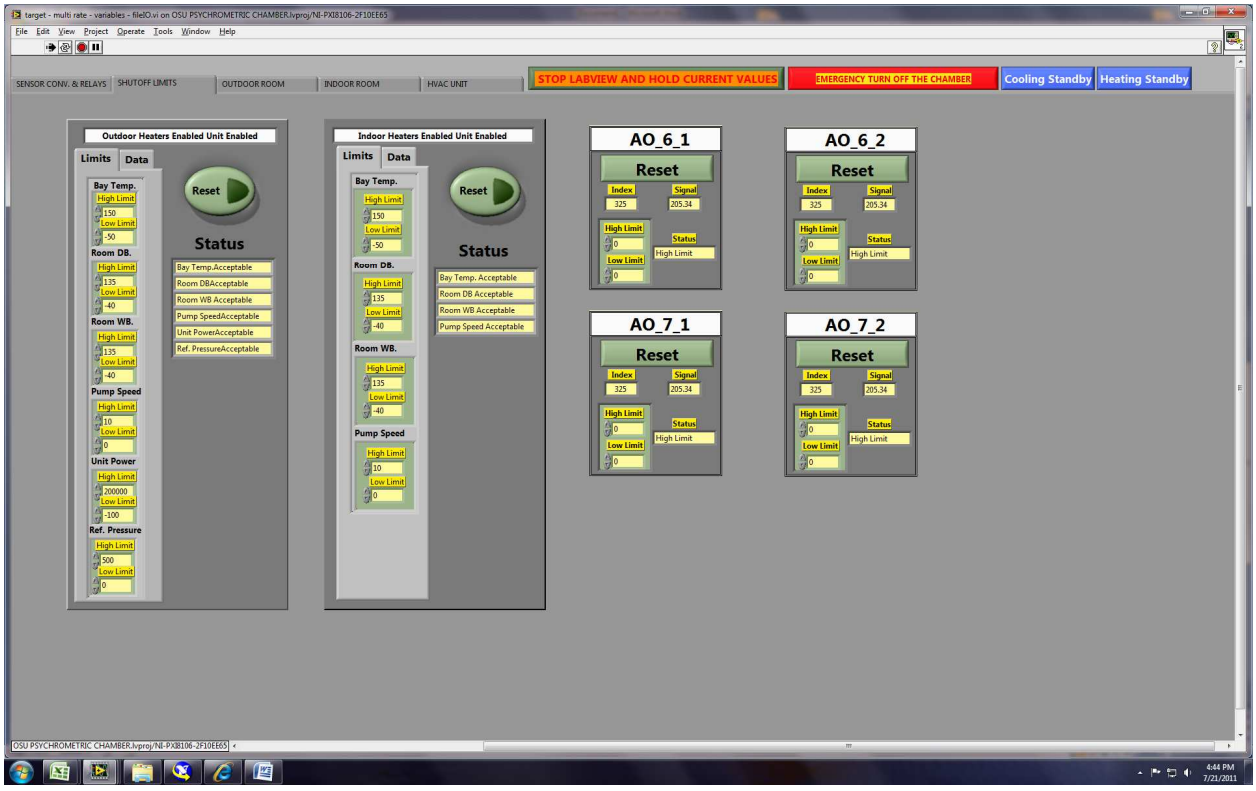
STOP LABVIEW AND HOLD CURRENT VALUES
EMERGENCY TURN OFF THE CHAMBER
Cooling Standby
Heating Standby
Outdoor Heaters Enabled Unit Enabled
Indoor Heaters Enabled Unit Enabled
Limits
Data
Reset
Status
AO_6_1
AO_6_2
AO_7_1
AO_7_2

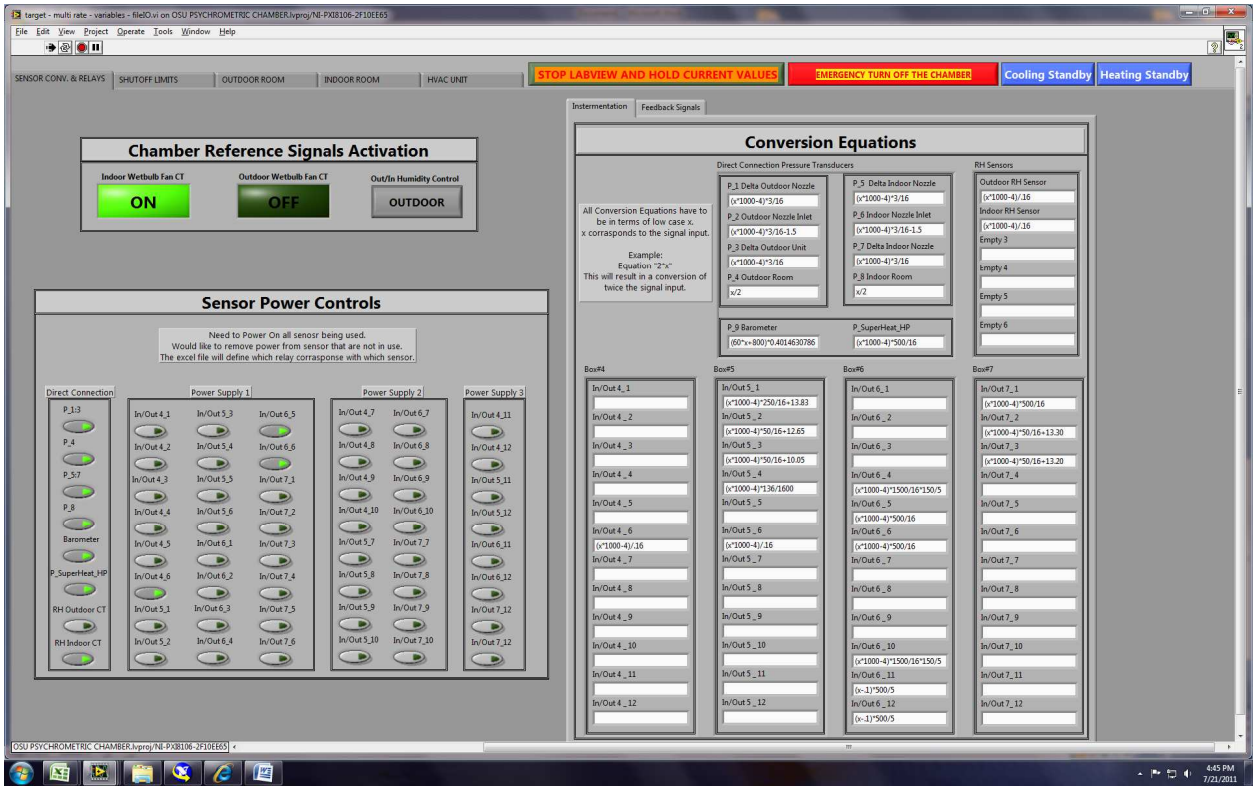
target - multi rate - variables - fileIO.vi on OSU PSYCHROMETRIC CHAMBER.lvproj/NI-PXI8106-2F10EE65
File Edit View Project Operate Tools Window Help
SENSOR CONV. & RELAYS
SHUTOFF LIMITS
OUTDOOR ROOM
INDOOR ROOM
HVAC UNIT
STOP LABVIEW AND HOLD CURRENT VALUES
EMERGENCY TURN OFF THE CHAMBER
Cooling Standby
Heating Standby
Chamber Reference Signals Activation
Indoor Wetbulb Fan CT
ON
Outdoor Wetbulb Fan CT
OFF
Out/In Humidity Control
OUTDOOR
Sensor Power Controls
Need to Power On all senosr being used.
Would like to remove power from sensor that are not in use.
The excel file will define which relay corrasponse with which sensor.
Direct Connection
Power Supply 1
Power Supply 2
Power Supply 3
P_1:3
P_4
P_5:7
P_8
Barometer
P_SuperHeat_HP
RH Outdoor CT
RH Indoor CT
Instermentation
Feedback Signals
Conversion Equations
All Conversion Equations have to be in terms of low case x.
x corrasponds to the signal input.
Example:
Equation "2*x"
This will result in a conversion of twice the signal input.
Direct Connection Pressure Transducers
P_1 Delta Outdoor Nozzle
P_2 Outdoor Nozzle Inlet
P_3 Delta Outdoor Unit
P_4 Outdoor Room
P_5 Delta Indoor Nozzle
P_6 Indoor Nozzle Inlet
P_7 Delta Indoor Nozzle
P_8 Indoor Room
P_9 Barometer
P_SuperHeat_HP
RH Sensors
Outdoor RH Sensor
Indoor RH Sensor
Box#4
Box#5
Box#6
Box#7

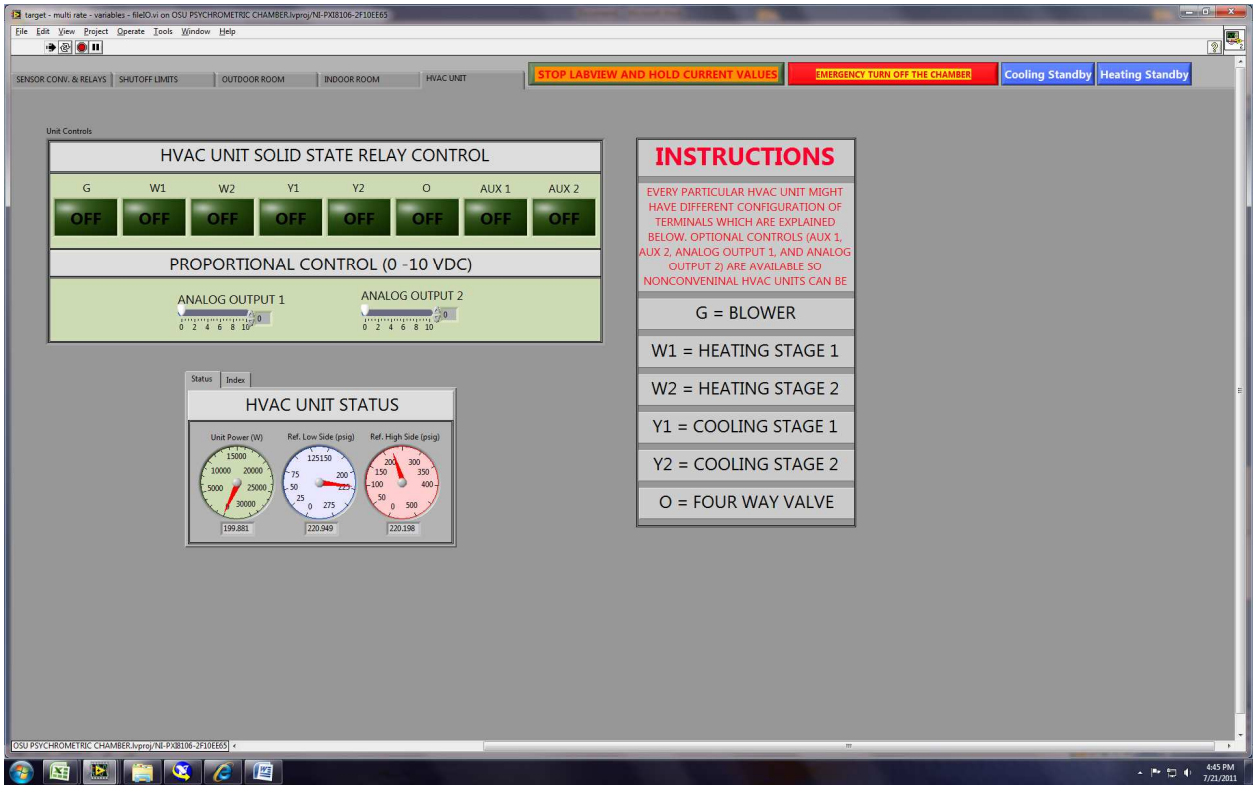
target - multi rate - variables - fileIO.vi on OSU PSYCHROMETRIC CHAMBER.lvproj/NI-PXI8106-2F10EE65
File Edit View Project Operate Tools Window Help
SENSOR CONV. & RELAYS
SHUTOFF LIMITS
OUTDOOR ROOM
INDOOR ROOM
HVAC UNIT
STOP LABVIEW AND HOLD CURRENT VALUES
EMERGENCY TURN OFF THE CHAMBER
Cooling Standby
Heating Standby
Unit Controls
HVAC UNIT SOLID STATE RELAY CONTROL
G
W1
W2
Y1
Y2
O
AUX 1
AUX 2
OFF
PROPORTIONAL CONTROL (0 -10 VDC)
ANALOG OUTPUT 1
ANALOG OUTPUT 2
Status
Index
HVAC UNIT STATUS
Unit Power (W)
Ref. Low Side (psig)
Ref. High Side (psig)
199.881
220.949
220.198
INSTRUCTIONS
EVERY PARTICULAR HVAC UNIT MIGHT HAVE DIFFERENT CONFIGURATION OF TERMINALS WHICH ARE EXPLAINED BELOW. OPTIONAL CONTROLS (AUX 1, AUX 2, ANALOG OUTPUT 1, AND ANALOG OUTPUT 2) ARE AVAILABLE SO NONCONVENINAL HVAC UNITS CAN BE
G = BLOWER
W1 = HEATING STAGE 1
W2 = HEATING STAGE 2
Y1 = COOLING STAGE 1
Y2 = COOLING STAGE 2
O = FOUR WAY VALVE

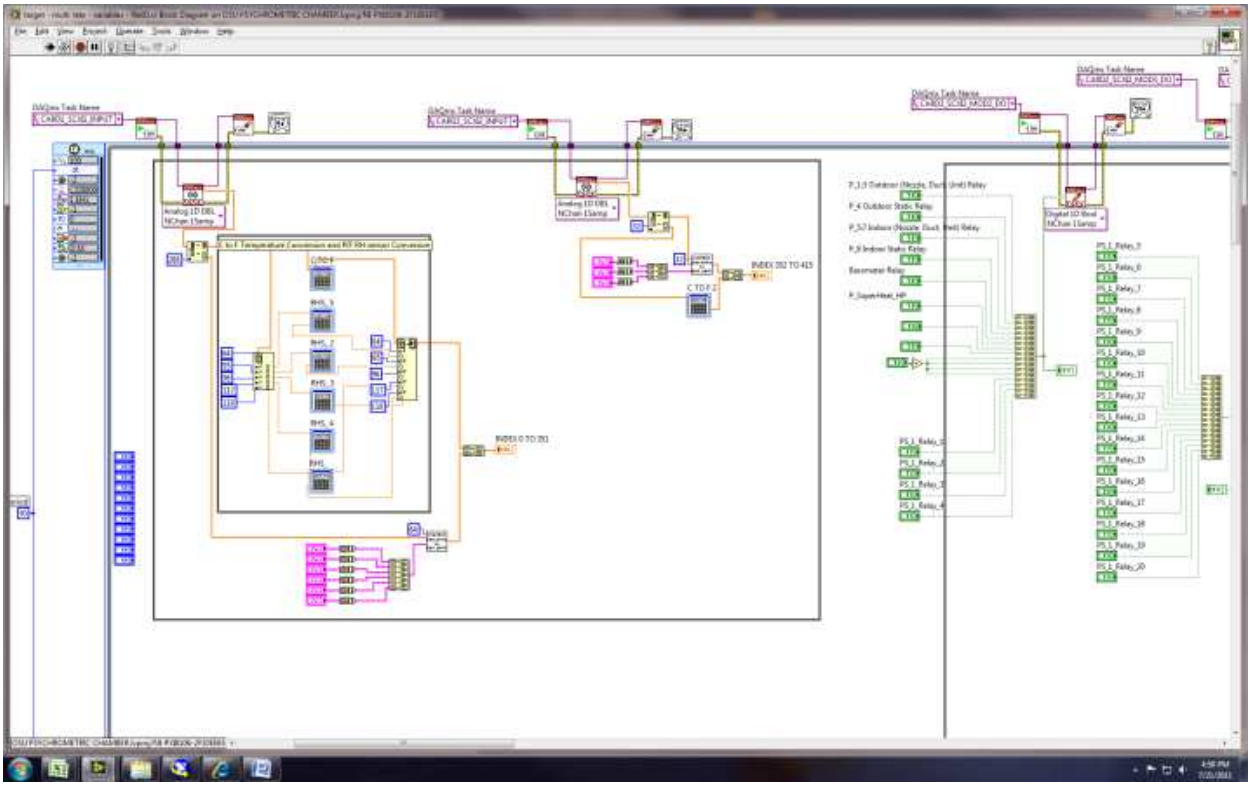

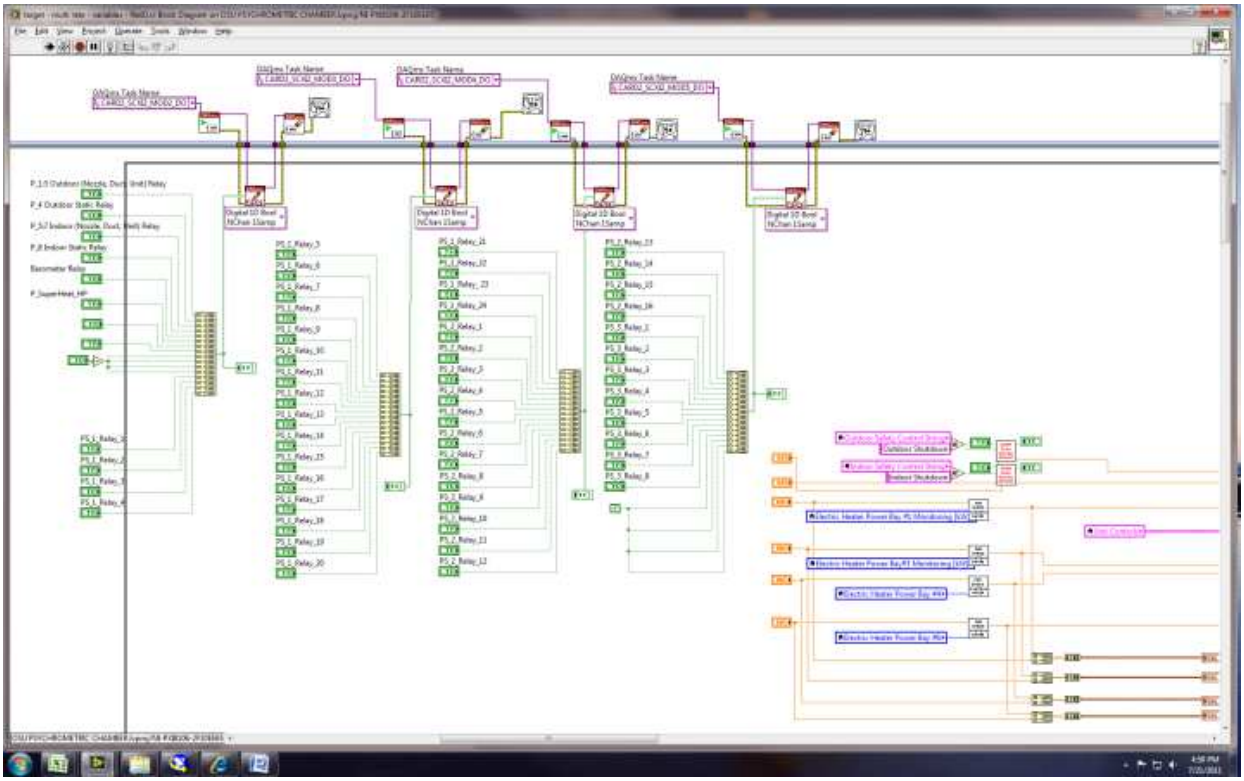

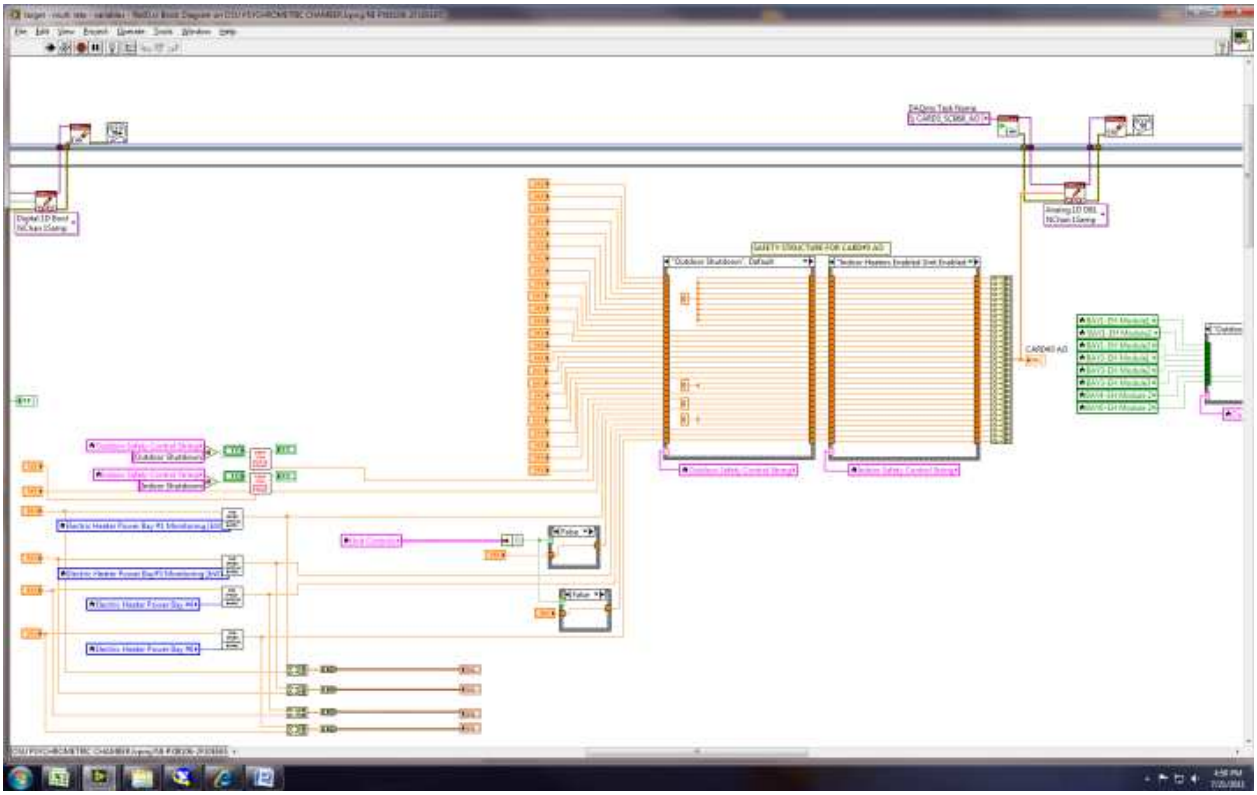

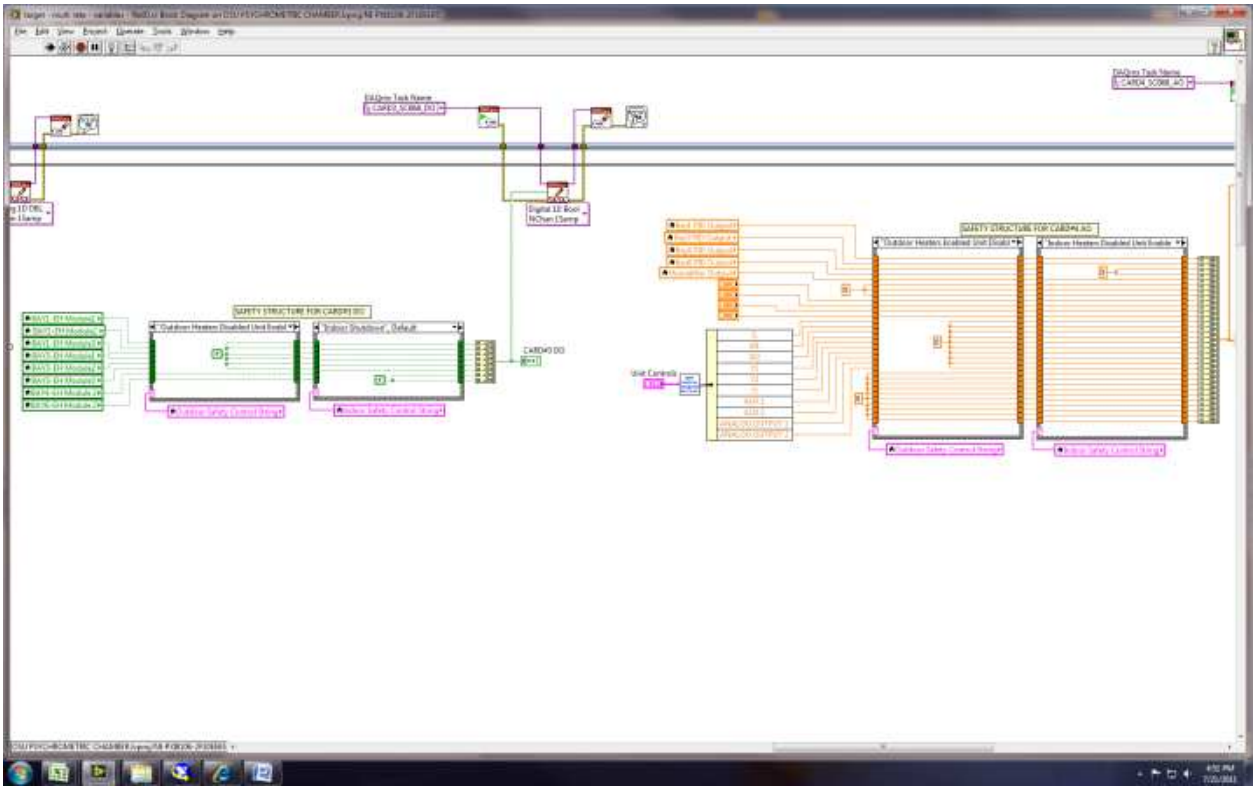

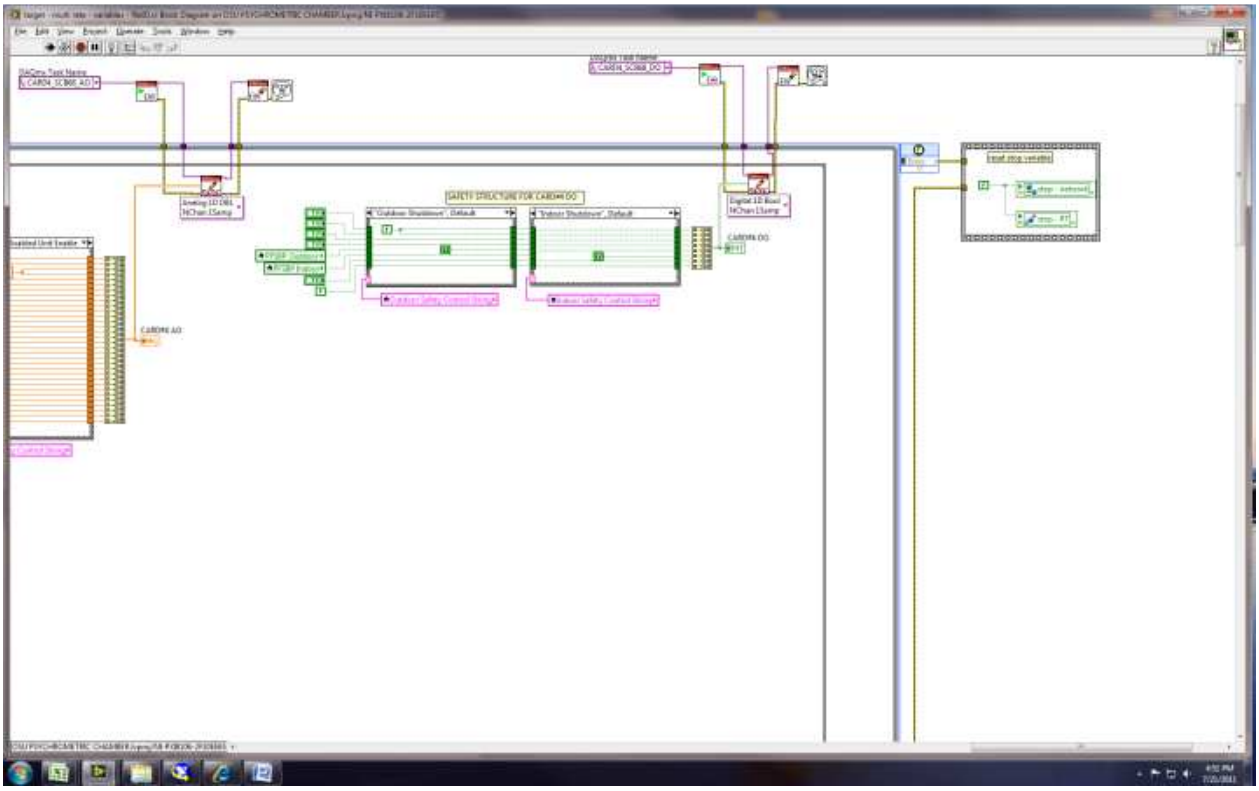

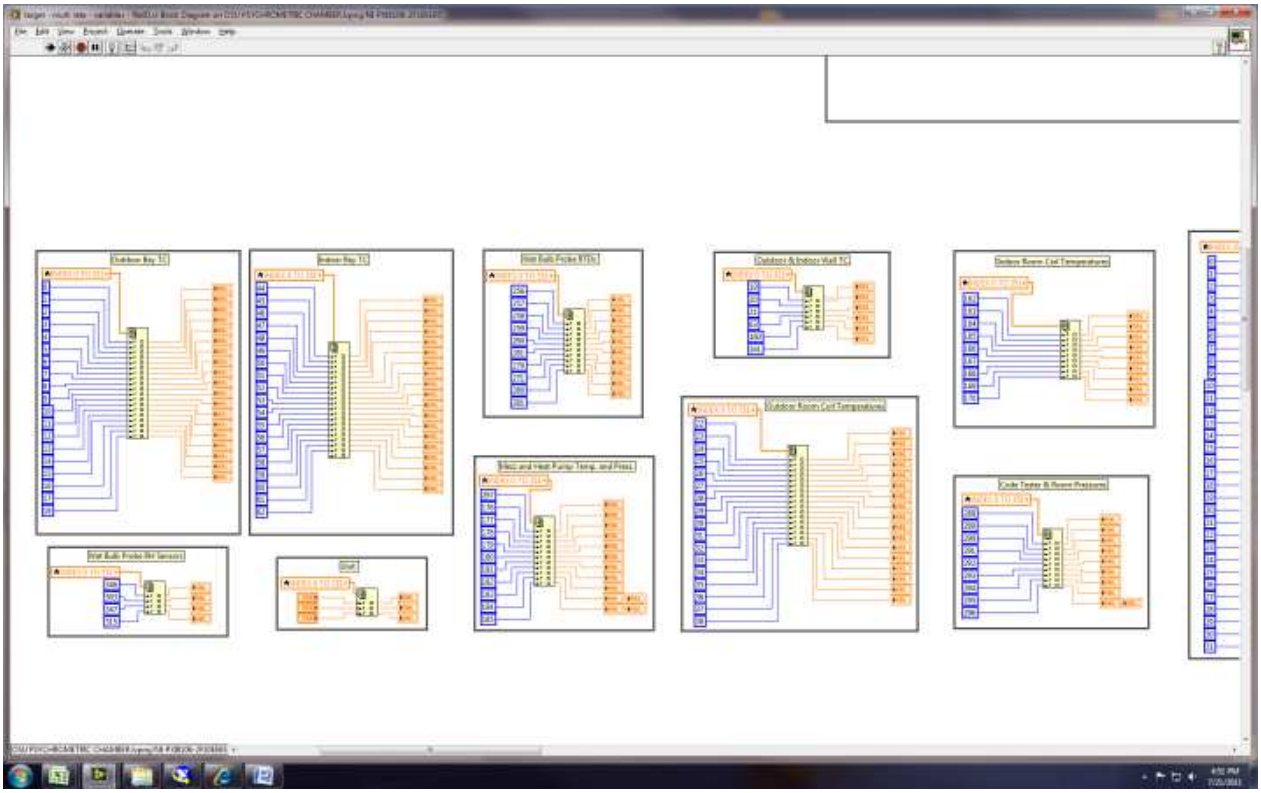

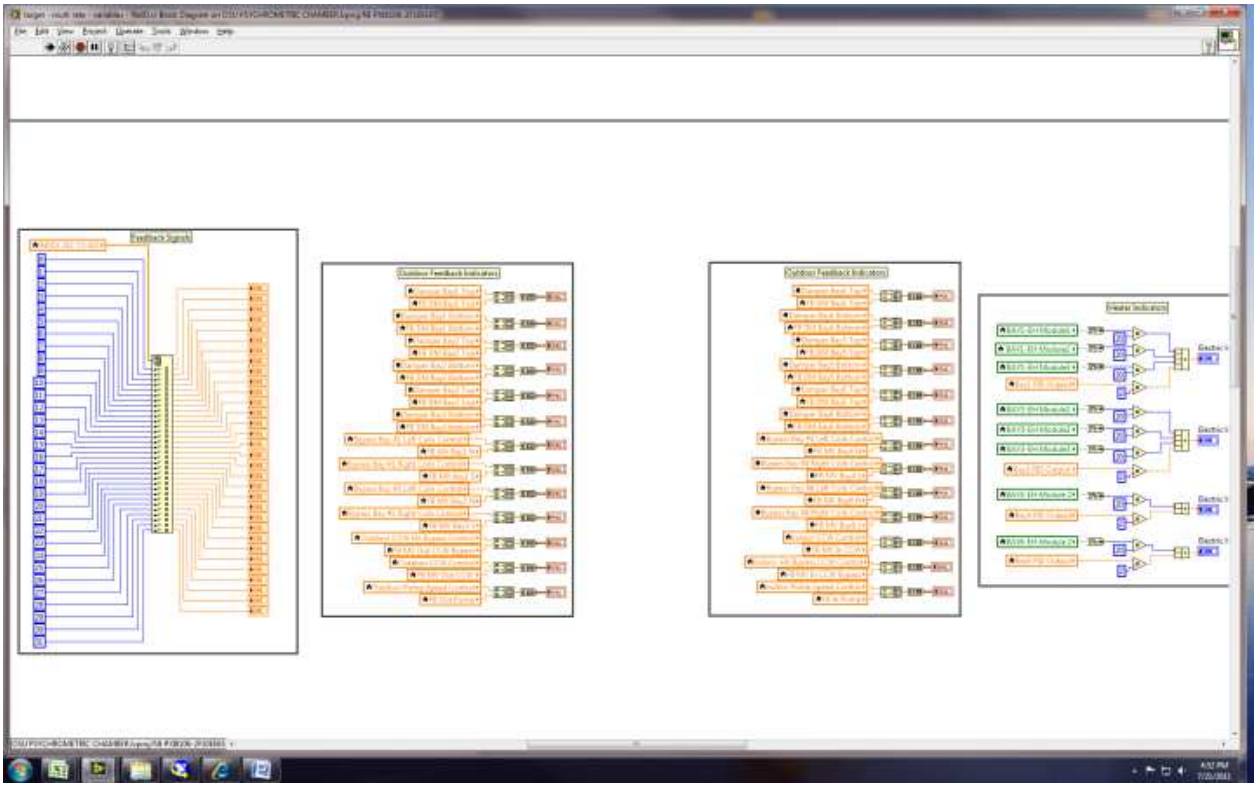

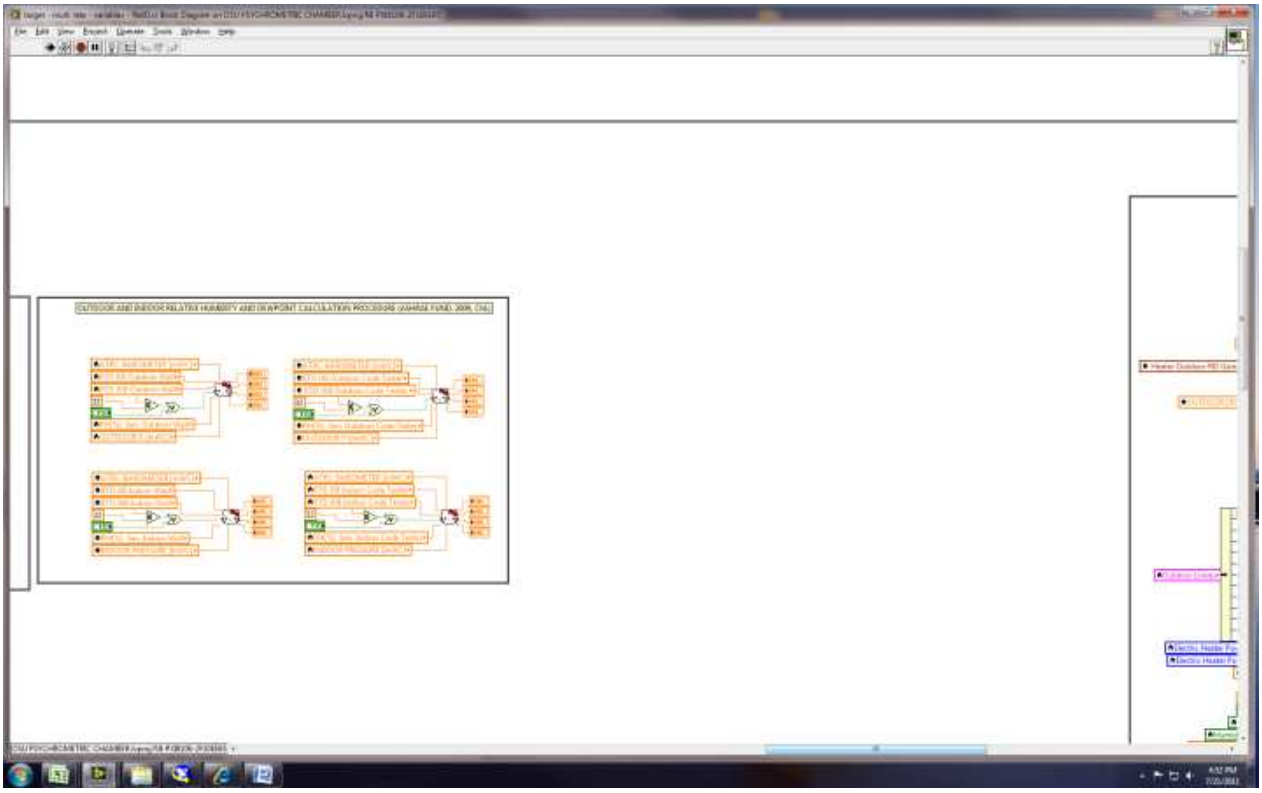

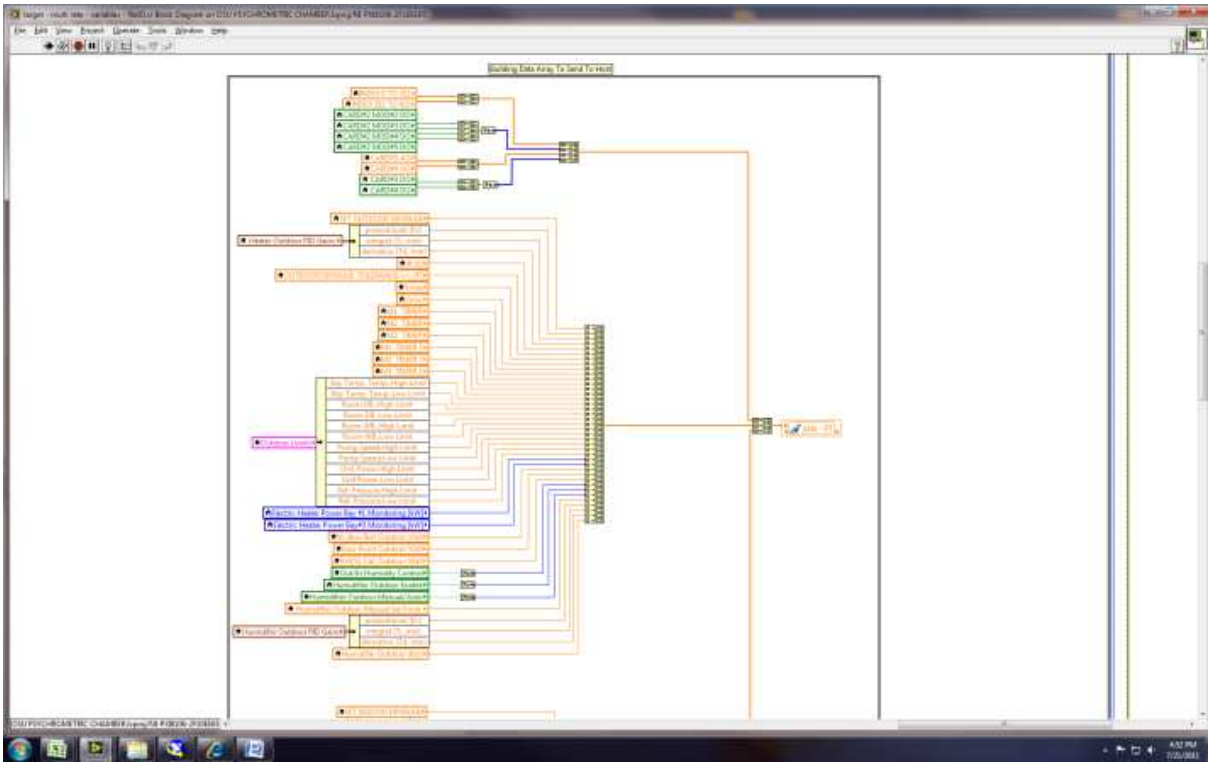

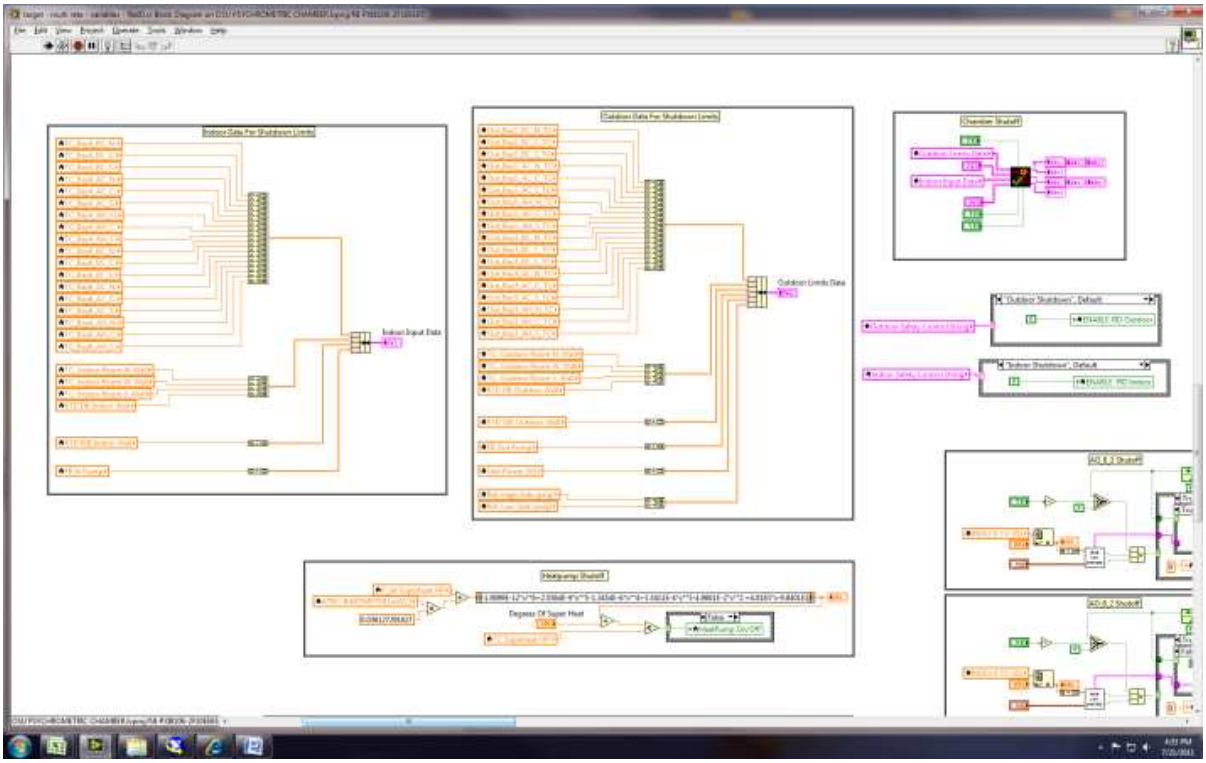

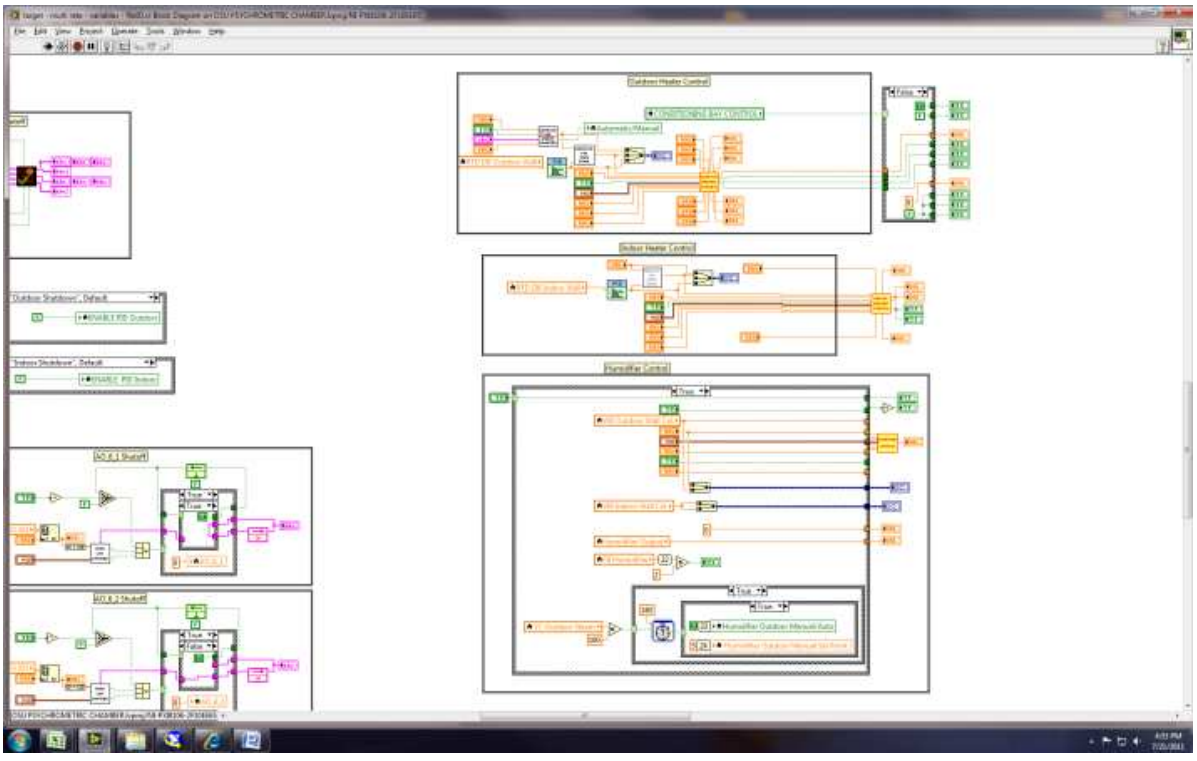

Appendix B - Temperature Distribution of Outdoor Room

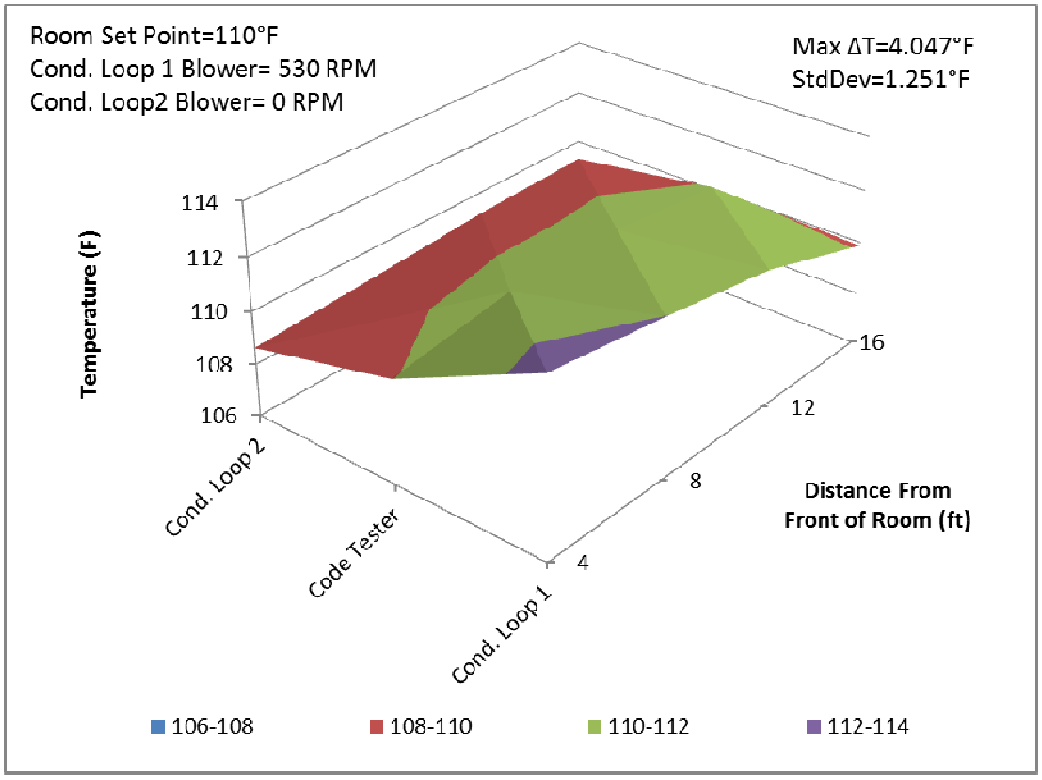

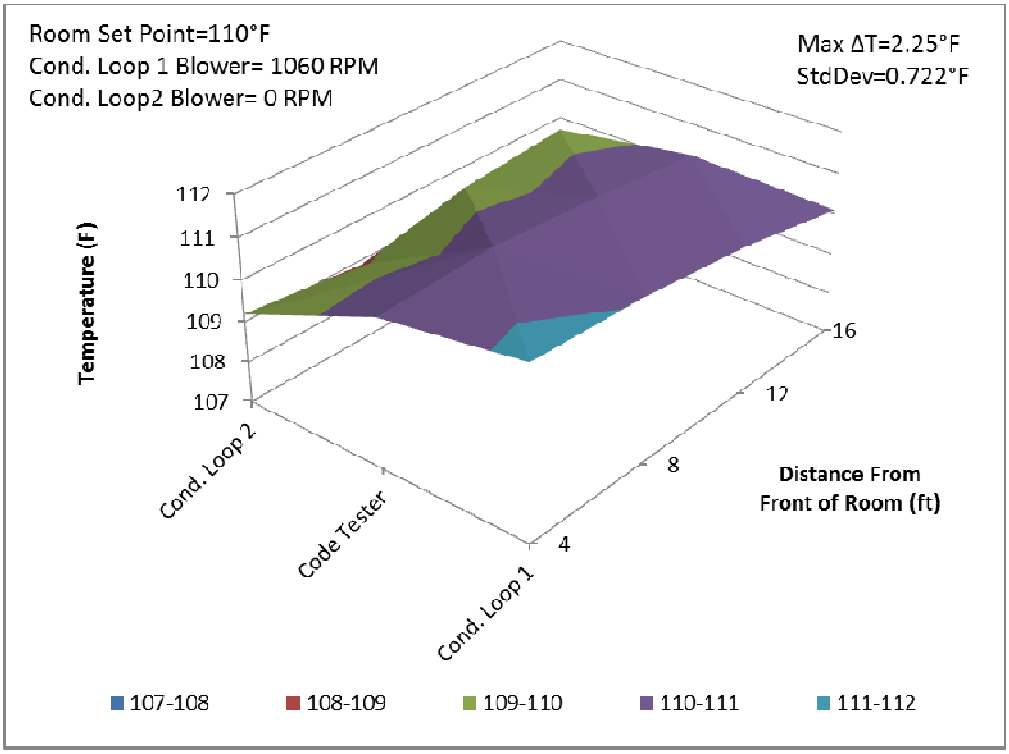

Appendix C EES Code For 11-ton rooftop Unit Uncertainty Analysis

```
"Calculations for moist air abs humidity ratio, specific volume,
 and density from ASHRAE fundamentals 1997,"
Procedure AirProp(t_db, t_wb, p : Wv, ρ, h)
"Absolute temperatures"
T_abs,db [R] := t_db + 459.67
T_abs,wb [R] := t_wb + 459.67
"Saturation pressure of water vapor as a function of wet bulb temperature"
C8 := -10440.39
C9 := -11.29465
C10 := -0.027022355 "above 32F"
C11 := 0.00001289036
C12 := -2.4780681 x 10^-9
C13 := 6.5459673
p_ws := exp[C8/T_abs,wb [R] + C9 + C10 · T_abs,wb [R] + C11 · T_abs,wb [R]^2 + C12 · T_abs,wb [R]^3 + C13 · ln(T_abs,wb [R])]
"Saturation humidity ratio function of wet bulb temperature and pressure"
W_wb,s := 0.62198 · [p_ws/(p - p_ws)]
"Humidity ratio"
W := ((1093 - 0.556 · t_wb) · W_wb,s - 0.24 · (t_db - t_wb))/(1093 + 0.444 · t_db - t_wb)
"Specific volume"
v [ft3/lbm] := 0.370486 · T_abs,db [R] · [(1 + 1.607858 · W)/p]
"Density of moist air"
ρ [lbm/ft3] := 1/v [ft3/lbm] · (1 + W)
"Enthalpy"
h := 0.24 · t_db + W · (1061 + 0.444 · t_db)
End AirProp
```

Determines Air Flow Rate and Density at the Indoor Nozzle Bank Depending on Measurements and Nozzle Configuration

Calculations from ASHRAE Standard 37-1988

Note: N1 through N10.....N(i)=1 for Open N(i)=0 for Closed

Procedure **IndoorNozzleBank** (Tdb, W, P_{inlet}, ΔP, N1, N2, N3, N4, N5, N6, N7, N8, N9, N10 : ρ, CFM, $\dot{m}$)

Absolute Temperature at Nozzle Inlet

$$T_{abs,db}\ [R] := Tdb + 459.67$$

Specific volume

$$v\ [ft3/lbm] := 0.370486 \cdot T_{abs,db}\ [R] \cdot \left[\frac{1 + 1.607858 \cdot W}{P_{inlet}}\right]$$

Density of moist air

$$\rho\ [lbm/ft3] := \frac{1}{v\ [ft3/lbm]} \cdot (1 + W)$$

Define Nozzle Diameters and which nozzle are being used

$$Dia_1 := N1 \cdot \frac{0.5}{12}$$

$$Dia_2 := N2 \cdot \frac{3}{12}$$

$$Dia_3 := N3 \cdot \frac{4}{12}$$

$$Dia_4 := N4 \cdot \frac{4}{12}$$

$$Dia_5 := N5 \cdot \frac{5.5}{12}$$

$$Dia_6 := N6 \cdot \frac{5.5}{12}$$

$$Dia_7 := N7 \cdot \frac{5.5}{12}$$

$$Dia_8 := N8 \cdot \frac{5.5}{12}$$

$$Dia_9 := N9 \cdot \frac{5.5}{12}$$

$$Dia_{10} := N10 \cdot \frac{5.5}{12}$$

Set initial CA and i value to zero

$CA := 0$

$i := 0$

Calculate the Total CA value by Summing for all nozzles that are open

Repeat

$i := i + 1$

Reynolds Number

$Re := 1.363 \times 10^{6} \cdot DIA_{i} \cdot (\Delta P \cdot \rho\ [lbm/ft3])^{0.5}$

Discharge Coefficient

$C := 2.2 \times 10^{-31} \cdot Re^{5} - 6.09 \times 10^{-25} \cdot Re^{4} + 6.77 \times 10^{-19} \cdot Re^{3} - 3.9 \times 10^{-13} \cdot Re^{2} + 1.28 \times 10^{-7} \cdot Re + 0.969$

Area of Nozzle Opening

$$A := \frac{\pi \cdot DIA_{i}^{2}}{4}$$

Summing the CA for each Nozzle

$CA := CA + C \cdot A$

Until $(i = 10)$

Alpha Ratio

$$\alpha := 1 - \frac{5.187 \cdot \Delta P}{\rho\ [lbm/ft3] \cdot 53.35 \cdot (Tdb + 459.7)}$$

Expansion Factor

$Y := 1 - 0.548 \cdot (1 - \alpha)$

$$CFM := 1096 \cdot CA \cdot Y \cdot \left[\frac{\Delta P}{\rho\ [lbm/ft3]}\right]^{0.5}$$

$$\dot{m} := CFM \cdot 60 \cdot \rho\ [lbm/ft3]$$

End **IndoorNozzleBank**

Pressure Unit Conversions

$\Delta P_{,Unit,psi} = \Delta P_{,Unit,in,wc} \cdot 0.3613$

$\Delta P_{,nozzle,psi} = \Delta P_{,nozzle,in,wc} \cdot 0.3613$

$P_{before,nozzle,psi} = 0.3613 \cdot P_{before,nozzle,in,wc}$

$P_{room,\psi} = P_{room,in,wc} \cdot 0.3613$

$Barometer_{\psi} = 0.00014504 \cdot Barometer_{pa}$

Defining the Static Pressure Throughout the Duct System

$P_{return} = P_{room,\psi} + Barometer_{\psi}$

$P_{supply} = P_{return} + \Delta_{P,Unit,psi}$

$P_{nozzle,inlet} = P_{before,nozzle,psi} + Barometer_{\psi}$

Finding the Properties of the Air at Supply and Return of Unit

Call **AirProp** (Tdb_{supply} , Twb_{supply} , P_{supply} : W_{supply} , v_{supply} , ρ_{supply} , h_{supply})

Call **AirProp** (Tdb_{return} , Twb_{return} , P_{return} : W_{return} , v_{return} , ρ_{return} , h_{return})

Determining the Flow Rate of the Unit

Call **IndoorNozzleBank** (Tdb_{nozzle} , W_{supply} , $P_{nozzle,inlet}$, $\Delta_{P,nozzle,in,wc}$, 0 , 1 , 1 , 1 , 1 , 1 , 1 , 1 , 1 : ρ_{nozzle} , CFM , $\dot{m}$)

Total Heat Transfer

$\dot{q}_{total} = \dot{m} \cdot (h_{supply} - h_{return})$

$\delta h = h_{supply} - h_{return}$

Defining the Static Pressure Throughout the Duct System

$P_{return} = P_{room,\psi} + Barometer_{\psi}$

$P_{supply} = P_{return} + \Delta_{P,Unit,psi}$

$P_{nozzle,inlet} = P_{before,nozzle,psi} + Barometer_{\psi}$

Finding the Properties of the Air at Supply and Return of Unit

Call **AirProp** (Tdb_{supply} , Twb_{supply} , P_{supply} : W_{supply} , v_{supply} , ρ_{supply} , h_{supply})

Call **AirProp** (Tdb_{return} , Twb_{return} , P_{return} : W_{return} , v_{return} , ρ_{return} , h_{return})

Determining the Flow Rate of the Unit

Call **IndoorNozzleBank** (Tdb_{nozzle} , W_{supply} , $P_{nozzle,inlet}$, $\Delta_{P,nozzle,in,wc}$, 0 , 1 , 1 , 1 , 1 , 1 , 1 , 1 , 1 : ρ_{nozzle} , CFM , $\dot{m}$)

Total Heat Transfer

$\dot{q}_{total} = \dot{m} \cdot (h_{supply} - h_{return})$

$\delta h = h_{supply} - h_{return}$

Singling Out Sensible and Latent Heat Transfer

$h_x = 0.24 \cdot Tdb_{return} + W_{supply} \cdot (1061 + 0.444 \cdot Tdb_{return})$

$\dot{q}_{sen} = \dot{m} \cdot (h_{supply} - h_x)$

$\dot{q}_{lat} = \dot{m} \cdot (h_x - h_{return})$

Coefficient Of Performance

$$COP = \frac{\left| \frac{\dot{q}_{total}}{Power_{unit}} \right|}{3.412}$$

$RH = RH ('AirH2O' , T = Tdb_{return} , B = Twb_{return} , P = P_{room,\psi} + Barometer_{\psi})$

Appendix D - Conditioning Loop Flow Rate

The flow rate of the air through the conditioning loop is needed to validate the coil model as well as the overall system model. Since at this point only the water side of the conditioning loop is being modeled; a direct relationship between the flow rate and fan RPM was developed. Within the conditioning loop there are electric resistance heating coils and the temperatures are being monitored before and after the coil. This configuration allows the conditioning loop to have a "built in" anemometer. It is relatively easy to measure the electrical resistance of the coil heater and the voltage being supplied to it, this makes it easy through Watt's and Ohm's Laws to calculate the power. Using the power of the heater and assuming that the heating coil has an extremely high efficiency, the power of the heater is the power or energy transfer to the air. Then using the heat transfer equation, the mass flow rate of the air can be estimated. The equations below summarize the calculations used.

$$P = \frac{V^2}{R}$$

$$P = \dot{q} = \dot{m} c_p (T_h - T_c)$$

This "built in" anemometer was used to estimate the airflow rate in the conditioning loop. Due to the high flow rate within the conditioning loop, the available instrumentation was limited and inaccurate, so the "built in" anemometer serves as the only option.

A series of experiments were run using different fan RPM. At each RPM the system was allowed to reach steady state; then three temperatures before and after the heaters was recorded every second for two minutes. The air flow rate was calculated for every second then averaged over the two minutes to achieve a value that relates the flow rate to RPM. The voltage and resistance of the heaters were measured before the experiment was started and was considered constant throughout the entire experiment. Below shows the results from the calculations and the curve that relates the different fan RPMs to their flow rates.

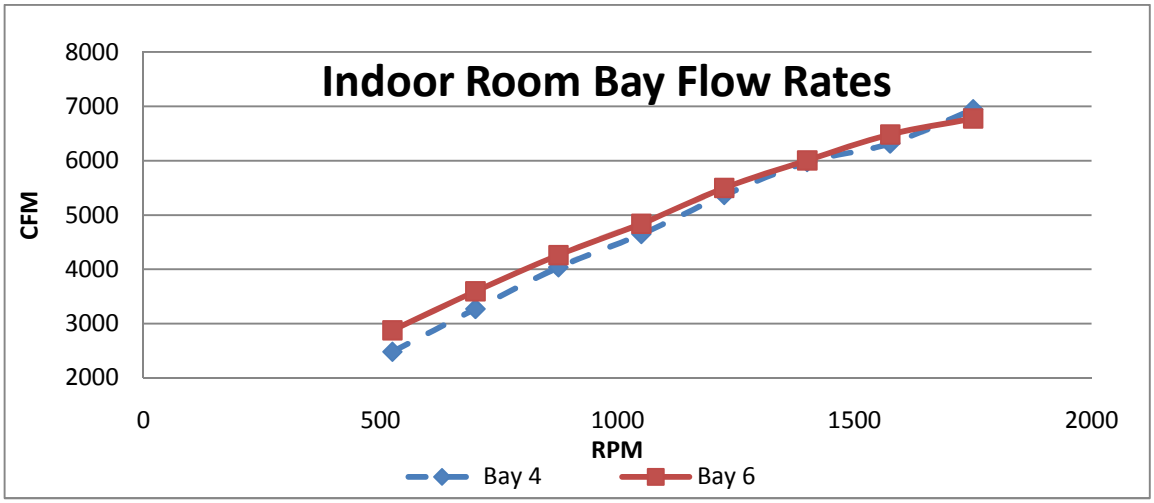

Appendix E - Assembly Drawing For PIT Apperatus

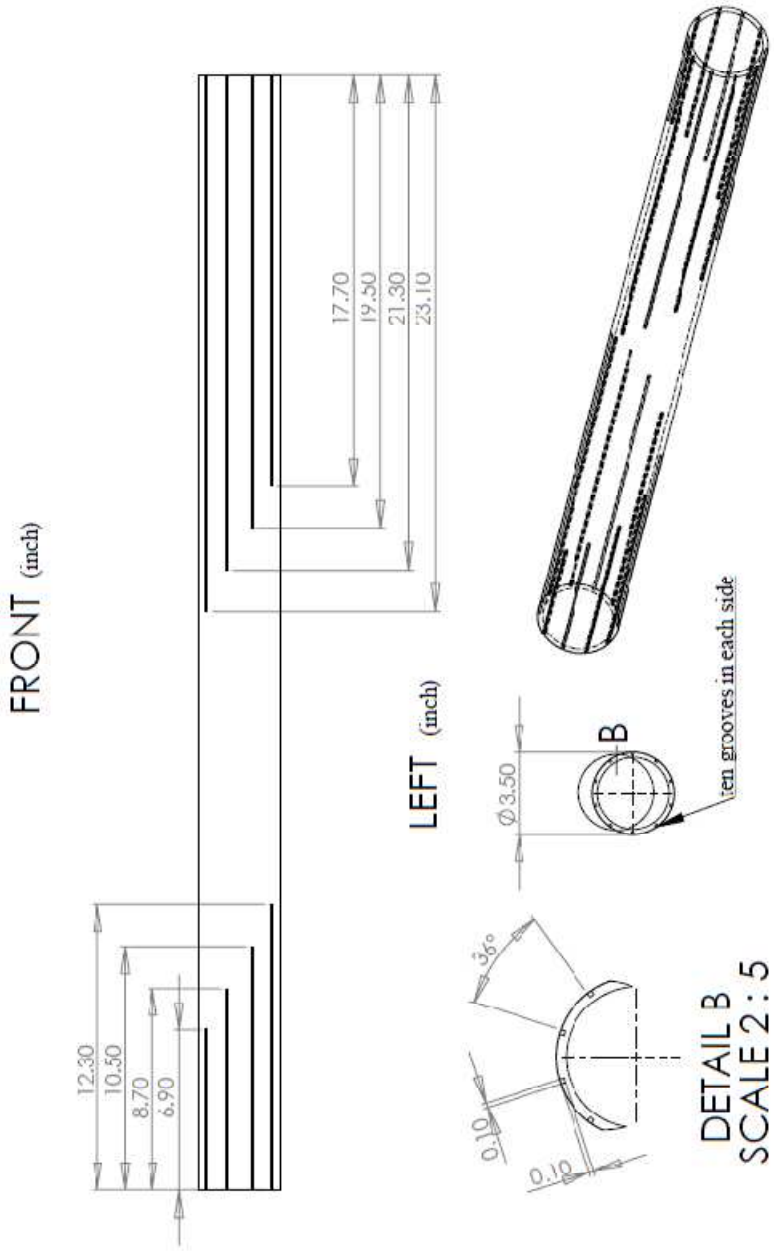

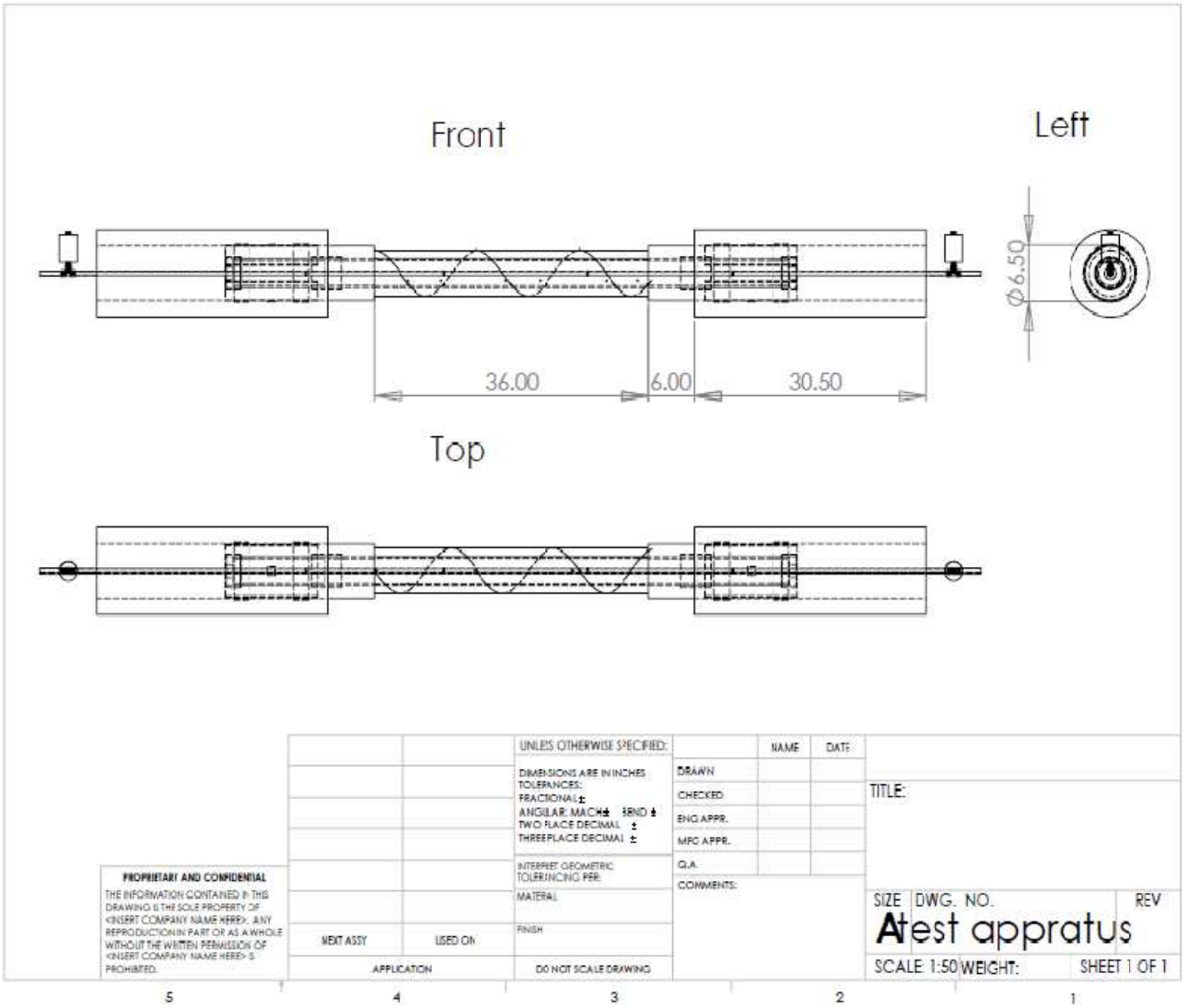
Front
Left
Ø6.50
36.00
6.00
30.50
Top
UNLESS OTHERWISE SPECIFIED:
NAME
DATE
DRAWN
CHECKED
ENG APPR.
MFG APPR.
Q.A.
COMMENTS:
DIMENSIONS ARE IN INCHES
TOLERANCES:
FRACTIONAL ±
ANGULAR: MACH ± BEND ±
TWO PLACE DECIMAL ±
THREE PLACE DECIMAL ±
INTERPRET GEOMETRIC TOLERANCING PER:
MATERIAL
FINISH
DO NOT SCALE DRAWING
NEXT ASSY
USED ON
APPLICATION
PROPRIETARY AND CONFIDENTIAL
THE INFORMATION CONTAINED IN THIS DRAWING IS THE SOLE PROPERTY OF <INSERT COMPANY NAME HERE>. ANY REPRODUCTION IN PART OR AS A WHOLE WITHOUT THE WRITTEN PERMISSION OF <INSERT COMPANY NAME HERE> IS PROHIBITED.
TITLE:
SIZE
DWG. NO.
REV
Atest appratus
SCALE: 1:50
WEIGHT:
SHEET 1 OF 1
5
4
3
2
1

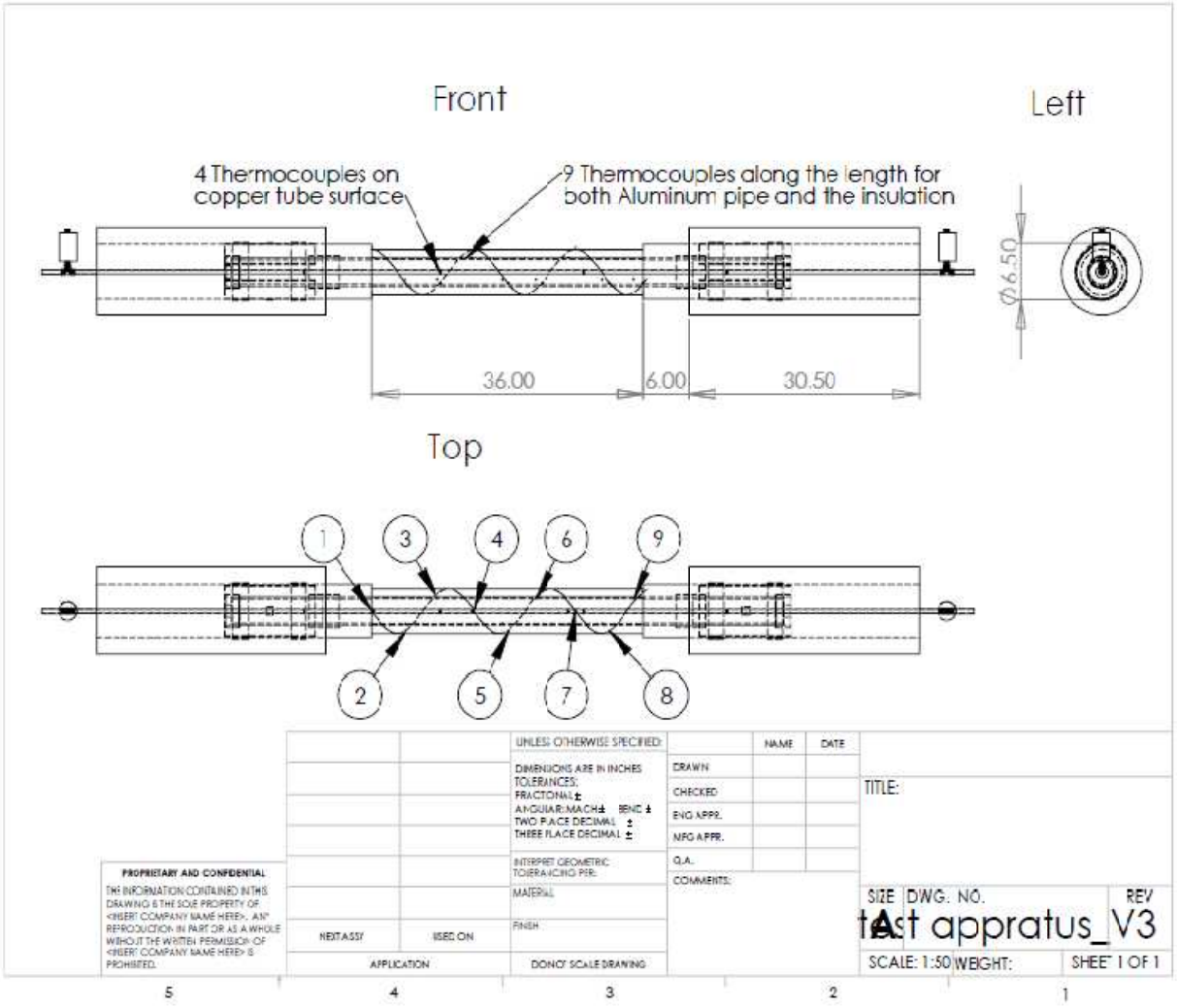
Front
Left
4 Thermocouples on copper tube surface
9 Thermocouples along the length for both Aluminum pipe and the insulation
Ø6.50
36.00
6.00
30.50
Top
1
3
4
6
9
2
5
7
8
UNLESS OTHERWISE SPECIFIED:
DIMENSIONS ARE IN INCHES
TOLERANCES:
FRACTIONAL ±
ANGULAR: MACH ± BEND ±
TWO PLACE DECIMAL ±
THREE PLACE DECIMAL ±
INTERPRET GEOMETRIC TOLERANCING PER:
MATERIAL
FINISH
NEXT ASSY
USED ON
APPLICATION
DO NOT SCALE DRAWING
NAME
DATE
DRAWN
CHECKED
ENG APPR.
MFG APPR.
Q.A.
COMMENTS:
TITLE:
SIZE
DWG. NO.
REV
A
test appratus_V3
SCALE: 1:50
WEIGHT:
SHEET 1 OF 1
PROPRIETARY AND CONFIDENTIAL
THE INFORMATION CONTAINED IN THIS DRAWING IS THE SOLE PROPERTY OF <INSERT COMPANY NAME HERE>. ANY REPRODUCTION IN PART OR AS A WHOLE WITHOUT THE WRITTEN PERMISSION OF <INSERT COMPANY NAME HERE> IS PROHIBITED.
5
4
3
2
1

Appendix F - ESS Code For Pipe Insulation Test Apparatus Uncertainty Analysis

The Effective Conductivity of the Sand

Inputs

$L_{testsection} = 0.9144$ [m] 3 [ft]

$ID_{cu} = 0.009525$ [m] 3/8 [in]

$OD_{cu} = 0.0127$ [m] 1/2 [in]

$ID_{Al} = 0.0762$ [m] 3 [in]

$OD_{Al} = 0.0889$ [m] 3.5 [in]

$OD_{outsideinsulation} = 0.2413$ [m] 9.5 [in]

Solutions

$$Q_{testsection} = -Q_{electric} + Q_{outsideinsulation}$$

$$Q_{outsideinsulation} = k_{outsideinsulation} \cdot 2 \cdot \pi \cdot L_{testsection} \cdot \left[\frac{T_{al} - T_{outsideinsulation}}{\ln\left(\frac{OD_{outsideinsulation}}{OD_{Al}} \right)} \right]$$

$$Q_{testsection} = k_{eff} \cdot 2 \cdot \pi \cdot L_{testsection} \cdot \left[\frac{T_{cu} - T_{al}}{\ln\left(\frac{ID_{Al}}{OD_{cu}} \right)} \right]$$

Conductivity of the Test Insulstion On the PIT

Inputs

$L_{testsection} = 0.9144$ [m] 3 [ft]

$ID_{cu} = 0.009525$ [m] 3/8 [in]

$OD_{cu} = 0.0127$ [m] 1/2 [in]

$ID_{Al} = 0.0762$ [m] 3 [in]

$OD_{Al} = 0.0889$ [m] 3.5 [in]

$OD_{testinsulation} = 2 \cdot OD_{Al} + testinsulationthickness$

Solutions

$$Q_{testsection} = Q_{testinsulation}$$

$$Q_{testinsulation} = k_{testinsulation} \cdot 2 \cdot \pi \cdot L_{testsection} \cdot \left[\frac{T_{al} - T_{testinsulation}}{\ln\left(\frac{OD_{testinsulation}}{OD_{Al}} \right)} \right]$$

$$Q_{testsection} = k_{eff} \cdot 2 \cdot \pi \cdot L_{testsection} \cdot \left[\frac{T_{cu} - T_{al}}{\ln\left(\frac{ID_{Al}}{OD_{cu}} \right)} \right]$$

VITA

Kasey M. Worthington

Candidate for the Degree of

Master of Science

Thesis: CALIBRATION OF THE OSU PSYCHROMETRIC CHAMBER AND FIRST EXPERIMENTS

Major Field: Mechanical and Aerospace Engineering

Biographical: From small town in north Texas (Bells). Family owned a HVAC sub-contract company. Raced Professional Motocross/Super cross prior to starting my Master's.

Education: BS from OSU "I bleed Orange"

Completed the requirements for the Master of Science in your major at Oklahoma State University, Stillwater, Oklahoma in July, 2011.

Completed the requirements for the Bachelor of Science/Arts in your major at Oklahoma State University, Stillwater, Oklahoma in May, 2009.

Experience:

Professional Memberships: ASHRAE

Name: Kasey Worthington Date of Degree: July, 2011

Institution: Oklahoma State University Location: OKC or Stillwater, Oklahoma

Title of Study: CALIBRATION OF THE OSU PSYCHROMETRIC CHAMBER AND FIRST EXPERIMENTS

Pages in Study: 115 Candidate for the Degree of Master of Science

Major Field: Mechanical and Aerospace Engineering

Scope and Method of Study:

Complete the construction of a new psychrometric chamber at OSU and demonstrate that the chamber is capable of performing accurate and precise experiments on thermal systems with and without a live thermal load.

Findings and Conclusions:

Completion of the chamber involved the development and fabrication of the control system. The control system included both the hardware and software needed to adjust and maintain the conditions in both the indoor and outdoor rooms. After completing the control system the chamber was ran in order to produce conditions needed to perform two experiments. These two experiments include the testing of an 11-ton (39 kW) rooftop air-conditioning unit and the establishment of thermal conductivity for different cold pipe insulation systems exposed to both moist air condensing and non-condensing conditions. Not only was these experiments performed but, the required experimental setup was also design and construct for both. An uncertainty analysis was performed on these setups and it shows to produce excellent theoretical uncertainty. The actual experiments results and accuracies confirm these finding as well as the experimental setups designs, fabrications, and abilities. Furthermore, the validation of the chamber and chamber control system was proven proficient at performing these two different experiments. These two experiments were different in nature; in both experiments a range of conditions were used, further validating the chamber and control system's capabilities.

ADVISER'S APPROVAL: Lorenzo Cremaschi